Department of Civil, Environmental and Geomatic Engineering

University College London

Engineering Properties of Hybrid Fibre Reinforced Strain-hardening Geopolymer Composites

Yi Wang

A thesis submitted for the degree of

Doctor of Philosophy

October 2021

Declaration

I, Yi Wang, confirm that the work presented in this thesis is my own. Where information has been derived from other sources, I confirm that this has been indicated in the thesis

Signed:

Date:

Abstract

Strain-hardening geopolymer composites (SHGC) is an alkali-activated material reinforced with randomly dispersed short fibres, which exhibits high ductility and strain-hardening behaviour with excellent crack control. Made from industrial by-products including fly ash (FA) and ground granulated blast-furnace slag (GGBS), SHGC is considered a promising and green alternative to its cement-based counterpart because of low carbon emissions, reduced energy consumption and superior mechanical properties. The incorporation of recycled tyre steel (RTS) fibre can further enhance the greenness of SHGC. Although the fresh and hardened properties of SHGC produced by various precursors have been increasingly investigated in recent years, a systematic study of strain-hardening behaviour and engineering properties of FA-GGBS based SHGC reinforced with hybrid polyvinyl alcohol (PVA) and RTS fibres and cured at ambient temperature is still lacking.

This thesis aims to develop a hybrid PVA-RTS fibre reinforced sustainable SHGC with desired engineering properties based on micromechanics and fracture mechanics theory and investigate the effects of sand and fibres on the engineering properties of SHGC. Firstly, a series of tests were conducted to explore the effect of sand and obtain the optimum sand content for SHGC with acceptable engineering properties. Then, the micromechanical analysis was undertaken to verify the strength- and energy-based pseudo strain-hardening criteria of SHGC. Afterwards, the effects of PVA fibre and hybrid PVA-RTS fibres on engineering properties of SHGC were studied in terms of flowability, drying shrinkage, static and dynamical mechanical properties, strain-hardening and multiple cracking behaviours, and failure mechanisms. Microstructural characterisation was employed to gain insight into the toughening mechanisms of hybrid fibre reinforced SHGC, including fibre bridging effect, fibre fracture, and fibre pull-out. This thesis provides a comprehensive understanding of the strain-hardening behaviour and engineering properties of FA-GGBS based SHGC reinforced with hybrid PVA-RTS fibre and cured at ambient temperature for civil infrastructure applications.

Impact Statement

In recent years, civil infrastructure has been increasingly challenged by devastating earthquakes, unprecedented winds and floods resulting from climate change, and other issues. Strain-hardening geopolymer composites (SHGC) appears as a promising material for civil infrastructure applications because of its low carbon emission, reduced energy consumption, and outstanding mechanical properties, such as high ductility and excellent crack control. However, strain-hardening behaviour and engineering properties of SHGC have not been systematically investigated, which hindered the wide application of SHGC in civil infrastructures. Hence, this thesis develops the SHGC based on micromechanical and microstructural theories, and investigates engineering properties of SHGC, which brings a series of impacts both inside and outside academia.

On the one hand, this thesis contributes to the research domain from three main aspects. Firstly, this thesis establishes an innovative material system of SHGC, which is produced by the blend of fly ash (FA) and ground granulated blast-furnace slag (GGBS) as the precursor, cured at ambient temperature, as well as reinforced with hybrid polyvinyl alcohol (PVA) and recycled tyre steel (RTS) fibres. Secondly, this thesis verifies the pseudo strain-hardening (PSH) criteria of SHGC by estimating its micromechanical parameters, as well as provides a systematic understanding of the effects of sand and fibres on engineering properties of SHGC. Thirdly, this thesis explores the potential application of RTS fibre and its effectiveness in enhancing the engineering properties of SHGC. Based on the studies, three papers have been published in journals in the field of construction and building materials.

On the other hand, the output of this thesis is promising to benefit society from three levels. From the infrastructure level, SHGC outperforms other building materials because of its strain-hardening behaviour, high ductility and energy absorption capacity, and excellent crack control, which enables SHGC to be used in important civil infrastructures for preventing damages caused by earthquakes and winds, water permeability, corrosion, and other issues. From the construction industry level, the application of FA and GGBS instead of ordinary cement could greatly reduce the carbon emission and energy

consumption of the material, which contributes to mitigating the climate change and achieving the goal of carbon neutrality. From the society level, the source materials of SHGC mainly come from industrial by-products (FA and GGBS) and recycled wastes (RTS fibre), which echoes the circular economy and further contributes to the sustainable development of the society.

Table of Contents

List of Tables

List of Figures

13

List of Abbreviations

FA   Fly ash

FRCC   Fibre reinforced cementitious composites

GGBS   Ground granulated blast-furnace slag

OPC   Ordinary Portland cement

PVA   Polyvinyl alcohol

RTS   Recycled tyre steel

SH   Sodium hydroxide

SHCC   Strain-hardening cementitious composites

SHGC   Strain-hardening geopolymer composites

SP   Superplasticiser

SS   Sodium silicate

DIF   Dynamic increase factor

PSH   Pseudo strain-hardening

Chapter 1 General Introduction

1.1 Research background

Ordinary Portland cement (OPC) concrete is the most widely used construction material in the world because of its affordability, availability and exceptional strength. However, concrete is brittle and prone to cracking. In order to limit the growth of cracks and the brittleness of the plain concrete, short fibres are incorporated into cementitious materials to produce fibre reinforced cementitious composites (FRCC). Strain-hardening cementitious composites (SHCC) is a new class of FRCC that demonstrates "bendable ability", superior ductility and tensile strain capacity with a typical range of 2%-5% against 0.01% of conventional concrete (Victor C. Li and Cynthia, Li, 2003). SHGC has extraordinary strain-hardening behaviour and steady-state microcrack propagation (typically with a mean crack width smaller than 100 μm), and therefore could be used in a wide range of engineering applications such as seismic resilient buildings, retrofitting projects aiming at longer service life, and hydraulic structures requiring tight crack width (Rokugo et al., 2009b, Paulay and Binney, Rokugo, 2013).

Despite the superior performance of SHCC materials, typical SHCC mixes are costly and contain 2-3 times higher ordinary Portland cement (OPC) content than conventional concrete. Given that the construction industry annually uses 4.3 billion tonnes of OPC as binder for concrete and the production of 1 tonne OPC generates 0.7-1.1 tonne of carbon emission, which is around 8% of global carbon emissions (Bosoaga et al., 2009, Lehne and Preston, 2018), the higher cement content in SHCC would make the current situation more severe. In recent years, an increasing number of attempts have been made to develop ultra-ductile cementitious composites with alternative binders to reduce carbon emissions. Geopolymers sourced from industrial or agricultural by-products such as fly ash (FA), ground granulated blast-furnace slag (GGBS), silica fume, and rice husk ash are increasingly considered as a promising alternative to OPC because of the low energy consumption, reduced greenhouse emissions, and superior mechanical properties, thermal performance and durability (Provis and Van Deventer, 2009). The substitution of OPC by geopolymers can lead to a substantial reduction of carbon emission by 55%-76% and

energy consumption by around 36% (Yang et al., 2013, Nematollahi et al., 2017d).

Strain-hardening geopolymer composites (SHGC), also known as engineered geopolymer composites (EGC), have been developed by combining the advantages of SHCC and geopolymers. Recent studies showed that low-calcium FA had low reactivity at ambient temperature, which resulted in long setting time and low early strength of FA-based SHGC (Ohno and Li, 2014, Shaikh, 2013, Kumar et al., 2010). As such, heat curing is required, which makes it unsuitable for in-situ construction (Somna et al., 2011, Fang et al., 2018b). GGBS-based SHGC has low workability, short setting time and large shrinkage, which may limit the large-scale and in-situ engineering applications of them. To address these limitations, there has been an increasing interest in the development of blended FA-GGBS based SHGC, in which GGBS plays a significant role in improving the mechanical properties of SHGC, while the workability of SHGC increases with increasing FA content (Nematollahi et al., 2017f, Nematollahi et al., 2017e). It was found that increasing the GGBS content in FA-based SHGC resulted in the improved compressive strength, tensile strength, and bond strength, but the reduced ductility of SHGC (Ling et al., 2019), the incorporation of sand in FA-GGBS based SHGC increased the compressive strength and fracture toughness of geopolymer matrix but impaired the strain-hardening and multiple micro-cracking behaviours of SHGC (Alrefaei and Dai, 2018). Although the mechanical properties of FA-GGBS based SHGC cured at ambient temperature have been increasingly studied in recent years, the effect of fine silica sand on the engineering properties including fresh and hardened properties of FA-GGBS based SHGC has not been systematically explored yet, and the deflection hardening and multiple cracking behaviours of SHGC have not been fully investigated.

Different fibres with various elastic modulus such as steel, polyvinyl alcohol (PVA), polyethylene (PE), polypropylene (PP) and polyethylene terephthalate (PET) fibres have been employed to produce SHGC, which have significant influences on the mechanical properties of SHGC (Singh et al., 2019, Maalej et al., 2012, Soe et al., 2013). Previous studies showed that the incorporation of steel fibre or chopped steel wool fibre in SHGC resulted in higher compressive strength (38.9-56.2 MPa) and tensile strength (2.1-5.35 MPa) but lower tensile strain capacity (0.12%-0.42%); in addition, SHGC containing PVA fibre or PP fibre presented lower compressive strength (19.2-41 MPa) and tensile strength (0.85-

3.35 MPa) but higher tensile strain capacity (0.52%-4%) (Farooq et al., 2019). Therefore, in order to achieve high strength and tensile strain capacity, SHCC and SHGC reinforced with hybrid fibres including both high and low modulus fibres have been developed to form synergistic effects. The hybridisation of steel and PVA fibres in SHCC indicated that the strengths and energy absorption of SHCC were enhanced, whilst workability was reduced by the incorporation of steel fibre (Mohammed et al., 2018, Wang et al., 2019, Li et al., 2019, Yu et al., 2018). The inclusion of hybrid metallic and polymeric fibres in SHGC is also a possible way to increase the cost-effectiveness of the resultant composites, as well as their engineering properties.

About 5.2 billion tyres are estimated to be at the verge of disposal worldwide, which could result in adverse environmental impact and health hazards (Liew and Akbar, 2020). In recent years, waste tyres have been increasingly utilised by energy recovery, recycling, and other approaches instead of ending up in landfills. The recycling of rubber particles, steel, and polymer fibres provides a promising way to mitigate the environmental and health problems, and produces economic benefits (Ramarad et al., 2015). For example, recycling waste tyres can help reduce carbon emissions by 1.52 tonnes annually (Gigli et al., 2019). Steel wire extracted from waste tyres, known as recycled tyre steel (RTS) fibre, was reported as a potential substitute for manufactured steel fibre due to its better ductility and higher tensile strength, as the raw steel used in tyre production can have better quality than commercially available manufactured steel fibres (Domski et al., 2017). Recently, an increasing number of studies have been focused on the effect of RTS fibre on the engineering properties of fibre reinforced concrete (FRC). It was reported that the addition of RTS fibre within the critical fibre content (approximately 0.5%) can result in the slight enhancement of compressive strength of FRC, whereas excessive fibre content can lead to a reduction in compressive strength (Aghaee et al., 2015, Martinelli et al., 2015, Leone et al., 2018, Mohammed et al., 2018). Under flexural loading, the composites containing RTS fibres show desired engineering properties, post-crack resistance and energy absorption ability due to sufficient crack restrain capacity, which is comparable with manufactured steel fibres reinforced material (Liew and Akbar, 2020, Zamanzadeh et al., 2015). An experimental study on engineering properties of hybrid RTS-PP fibre reinforced mortar found that the inclusion of RTS fibre was effective in restraining the drying

shrinkage and improving the flexural strength. The optimal mixture was found to be that with hybrid 0.5% RTS and 0.5% PP fibres, which resulted in the significantly enhanced post-cracking behaviour in terms of toughness indices and residual strength factors (Zhong and Zhang, 2020). The effect of hybrid RTS and PVA fibres on engineering properties of the composites was studied, and it was observed that the combination of 0.5% PVA and 1.5% RTS fibres can lead to the optimum strengths (e.g. flexural strength and direct tensile strength). Moreover, an optimal ratio of 0.5% tyre wire and 1.5% PVA fibre was reported in SHCC considering the flexural strength, tensile strength, elastic modulus and shrinkage (Mohammed et al., 2018). To date, the feasibility of hybridising RTS and PVA fibre to enhance the engineering properties of FA-GGBS based SHGC has not been studied.

In summary, the following aspects regarding the engineering properties of FA-GGBS based SHGC are still lacking:

- Investigation of the effect of fine silica sand and optimisation of sand content in SHGC to achieve desired engineering properties of SHGC.
- Study of micromechanical parameters of SHGC and verification of pseudo strain-hardening (PSH) criteria.
- Systematic study of static and dynamic properties of SHGC.
- Development of hybrid fibre reinforced SHGC with desired engineering properties.

Based on a critical review of the engineering properties of SHGC and micromechanics-based mix design, the aim, objectives, and strategy of this research are described below.

1.2 Aim, objectives and scope

The overall aim of this thesis is to develop a hybrid PVA-RTS fibre reinforced sustainable SHGC with desired engineering properties. Effects of sand and fibres on engineering properties of SHGC are systematically investigated, meanwhile, micromechanical parameters are measured to verify the micromechanics and fracture mechanics theory of SHGC. This study will provide a comprehensive understanding of mix design and engineering properties of FA-GGBS based SHGC reinforced with hybrid PVA-RTS fibres and cured at ambient temperature for civil infrastructure applications. The main

objectives of this study are as follows:

- To explore the effect of fine silica sand (ranging from 0% to 40% by weight of the geopolymer matrix) and obtain the optimal sand content for FA-GGBS based SHGC with acceptable engineering properties including flowability, setting time, drying shrinkage, compressive strength, and strain-hardening behaviour.

- To characterise the micromechanical parameters of FA-GGBS based SHGC containing 2% PVA fibre, which has been widely used to reinforce SHGC, and verify the pseudo strain-hardening (PSH) criteria based on strength and energy criteria.

- To study the engineering properties of SHGC containing various volume fractions of PVA fibre (0%, 1%, 1.5%, and 2%), and explore the toughening mechanisms of PVA fibre reinforced SHGC under static and dynamic loadings, which is entirely novel.

- To investigate the effect of incorporating RTS fibre (0.25% and 0.5% by volume) on static and dynamic mechanical properties of SHGC in comparison with SHGC reinforced with mono PVA fibre, which has not been addressed elsewhere.

1.3 Research strategy

In order to accomplish these objectives, this thesis develops and applies the following strategies:

- To begin with, the effect of fine silica sand content on the engineering properties of PVA fibre reinforced blended FA-GGBS based SHGC cured at ambient temperature is investigated by a series of tests including workability, setting time, drying shrinkage, compressive strength, flexural strength and flexural toughness of SHGC with various sand content ranging from 0% to 40% by weight of the geopolymer binder. The influence of fine silica sand on the deflection-hardening behaviour of SHGC including stress-deflection response, failure mode and cracking, flexural toughness and toughening mechanism is then estimated and discussed in detail. The cracking process and fibre-matrix interactions are monitored using a digital microscope, which are used to gain insights into the toughening mechanisms of SHGC specimens. Afterwards, the optimal sand content for SHGC is proposed.

- Moreover, the optimal sand content is used to develop FA-GGBS based SHGC. Based on previous studies, SHGC containing 2% PVA fibre is prepared and tested to obtain the micromechanical parameters relating to matrix, fibre, and fibre-matrix

interface properties, which are applied to verify the micromechanics criteria, including both strength and energy-based criteria.

- Based on the developed and micromechanically verified SHGC, the effect of PVA fibre on engineering properties of FA-GGBS based SHGC containing various fibre volume fractions (0%, 1%, 1.5%, and 2%) is studied through a series of tests including flow table, drying shrinkage, static compression, static uniaxial tension, static splitting tension, and split Hopkinson pressure bar (SHPB) tests. Based on the obtained experimental results, the optimal mix proportion for SHGC is proposed.

- Furthermore, the synergetic effects of PVA and RTS fibres on the engineering properties of SHGC is investigated. Three series of fibre incorporation are considered for the ease of comparison (i.e. mono, hybrid addition and hybrid replacement): (1) increasing PVA fibre volume fractions from 1.5% to 2%; (2) addition of 0.5% RTS fibre in SHGC with 1.5% PVA fibre; (3) RTS fibre partial replacement for PVA fibre in SHGC containing 2% PVA fibre at replacement levels of 0%, 0.25%, and 0.5%. A series of tests are conducted to study the flowability, drying shrinkage, static and dynamic mechanical properties of SHGC.

1.4 Thesis outline

This thesis consists of seven chapters as follows:

Chapter 1 is the general introduction, which presents the research background, research aim, objectives, and scope, research strategy, and outline of this thesis.

Chapter 2 provides a state-of-the-art literature review of SHGC. A brief introduction of SHGC is given, including the constituents, characteristics, and micromechanics criteria. Then, the engineering properties of SHGC are reviewed based on fresh properties and shrinkage, static mechanical properties, dynamic mechanical properties, and durability of SHGC. Different influencing factors are considered, such as the geopolymer binder and fibres. Moreover, sustainability assessment and potential applications of SHGC are briefly surveyed. The literature review gives and discusses the main challenges and limitations in this field.

Chapter 3 experimentally explores the effect of fine silica sand and determine the optimal sand content for SHGC with acceptable engineering properties based on flowability, setting time, drying shrinkage, compressive behaviour, and deflection

hardening behaviour.

Chapter 4 conducts the micromechanics-based design of SHGC and verifies the strength and energy-based criteria. The optimal sand content is used to develop SHGC and evaluate micromechanical parameters through the uniaxial tension test, single-crack tension test, and three-point bending test.

Chapter 5 provides a comprehensive understanding of the effect of PVA fibre on engineering properties of FA-GGBS based SHGC cured at ambient temperature, with a special focus on static tensile behaviour and dynamic compressive behaviour. A series of tests were conducted on SHGC containing various fibre volume fractions (0%, 1%, 1.5%, and 2%) to measure their engineering properties including flowability, drying shrinkage, tensile properties, strain-hardening behaviour, and static and dynamic compressive behaviour. The effects of PVA fibre content on these engineering properties of SHGC were estimated, based on which the toughening mechanism was explored, and the optimal mix proportion for SHGC was obtained.

Chapter 6 investigates the effect of hybrid PVA and RTS fibres on engineering properties of FA-GGBS based SHGC cured at ambient temperature, with a special focus on uniaxial tensile behaviour and dynamic mechanical properties. A series of tests were conducted on SHGC containing various volume fractions of hybrid PVA and RTS fibres (1.5% PVA, 2% PVA, 1.75% PVA + 0.25% RTS, and 1.5% PVA + 0.5% RTS) to study the engineering properties of SHGC, including flowability, drying shrinkage, tensile strain-hardening behaviour, and static and dynamic compressive behaviour. Based on the experimental results obtained, the toughening mechanisms of PVA and RTS fibres in FA-GGBS based geopolymer concrete were explored.

Chapter 7 draws the main conclusions of this thesis and critically summarises the limitations of this thesis and provides some recommendations for the future research.

Chapter 2 Literature Review

This chapter provides a state-of-the-art literature review on the engineering properties of SHGC. To begin with, a brief introduction of SHGC is presented, which describes the constituents, characteristics, and micromechanics criteria of SHGC. Moreover, fresh and mechanical properties of SHGC are reviewed. Afterwards, the sustainability assessment of SHGC is discussed. The remaining challenges to address are identified.

2.1 Introduction of strain-hardening geopolymer composites (SHGC)

SHGC is an alkali-activated material reinforced with randomly dispersed short fibres, exhibiting high ductility and strain-hardening behaviour with excellent crack controls, which is governed by the micromechanics criteria. Herein, SHGC is briefly introduced in terms of its constituents, characteristics, and micromechanics criteria.

2.1.1   Constituents

SHGC is produced by adding sand and short randomly dispersed fibre into geopolymer binder, which is obtained by alkaline activation of aluminosilicate precursors. Major constituents of SHGC are briefly reviewed below.

2.1.1.1 Precursor

Theoretically, any material rich in silicon and aluminium can be the possible source material as the precursor, such as FA, GGBS, metakaolin, bottom ash, silica fume, and rice husk ash, where FA and GGBS are favoured in particular.

FA, the most favoured source material, is a by-product of coal-fired electricity plants and can be classified as Class F and Class C types based on the calcium oxide contents per ASTM C618 (ASTM, 2019a). Class F FA has a low calcium content, i.e., less than 10% CaO, with a total content of SiO_2, Al_2O_3 and Fe_2O_3 of up to 70% by weight. Class C FA has a high calcium content, i.e., more than 20 % of CaO, and the total content of SiO_2, Al_2O_3, Fe_2O_3 is between 50% and 70%. GGBS, another widely used raw material, is the by-product of the iron production industry. Unlike FA, GGBS has a plentiful proportion of CaO, i.e., 30%-50% of total weight, while the components of SiO_2, Al_2O_3, and MgO take up 37%-80% altogether.

Geopolymers produced by various source materials and mix proportions have

23

different properties due to the chemical compositions of the raw materials. It was reported that FA-based geopolymer concrete has good mechanical properties and durability but low early strength (Fernandez-Jimenez et al., 2007, de Vargas et al., 2011), whereas GGBS-based geopolymer concrete has high early strength and better acid-resistance but less flowability (Singh et al., 2015). Thus, the blended FA-GGBS based geopolymer concrete cured at ambient temperature has been increasingly studied because of the good flowability and mechanical properties. Previous studies indicated that the optimum results can be achieved when 20%-30% GGBS was added into FA-based system (Fang et al., 2018b, Nath et al., 2016).

2.1.1.2 Alkaline activator

Alkaline activators are usually applied to activate the geopolymerisation, due to the limited reactivity of precursors. In general, sodium hydroxide (SH), sodium silicate (SS), potassium hydroxide (KOH), potassium silicates (K_2SiO_3) and calcium hydroxide ($Ca(OH)_2$) all can be used as the activator, while a combination of SH and SS is favoured by many researchers. Engineering properties of geopolymer concrete can be affected by the activator/binder ratio, molarity of SH, and SS/SH ratio (Fang et al., 2018b). It was reported that either higher SS/SH ratio or higher molarity of SH (molarity of SH ranging from 8M to 16M) in FA-based geopolymer concrete can lead to improved compressive strength (Hardjito et al., 2004). For FA-GGBS based geopolymer concrete, the optimal mixture was suggested to be AL/B ratio of 0.4, SH concentration of 10M, and SS/SH ratio in the range of 1.5-2.5 considering the performance criteria of flowability, setting time, and compressive strength (Fang et al., 2018b).

2.1.1.3 Sand

Aggregate occupies a significant volume fraction (usually 50%-80%) in concrete and has an important effect on material properties. The addition of aggregates in cement-based materials can lower the cost, keep the dimensional stability, and increase the fracture toughness of cement-based materials. However, in fibre reinforced composites, the presence of aggregates, especially large aggregate particles, can lead to clumping and interaction of fibres, which can negatively affect the properties of the resultant composites. For SHCC and SHGC, the micromechanics criteria require limited matrix fracture toughness to avoid the failure of fibre bridging effect and achieve strain-hardening, where

steady-state crack initiates before the tensile load reaches the maximum fibre bridging stress. Hence, the addition of aggregate should consider the type, size, and content to achieve the expected properties. It was indicated that fine silica sand with a very tiny particle size (usually 100-212 μm) should be used for SHCC and SHGC to obtain the desired strain-hardening behaviour and other engineering properties (Lee et al., 2012, Ohno and Li, 2014, Nematollahi et al., 2016b)

2.1.1.4 Superplasticiser (SP)

Superplasticiser (SP) is the high range water reducing admixture. SPs are added to concrete either to reduce the water content while keeping constant workability, or to increase the flowability while keeping a constant water content. The commonly used SPs include naphthalene, melamine-based, lignosulphonates, and modified polycarboxylates (Nematollahi and Sanjayan, 2014). The incorporation of naphthalene-based SP can improve the workability of fresh geopolymer, but adding over 2% SP can result in a significant reduction of the compressive strength (Hardjito et al., 2004). Modified polycarboxylates-based SP was found to be effective in multi-compound activators, but the addition of 3.3% SP can cause a significant reduction (54%) in compressive strength of potassium hydroxide (KOH) and SS activated FA-based geopolymer (Puertas et al., 2003b).

2.1.1.5 Fibres

Various forms of fibres, such as threads and filaments, have been used to improve the flexural behaviour and energy absorption capacity of geopolymer composites (Ranjbar and Zhang, 2020). In SHGC, fibres compatible with geopolymers should be used with an optimum aspect ratio and volume fraction to secure the strain-hardening behaviour. Table 2-1 shows the typical physical and mechanical properties of fibres applied in SHGC.

Industry manufactured steel fibres were widely used to produce fibre reinforced composites because of their high strength and elastic modulus (Bentur and Mindess, 1990). The tensile strength of steel fibre ranges from 345 MPa to 2100 MPa, and the elastic modulus is around 200 GPa. The main factors affecting the properties of steel fibre reinforced concrete are fibre volume fraction and aspect ratio (length/diameter) (Yazıcı et al., 2007). In recent years, steel fibres recycled from waste tyres have been increasingly used in producing fibre reinforced composite to mitigate the environmental and health problems, and bring economic benefits (Ramarad et al., 2015, Wang et al., 2020a).

Table 2-1 Physical and mechanical properties of fibres for geopolymers

Fibre type	Diameter (µm)	Length (mm)	Density (g/cm^3)	Tensile strength (MPa)	Elastic modulus (GPa)
Steel (Farooq et al., 2019, Al-Majidi et al., 2017)	160-1000	6-50	7.85	1150-2750	200
PVA (Farooq et al., 2019, Al-Majidi et al., 2017)	15-40	8-12	1.30	1100-1885	29.5-40
PP (Farooq et al., 2019, Shaikh, 2020)	22-50	12-19	0.91	600-700	3-3.5
PE (Shaikh et al., 2018)	12	12	0.97	3500	123
PET (Shaikh, 2020)	38	12	1.37	1160	11.5

Note: PVA – polyvinyl alcohol; PP – polypropylene, PE – polyethylene, PET - polyethylene terephthalate.

PVA fibre is a hydrophilic material that contains hydroxyl groups (OH) and has a good surface bond strength with the matrix (Xu et al., 2010). PVA fibre is featured by high aspect ratio and ultimate tensile strength, relatively high modulus of elasticity, good chemical compatibility with OPC, good affinity with water and no health risks. PVA fibre generally has positive effects on the bending strength and other mechanical properties of the composites, since it is stiffer than the concrete matrix and provides good interfacial bonds with the matrix (Wang and Li, 2011). The high tensile strength of PVA fibre contributes to sustaining the first crack stress and resisting pull out force due to the strong bond between the fibre and the cementitious matrix (Victor C. Li and Cynthia, 2001). In contrast, the low lateral resistance of the fibres may also lead to premature fibre rupture before pulling out from the matrix. PVA fibre elongates and transfers the load to different parts of the matrix, and as a result, the load applied is distributed more evenly between the loading surfaces (Toutanji et al., 2010). Most studies applied fibre content of no more than 2%, usually with oil coating to increase the ductility and impact toughness of the composite (Yunsheng et al., 2008).

PP fibre is derived from the monomeric C_3H_6 (Mwangi, 2001). The main advantages of PP fibre include high alkali resistance, relatively high melting point (165 °C), and low price. PP fibre has disadvantages such as poor fire resistance, sensitive to sunlight and oxygen, low elastic modulus (1-8 GPa) and poor bond with the matrix, while the mechanical properties, in particular elastic modulus and bond, can readily be enhanced

(Bentur and Mindess, 1990). The addition of PP fibre has marginal effect on compressive strength of FRGC but could increase the fracture toughness and other mechanical performance in low fibre content (less than 1.0%) (Yang et al., 2014, Puertas et al., 2003a).

PE fibre has a tensile strength in the range of 80-590 MPa, and an elastic modulus of about 5 GPa, but others have been reported to have elastic moduli in the range of 15.4-31.5 GPa, similar to those of the concrete matrix (Bentur and Mindess, 1990). PET fibre is sourced from the recycled plastics, such as containers for liquids and foods. PET fibre is produced by shredding PET bottles and containers into short fibres with different lengths and diameters. PET fibre reinforced SHGC exhibits strain-hardening behaviour (Shaikh, 2020).

2.1.2   Characteristics

SHGC differs from FRGC and geopolymer concrete in terms of tensile stress-strain behaviour after first crack under uniaxial tension, as illustrated in Figure 2-1. In general, concrete fails immediately after the first crack is initiated and shows a brittle failure. FRGC exhibits a tension-softening behaviour, as first crack appears and propagates with fibre pulling out or breaking, leading to deformation localisation of the composite and drops of load carrying capacity. On the contrary, SHGC displays multiple microcracks and strain-hardening behaviour, as microcracks formed over the composites and deformation distributed along the composites. During this process, the tensile stress and strain continue to rise. Typically, the average crack width of SHGC is less than 100 μm at the failure point, resulting in the superior ultimate tensile strain of SHGC.

It is known that brittle geopolymer concrete can be reinforced with short fibres, which limit the growth of cracks, to produce FRGC. However, the transition from tension-softening to strain-hardening behaviour is governed by matrix properties, fibre properties, and fibre-matrix interfacial properties of the composite. Hence, according to micromechanics-based theory, strain-hardening behaviour of SHGC can be tailored by modifying matrix properties, fibre properties, and fibre-matrix interfacial properties of the material (Li, 2019).
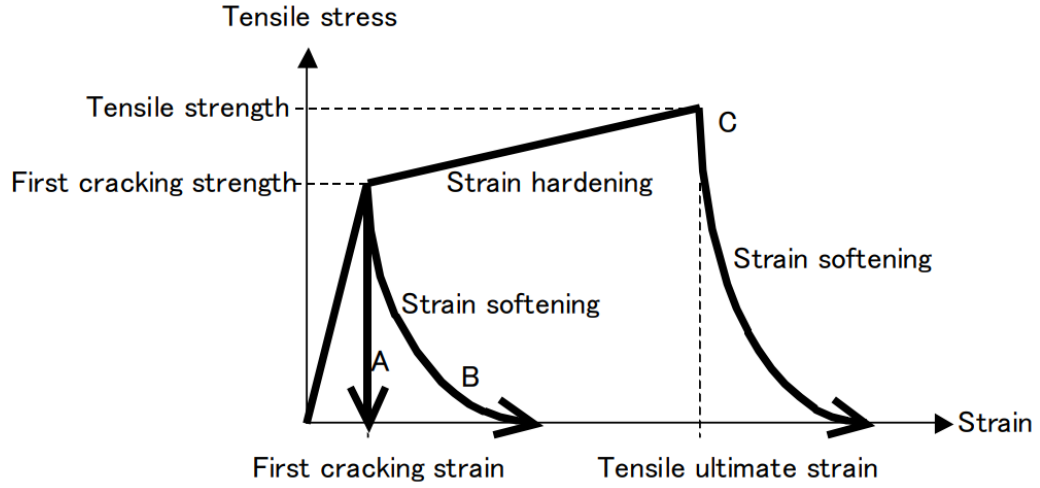
Figure 2-1 Stress-strain curves of different materials (A: brittle, B: quasi brittle, and C: ductile behaviour) under uniaxial tension (Matsumoto and Mihashi, 2002).

2.1.3 Micromechanics criteria

Strain-hardening behaviour along with the formation of multiple microcracks is achieved when micromechanics criteria is fulfilled, including strength and energy-based criteria (Kanda and Li, 2006a). Regarding the strength-based criterion, it governs the initiation of crack at the defect sites within material by the following equation:

$$\sigma_{fc} \leq \sigma_0 \tag{2-1}$$

where σ_{fc} represents the first-crack strength of the matrix, and σ_0 denotes the maximum fibre bridging strength.

The energy-based criterion controls the crack propagation mode by:

$$J_{tip} \leq \sigma_o \delta_o - \int_0^{\delta_o} \sigma(\delta)d\delta = J_b' \tag{2-2}$$

$$J_{tip} = K_m^2 / E_m \tag{2-3}$$

Where J_{tip} represents crack tip toughness, J_b' stands for complementary energy, σ_0 is the maximum bridging stress at the flat crack opening δ_0, K_m is the matrix toughness, and E_m is the elastic modulus of the matrix.

2.2 Fresh and hardened properties of SHGC

This section reviews the fresh and hardened properties of SHGC, including fresh properties, drying shrinkage, static mechanical properties, and dynamic properties, focusing on the effects of geopolymer matrix and different fibres (type and content), which is summarised in Table 2-2.

Table 2-2 Literature review of strain-hardening geopolymer composites (SHGC).

Refs.	Binder	Alkaline activator	Aggregate	Fibre	Curing condition	Major findings
Nematollahi et al. (Nematollahi et al., 2017a)	FA	SS & SH	N/A	PVA	Oven, 60 °C, 24 h	• In FA-SHGCs, critical fibre content required to display saturated pseudo-strain-hardening behaviour is primarily governed by energy-based criterion. • Critical fibre content could be reduced by the fibre surface oil coating, the increase of fibre length, and the reduction of matrix fracture toughness.
Nematollahi et al. (Nematollahi et al., 2014)	FA	Na-, K-, Ca-based	N/A	PVA	Oven, 60 °C, 24 h	• All SHGC exhibited deflection hardening behaviour accompanied by multiple micro-cracks in bending, regardless of activator type. • SHGC-Na-1 displayed the superior deflection capacity, matrix fracture properties, compressive and flexural strengths, ductility and toughness.
Nematollahi et al. (Nematollahi et al., 2015b)	FA	Na-, K-, Ca-based	N/A	PVA	Oven, 60 °C, 24 h	• Na-based activator combination (8 M NaOH solution, SiO_2/Na_2O ratio of 2.0) was superior in terms of higher compressive strength, matrix fracture properties and uniaxial tensile behaviour as well as lower cost.
Nematollahi et al. (Nematollahi et al., 2017b)	FA	Na-, K-, Ca-based	N/A	PVA	Oven, 60 °C, 24 h	• Regardless of activator type and w/b ratio, the chemical bond and slip hardening coefficient of oil-coated PVA fibre were lower than virgin fibre. • The frictional bond between fibre and matrix depended on activator type: in Na-based activator, oil-coated PVA fibre outperforms virgin fibre (reverse in K-based activator).

						• Reducing w/b ratio increased chemical bond but decreased the frictional bond of PVA fibre with Na-based matrix.
Ahmed and Ronnie ([Ahmed and Ronnie, 2017])	FA	SS&SH	N/A	PE	Oven, 85 °C, 24 h	• Optimum fibre volume content: 1% (among 0.5%, 1%, 1.5%, and 2%) for strain and deflection hardening behaviour in uniaxial tension and three-point bending tests. • Compressive strength of the composites decreased with the increase of volume content of PE fibre. • Alkaline geopolymer matrix had no significant damage to PE fibre.
Zahid et al. ([Zahid et al., 2018])	FA	SS&SH	silica sand	PVA	Oven, 45-90 °C, 24 h	• Simulation results agreed well with experimental data (less than 5% difference).
Shaikh ([Shaikh, 2013])	FA	SS&SH	Fine & coarse aggregate	Steel; PVA	Steam, 60 °C, 24 h	• Derived deflection hardening behaviour with multiple cracks • Cement and geopolymer-based composites showed comparable deflection hardening behaviour, ultimate flexural strength, and deflection at peak load. • Geopolymer matrix did not degrade PVA and steel fibres.
Farooq et al. ([Farooq et al., 2019])	FA	SS&SH	Natural sand	PVA; high strength steel; chopped steel wool; PP	Oven, 80 °C, 4 h	• Workability was affected by fibre geometry, most by chopped steel wool and least by high strength steel; • High strength steel and chopped steel wool notably improved the compressive strength; • Pseudo strain-hardening behaviour was observed in all specimens reinforced with PVA and high strength steel fibre;

Reference	Binder	Activator	Aggregate	Fibre	Curing	Key findings
						• Specimens reinforced with PP fibres showed low post-cracking bridging tensile strength but high tensile strain capacity (over 4%).
Nematollahi et al. ([Nematollahi et al., 2017c](#))	FA	SS&SH	silica sand; Expanded glass; ceramic microsphere; expanded perlite.	PVA	Oven, 60 °C, 24 h	• All SHGC developed by lightweight aggregates meet the criteria (i.e. density and compressive strength) for structural lightweight concrete. • Compressive and tensile strength: SHGC (lightweight aggregates) < SHGC (normal weight micro-silica sand). • Tensile ductility: SHGC (lightweight aggregates) ~ SHGC (normal weight micro-silica sand). • Thermal conductivity: SHGC (lightweight aggregates) < SHGC (normal weight micro-silica sand).
Nematollahi et al. ([Nematollahi et al., 2016a](#))	FA	SS&SH	Fine & coarse aggregate	PVA	Oven, 60 °C, 24 h	• Lowering water to geopolymer solids ratio and the addition of sand enhanced the elastic modulus of the geopolymer matrix and composite in all cases. • Excessive use of fine sand and the use of coarse sand result in the increase of the matrix fracture toughness and the first crack strength of the composite, which adversely affect the strain-hardening behaviour of SHGC. • Desirable tensile ductility of SHGC could be only maintained by geopolymer matrices with suitable fracture toughness as defined by the micromechanics design model.
Ohno and Li ([Ohno and Li, 2014](#))	FA	SS&SH	Fine silica sand	PVA	Ambient curing;	• SHGC exhibited tensile strain-hardening behaviour with very high ductility of over 4%.

Reference	Binder	Activator	Aggregate	Fiber	Curing	Key findings
					Oven, 60 °C, 4-8 h	• Temperature curing methods could improve compressive strength, tensile strength and tensile ductility. • Maximum and average crack widths were 117 µm and 45 µm (even at strain level of 4.5%).
Ohno and Li (Ohno and Li, 2018)	FA	SS&SH	Fine silica sand	PVA	Oven, 60 °C, 4-8 h	• The systematic design process could optimise SHGC to achieve improved compressive strength (43.1%), high tensile ductility (4.7%), less embodied energy (11% less than SHCC), and CO_2 equivalent emissions (55% less than SHCC).
Guo et al. (Guo et al., 2020)	FA			PVA		• All specimens showed increase of UPV, while A7d had the highest UPV after self-healing for 28 d; • There was a strong correlation between the tensile strength and UPV with R2 close to 1, which indicates that UPV could be a prediction to tensile strength according to the fitting equations.
Kan et al. (Kan et al., 2020b)	FA, Zeolite	SS&SH	Micro silica sand	PVA	Oven, 80 °C, 2 h	• Specimens showed high tensile strain capacities with the maximum strain capacity up to 8.62%; • The optimal zeolite replacement ratio was 3% in respect of the tensile properties; • The main reaction products were the amorphous aluminosilicate phases, i.e. gel-like materials resulted from geopolymerisation reactions.
Choi et al. (Choi et al., 2016)	GGBS	$Ca(OH)_2$ & Na_2SO_4 (powder)	N/A	PE	Cured at ambient temperature in water	• The average tensile strength to compressive strength ratio of the composites was 19.8%, nearly double that of normal concrete. • Average crack width was 101 µm at failure point. • The composite could reach tensile strain capacity and tensile strength of up to 7.5% and 13.06 MPa, respectively.

Lee et al. (Lee et al., 2012)	GGBS	Ca(OH)$_2$ & Na$_2$SO$_4$; Ca(OH)$_2$ & SS	N/A	PVA	Cured at ambient temperature in water	• Achieved high ultimate tensile strain of 4.7%, compared with 0.02% for the mortar matrix alone.
Nguyen et al. (Nguyen et al., 2018)	Ladle slag	SS& KOH	Fine sand	PP	Bagged-curing at room temperature	• The composite could gain very high ductility with an appropriate fibrous reinforcement. • PP fibre reinforced composite has higher flexural strength, fracture energy and fracture toughness compared to unreinforced material. • Samples showed pseudo strain-hardening behaviour with multi-cracking under uniaxial tension test. • High mechanical performance of the PP-reinforced composite is obtained by local fibre bridging effect.
Nguyen et al. (Nguyen et al., 2019)	Ladle slag; gypsum; Fluidised bed combustion FA	N/A	Fine sand	PP; PVA	23 °C, 95% RH	• All composites showed strain-hardening behaviour with multi-cracks under tensile and flexural loading. • The compressive strength of the composites is higher than the plain material. • PP micro-fibre reinforced composites is the best mixture to balance the mechanical and economic aspects, based on a multi-criterion ranking method.
Alshaaer et al. (Alshaaer et al., 2017)	MK	SS&SH	N/A	Luffa cylindrical fibre	Ventilated oven, 40 °C, 24 h	• The hydrophobicity of rough LCF contributes to the strengthening of bonding between fibre and geopolymer matrix.

						• The crack healing and improved tensile strength and toughness of SHGC is due to the fibre-like and cubic crystals formed by the incorporation of LCF. • The addition of LCF increased the compressive and flexural strength of SHGC. • LCF reinforced SHGC exhibited strain-hardening behaviour with elastic modulus of 72 MPa.
Trindade et al. (Trindade et al., 2019)	MK	SS&SH	River sand	Jute; Sisal; Curauá; PVA	Ambient temperature	• All SHGC exhibited strain-hardening behaviour with multiple cracking formations.
Trindade et al. (Constâncio Trindade et al., 2020)	MK	Na-, K-based watergla ss, NaOH, KOH	Quartz sand	PVA	Ambient temperature	• With fine-grained sand, SHGC-Na showed strain-hardening behaviour and multiple cracking, with a strain capacity of approximately 4.5%, whereas SHGC-K showed strain softening behaviour; • When compared to typical SHCC responses, SHGC-Na showed a mechanically improved multiple cracking behaviour.
Trindade et al. (Trindade et al., 2020)	MK	SS&SH	Quartz sand	PVA; ultrahigh molecular-weight PE	Ambient temperature	• SHGC reinforced with UHMWPE fibres exhibited superior mechanical performance compared to the composite with PVA fibres both under quasi-static tensile loading and impact tensile loading; • Compared with normal-strength SHCC, SHGC showed higher dynamic tensile strength and energy dissipation capacity.

Salami et al. (Salami et al., 2017)	POFA	SS&SH	Dune sand	PVA	65 °C, 24 h	• POFA-SHGC had better durability performance when exposed to 5% $MgSO_4$ than 5% Na_2SO_4.
Salami et al. (Salami et al., 2016)	POFA	SS&SH	Dune sand	PVA	60 °C, 24 h	• Compressive strength: specimens with extra water > specimens with superplasticiser > specimens with both water and superplasticiser; •
Nematollahi et al. (Nematollahi et al., 2017f)	FA & GGBS	SS (powder)	Micro-silica sand	PVA	Oven, 60 °C, 24 h; ambient temperature	• SHGC demonstrated strong strain-hardening behaviour with high tensile strength (4.6 MPa) and very high tensile strain capacity (4.2%). • The ambient temperature cured one-part SHGC offers 76% fewer carbon emissions and 36% less energy consumption than typical SHCC.
Nematollahi et al. (Nematollahi et al., 2017e)	FA & GGBS	SS (powder)	N/A	PVA; PE	Oven, 60 °C, 24 h; ambient temperature	• For one-part PE-SHGCs, the ambient temperature curing increased the compressive strength and tensile strengths, but reduced the tensile ductility. • Compared to one-part PVA-SHGC, PE-SHGCs exhibited lower compressive and tensile strengths, but higher tensile strain.
Shaikh et al. (Shaikh et al., 2018)	FA & GGBS	SS&SH	N/A	PE	Oven, 80 °C, 24 h; ambient temperature	• Strain-hardening behaviour (tension test) and deflection-hardening behaviour (three-point bending test): SHGC (both ambient and heat-cured) > SHCC. • Deflection and uniaxial tension capacity: ambient cured SHGC > heat-cured SHGC. • Compressive strength: SHGC (both ambient and heat-cured) < SHCC.

						• PE fibre volume fractions to achieve optimum tensile strain, deflection at peak load and maximum number of multiple cracks: 0.75-1.0% (both SHGC and SHCC). • Cement matrix and geopolymer gel adhered on PE fibres (possibly higher frictional bond of PE fibre): ambient cured SHGC < heat-cured SHGC.
Shaikh (Shaikh, 2020)	FA & GGBS	SS&SH	N/A	PET; PP	Ambient temperature	• Specimens reinforced with PP fibre had slightly higher compressive strength than that of PET fibre composites; • The increase of fibre volume fraction from 1% to 1.5% showed reduction in compressive strength in all specimens reinforced by both fibres; • SHGC specimens reinforced with PET fibre showed strain-hardening and deflection hardening behaviour; • No significant damage was observed on PET fibre in SHGC.
Ling et al. (Ling et al., 2019)	FA & GGBS	SS&SH	N/A	PVA	Oven, 50 °C	• All SHGC exhibited strain-hardening behaviour under tension and flexure. • Increasing GGBS content enhanced strength-related properties but reduced ductility-related properties of SHGC, mainly due to the improved density of SHGC matrix and bond between matrix and fibre. • 20% GGBS replacement shows optimum strength-related properties (compressive, flexural, and bond strengths) but not for ductility-related properties (tensile strain capacity, maximum flexural deformation, ultimate slip, and toughness).

Reference	Binder	Activator	Aggregate	Fibre	Curing	Findings
Nedeljković et al. (Nedeljković et al., 2018)	FA & GGBS	SS&SH	Sand	PVA	22 °C, ~ 99% RH	• Mixture sets in less than 30 min; • Large volume casting (45 L compared to 3 L) did not affect the workability and the setting time of the mixture, and flexural and compressive strength; • The mixture with PVA fibres exhibited deflection hardening behaviour even with aggregate particles as large as 4 mm, although single crack localization led to failure; • Combined fibre pull-out and fibre rupture occurred with the latter one causing the final failure.
Zhang et al. (Zhang et al., 2020)	FA & GGBS	SS&SH	N/A	PVA	50 °C, ≥98% RH	• Experimentally verified the micromechanics as the design basis; • Systematically developed the FA-GGBS based SHGC with tensile strength of over 3.8 MPa and tensile strain capacity of 4.8% following the micromechanics-based design.
Alrefaei and Dai (Alrefaei and Dai, 2018)	FA & GGBS	SS	Fine silica sand	Steel & PE	Ambient temperature in water	• GGBS-based SHGC and FA-GGBS based SHGC achieved comparable compressive strength, but the former exhibited a relatively better tensile response in strain-hardening and multi-cracking behaviours. • The matrix of GGBS-based SHGC was relatively denser and more compacted than FA-GGBS based SHGC. • For both GGBS-based and FA-GGBS based SHGC, additional sand reduced the strain-hardening and multi-cracking behaviours but increased the compressive strength and fracture properties of the geopolymer matrices.

Wan et al. (Wan et al., 2020)	FA & GGBS	SS&SH	Quartz sand	PVA	20 °C; 60 °C; 80 °C	• With 20 wt% GGBS and cured at 60 °C, specimens showed strain-hardening behaviour with multiple cracks, and had an average tensile strain of more than 3%; • The addition of PVA fibre improved both initial fracture toughness and unstable fracture toughness; • The fracture energy of SHGC reinforced with 2 vol% fibre was 77 times than that of plain geopolymer; • The increase of curing temperature resulted in the increase of elastic modulus, but slight decrease of fracture energy.
Wang et al. (Wang et al., 2021)	FA & GGBS	SS&SH	Fine silica sand	PVA	Ambient temperature	• SHGC specimens showed deflection hardening behaviour with large deflection and multiple microcracks; • The widths of microcracks were within 300 μm and mostly smaller than 45 μm. • The flowability, setting time, drying shrinkage and compressive strength of SHGC reduced with the increase of sand content at early ages up to 28 d. • At 28 d, the incorporation of sand up to 20 wt% increased the flexural strength and toughness of SHGC, but the further increase of sand content up to 40 wt% resulted in decrease in flexural strength and toughness.
Wang et al. (Wang et al., 2020a)	FA & GGBS	SS&SH	Fine silica sand	PVA; RTS	Ambient temperature	• SHGC specimens showed deflection hardening behaviour with large deflection and multiple microcracks; • The hybridisation of PVA and RTS fibre reduced the flowability, setting time, and flexural strength of SHGC, but

						greatly improved the resistance of drying shrinkage and compressive strength; • The addition of RTS fibre resulted in reduced crack widths in specimens where over 90% of cracks had a width of smaller than 60 μm; • The mixture containing 2.0 vol% PVA fibre can be regarded as the optimal mixture for SHGC considering the strengths and deflection (or strain) hardening behaviour.
Zhong and zhang (Zhong and Zhang, 2021)	FA & GGBS	SS&SH	Fine silica sand	PVA; RTP	Ambient temperature	• Incorporation of RTP fibre reduced the adverse effect of PVA fibre on flowability and compressive strength; • Optimum mixture is SHGC containing 1.75% PVA fibre and 0.25% RTP fibre in terms of high tensile strain capacity, low material cost and environmental impact than that of SHGC with 2% PVA fibre.
Hossain et al. (Hossain et al., 2020)	FA & GGBS	SS & Ca(OH)$_2$	Fine silica sand	PVA	N/A	• The addition of MgO delayed the setting time of both the SHGC mixes; • The binary geopolymer mix exhibited superior performance as compared to its ternary counterpart; • Strain-hardening behaviour was observed for both SHGC mixes under direct tension test.
Kan et al. (Kan et al., 2020a)	FA & MK	SS&SH	Micro silica sand	PVA	Oven, 80 °C, 2h; then 20 °C, 70% RH	• The ultimate tensile strain of the optimal mix reached 6.8%, 6.4%, and 5.2% at 3, 7, and 28d, respectively; • Multiple cracks had uniform distribution with specing of 2-5μm and average crack width of only 25μm;

						• The MFA-SHGC met the energy and strength criteria of strain-hardening behaviour and saturated multi-cracking; • The main reaction product of MFA-SHGC was amorphous aluminosilicate phase.
Kan et al. (Kan et al., 2019)	FA & MK	SS&SH	Micro silica sand	PVA	Oven, 80 °C, 2h; then 20 °C, 70% RH	• Specimens showed strain-hardening behaviour with pronounced multiple cracking; • After self-healing, number of cracks decreased significantly; • Specimens showed high recovery ratios of the tensile strains and the ultimate tensile strengths, while some showing even better tensile properties than the control specimens; • Air exposure seems to be more favourable than exposure to the wet-dry cycles for the self-healing of specimens; • The main healing products were amorphous aluminosilicate phases.
Al-Majidi et al. (Al-Majidi et al., 2017)	FA & GGBS & SF	K_2SiO_3	Silica sand	Steel; Glass; PVA.	Ambient temperature	• Additional steel and PVA fibres increase the flexural and tensile strength of the ambient cured examined geopolymer matrix. • Superior deflection capacity can be obtained by SHGC reinforced by 2% PVA fibre or 2% and 3% of 13 mm length steel fibre.
Batista et al. (Batista et al., 2019)	MK & SF	SS&SH	Fine sand	PVA	Ambient temperature	• The employment of SF could reduce the demand for sodium silicate in the alkaline activator, and further lower environmental impact (reduced CO_2 emissions). • Adjusting the formulations could improve flexion toughness in 170% with 30 wt% reduction of sodium silicate in the activator and improve deformation capability in tension.

| Li et al. (Li et al., 2021a) | FA & GGBS & MK & SF | SS&SH | Fine silica sand | Multi-walled carbon nanotubes, PVA | Ambient temperature, 95% RH | • Ultra-high SHGC showed excellent saturated multiple cracking properties and strain-hardening;
• At the maximum limit, the residual crack width and crack spacing of ultra-high SHGC were generally less than 70 μm and 2 mm, respectively;
• Ultra-high SHGC displayed strain-hardening behaviour with an ultimate tensile strain greater than 8%, and compressive strength of greater than 45 MPa;
• The main reaction products was the amorphous aluminosilicate phases, i.e., N-A-S-H. |

2.2.1 Fresh properties

Flowability is used to represent the workability of SHGC. SHGC with higher flowability indicates better fluidity and workability, and is easier for casting and compacting. Flowability of SHGC can be affected by the mix design of geopolymer matrix. The flowability of SHGC produced by typical GGBS showed 32% lower flowability compared with that of SHGC produced by gypsum free slag (Nematollahi et al., 2017f). Compared to GGBS-based SHGC, the incorporation of FA resulted in slightly higher flowability due to the ball-bearing effect of FA particles (Alrefaei and Dai, 2018). In metakaolin-based SHGC, the addition of silica fume had marginal effect on the flowability of SHGC, because both metakaolin and silica fume had spherical particles, and the particles of silica fume were thinner than that of metakaolin, which led to a lower solution demand to maintain the same workability (Batista et al., 2019). Moreover, the incorporation of aggregate influences the flowability of SHGC due to different water absorption ability of the aggregate. It was observed that SHGC with fine silica sand exhibited higher matrix flowability than those containing ceramic microsphere, expanded perlite, and expanded glass, which can be attributed to higher water absorption ability of ceramic microsphere, expanded perlite, and expanded glass particles (Nematollahi et al., 2017c).

2.2.2 Drying shrinkage

Drying shrinkage is the net volumetric contraction caused by the high capillary pressures generated by the loss of water, which could result in cracking in the microstructure (Wang et al., 2021). Drying shrinkage of SHGC can be affected by the geopolymer matrix and fibres. Geopolymer mortars had lower shrinkage than geopolymer pastes, because the sand in geopolymer mortar had a restraining effect on drying shrinkage due to its stability in shape and therefore controlled the volume stability of SHGC (Yang et al., 2017).

2.2.3 Static mechanical properties of SHGC

The unique characteristic of SHCC is the strain-hardening behaviour under tensile or flexural load, showing increased stress and strain with multiple microcracks rather than strain-softening with few wide cracks (Li and Kanda, 1998). This section provides a review on static mechanical properties of SHGC, focusing on the effects of geopolymer matrix

and short fibres.

2.2.3.1 Effect of geopolymer matrix

Static mechanical properties of SHGC can be affected by the mix design of the geopolymer matrix. It was reported that GGBS-based SHGC outperformed the blended FA-GGBS based SHGC in terms of tensile strain-hardening and multiple micro-cracking behaviour, because the GGBS-based SHGC had a relatively denser and more compacted geopolymer matrix (Alrefaei and Dai, 2018). The increase of GGBS content enhanced the strengths but reduced the ductility and toughness of SHGC due to the increased density of matrix and fibre-matrix bond strength, and the optimal FA/GGBS ratio was 8:2 (Ling et al., 2019). Ladle slag was also used to produce SHGC, which formed an ettringite-based binder, and the ladle slag-based SHGC attained a very high ductility and formed multiple microcracks under uniaxial tension (Nguyen et al., 2018, Nguyen et al., 2019). For metakaolin-based SHGC, the addition of silica fume improved the flexural toughness by 170% and deformation capability in tension but reduced the demand of sodium silicate (30%), which further reduced the CO_2 emissions (Batista et al., 2019). In FA-GGBS based SHGC, the optimal mixture was suggested to be 70% FA and 30% GGBS activated by the alkaline activator with a silicate modulus of 1.2, which achieved a ultimate tensile strength of over 3.8 MPa and tensile strain of 4.8% (Zhang et al., 2020).

Moreover, the incorporation of sand in SHGC resulted in the increase of the compressive strength and fracture properties of geopolymer matrix but impaired the strain-hardening and multiple micro-cracking behaviour of both GGBS-based and blended FA-GGBS based SHGC (Nematollahi et al., 2017f, Nematollahi et al., 2017e). The effects of geopolymer matrix properties on the strain-hardening behaviour of SHGC were quantitatively evaluated, and it was concluded that lower water/solids ratio and additional sand could increase the elastic modulus, but the excessive use of fine sand and coarse sand could lead to increased matrix fracture toughness and the first-crack strength of the composite, which could adversely affect the strain-hardening behaviour of SHGC (Nematollahi et al., 2016b). The development of FA-based SHGC mortar was studied by considering three design techniques, including design of experiment, micromechanical modelling, and material sustainability indices, which provided a comprehensive approach

to maintain high tensile ductility of SHGC and meanwhile enhance the compressive strength and material greenness (Ohno and Li, 2014, Ohno and Li, 2018). The tailored SHGC presented a 43.1 MPa improvement in compressive strength and 4.7% higher tensile ductility, but 11% lower embodied energy and 55% less embodied carbon compared to SHCC.

2.2.3.2 Effect of fibres

Various fibres have been used to produce SHGC, such as steel and PVA fibres. A comparison was conducted on SHGC containing PVA, glass, straight/hooked end steel fibres with various content and aspect ratios, indicating that SHGC reinforced with 2% PVA fibre or 2 vol% and 3 vol% steel fibre of 13 mm length led to superior deflection capacity (Al-Majidi et al., 2017). Compared with PVA fibre reinforced SHGC, it was reported that SHGC containing PE fibre had lower compressive and tensile strengths but higher tensile ductility (Nematollahi et al., 2017f, Nematollahi et al., 2017e). Moreover, the increase of PE fibre content in FA-based SHGC resulted in a decline in the compressive strength of SHGC, and SHGC containing 1 vol% PE fibre exhibited optimal strain-hardening and deflection-hardening behaviour (Ahmed and Ronnie, 2017).

In general, SHGC reinforced with low-modulus fibres, e.g., PP fibre with an elastic modulus of 1.5-10 GPa tends to possess low strength, high tensile strain capacity and large crack width. By contrast, SHGC containing high-modulus fibres, e.g., steel fibre with an elastic modulus of 200-210 GPa exhibits high strength, low tensile strain capacity and fine crack width (Ranjbar and Zhang, 2020, Pakravan et al., 2016, Li et al., 1996). It has been reported that the addition of hybrid steel and PVA fibres into SHCC results in enhanced strengths and energy absorption, while the incorporation of steel fibre leads to a reduction in workability (Mohammed et al., 2018, Wang et al., 2019, Li et al., 2019, Yu et al., 2018). When PVA fibre is partially replaced with 0.5% steel fibre, SHCC exhibits a slight improvement in flexural strength and peak energy absorption by around 2 MPa and 5 kJ/m^3, while the addition of 0.5% steel fibre results in an increase in ultimate tensile strength from 2.84 MPa to 3.51 MPa (Wang et al., 2019). Moreover, the inclusion of steel fibre in SHCC can improve the crack width control ability of SHCC (Li et al., 2019, Yu et al., 2018), but the fibre-balling effect can be observed in SHCC containing more than 0.5% tyre steel fibre

(Mohammed et al., 2018). In SHGC reinforced with hybrid steel and PP fibres, the increase of steel fibre can lead to an enhancement of toughness and equivalent flexural strength, but a reduction when the total fibre volume fraction exceeds 1%. For FA-based SHGC reinforced with hybrid PVA and steel fibres, the SHGC containing 1% PVA and 1% steel fibres shows superior deflection hardening behaviour (Shaikh, 2013).

Natural fibres such as luffa cylindrical fibre and fibres sourced from jute, sisal and curauá, were used to reinforce geopolymers. The incorporation of luffa cylindrical fibre into metakaolin-based geopolymer led to the formation of fibre-like crystals and cubic-shaped fine crystals, which increased the tensile strength and toughness and contributed to the crack healing of SHGC (Alshaaer et al., 2017). Moreover, metakaolin-based SHGC reinforced with distinct natural (jute, sisal and curauá) fibres was observed to exhibit strain-hardening behaviour with the formation of multiple cracks in all specimens (Trindade et al., 2019).

2.2.4   Dynamic mechanical properties of SHGC

Dynamic compressive properties are affected by strain rate, fibre content and fibre type. The most critical rate sensitivity is determined by the interface chemical bond. The increase of the strain rate could result in the increase of interface chemical bond, and then the decreased complementary energy and tensile ductility. At the high-level strain rate, the enhancement of ductility can be achieved by two ways. First, using more FA that has less reactivity would lead to the decreased crack tip toughness but increased complementary energy. Second, replacing hydrophilic fibre by hydrophobic fibres would result in the decrease of interface chemical bond. It was found that FA-GGBS based geopolymer composites reinforced with steel fibre (spiral and hooked end) and high-strength polyethylene fibres exhibited strong dependency on strain rate under splitting tensile load, and the high-strength polyethylene fibre complemented the bonding between steel fibre and matrix (Khan et al., 2019).

2.3 Sustainability assessment of SHGC

Sustainability of SHGC can be analysed through life cycle analysis (LCA). LCA framework captures externalities related to upstream environmental costs related to construction materials (pollution from mining, processing, and transportation) and

downstream environment costs related to reconstruction events. LCA provides a quantitative assessment of the dominant source of environmental costs, which could be used to adjust the material ingredients for SHGC. Likewise, the sustainability indicator could also be deployed to alter designs at the structural and infrastructure system level. The environmental impacts investigated include resource consumption and global warming potential. The global warming impact is characterised by greenhouse gas (GHG) emissions in metric tons of CO_2 equivalent, which is calculated by multiplying the mass of each GHG emission by its global warming potential (GWP). Previous studies showed that the partial replacement of cement with FA or GGBS could reduce the carbon emissions of the material, which contributes to the reduction of global warming (Wang and Li, 2007, Yang et al., 2007). According to Nematollahi et al., the FA-based SHGC had 50%-76% less carbon emissions compared with cement-based SHCC, and the embodied energy of SHGC is 22%-36% less than that of cement-based SHCC (Nematollahi et al., 2017d).

About 5.2 billion tyres are estimated to be at the verge of disposal worldwide, which could result in adverse environmental impact and health hazards (Liew and Akbar, 2020). In recent years, waste tyres have been increasingly utilised by energy recovery, recycling, and other approaches instead of ending up in landfills. The recycling of rubber particles, steel, and polymer fibres provides a promising way to mitigate the environmental and health problems, and leads to economic benefits (Ramarad et al., 2015). For example, recycling of waste tyres can help reduce carbon emissions by 1.52 tonnes annually (Gigli et al., 2019). Steel wire extracted from waste tyres, known as recycled tyre steel (RTS) fibre, was reported as a potential substitute for manufactured steel fibre because of its better ductility and higher tensile strength, as the raw steel used in tyre production has better quality than commercially available manufactured steel fibres (Domski et al., 2017).

SHGC can be applied in structures that require ultra-high ductility and important civil infrastructures, which could prevent damages caused by earthquakes and winds, water permeability, corrosion, and other issues. After decades of research and development, SHCC has been used in seismic resistant structures (Gregor and Victor, 2002, Fischer and Li, 2002, Parra-Montesinos and Wight, 2000, Fischer and Li, 2003), durable structures under severe

environmental conditions (Lepech and Li, 2011, Mustafa Sahmaran and Victor, 2007, Suthiwarapirak et al., 2002, Li and Li, 2011), and advanced processing technologies such as spray-applied fire-resistive materials and extrusion process that lead to efficient construction productivity (Zhang and Li, 2016, Stang and Li, 2003, Takashima et al., 2003). In the future, SHGC has the potential to be applied in the civil infrastructures.

2.4 Concluding remarks

This chapter provides a review on SHGC, with special focus on the micromechanics-based design and the effects of different factors such as matrix, sand content, and fibres in terms of type, content and length on the fresh and hardened properties as well as sustainability. Based on the literature review, the key findings and remaining challenges can be summarised as follows:

- Flowability of SHGC can be influenced by the mix design of geopolymer matrix, as the incorporation of FA tends to enhance the flowability of GGBS-based SHGC, and the aggregate with higher water absorption ability can result in lower flowability. However, the effect of fine silica sand on the engineering properties including fresh and hardened properties of FA-GGBS based SHGC has not been systematically explored yet, and the deflection hardening and multiple cracking behaviour of SHGC have not been fully investigated.

- Previous studies have been conducted to validate the micromechanical properties of SHCC and found that strength and energy-based criteria were the basic principle in strain-hardening behaviours, however, the micromechanical parameters of SHGC and verification of pseudo strain-hardening (PSH) criteria have not been studied yet.

- Many studies have investigated the fresh properties and static mechanical properties of SHGC, however, a systematic study on dynamic properties of FA-GGBS based SHGC concerning the effects of mono PVA fibre and hybrid PVA-RTS fibres is still lacking.

- RTS fibre has been used to reinforce geopolymer composites, however, hybrid PVA-RTS fibre reinforced FA-GGBS based SHGC with desired static and dynamic properties has not been developed yet.

Chapter 3 Effect of Sand on Engineering Properties of SHGC

3.1 Introduction

As introduced above, concrete is brittle and prone to cracking, and fibre reinforced cementitious composites (FRCC) are produced by incorporating short fibres into cementitious materials to inhibit the growth of cracks and the brittleness of concrete. As a tailored group of FRCC, strain-hardening cementitious composites (SHCC), also called engineered cementitious composites (ECC), have been widely investigated to achieve ultra-high-ductile performance and produce "bendable concrete" (Li, 2003, Li, 2019). In recent years, alternative binders, such as FA and ground granulated blast-furnace GGBS, have been increasingly used to develop SHGC.

This chapter aims to develop the SHGC, i.e., "bendable" geopolymer composites, by incorporating short and randomly distributed PVA fibre into blended FA-GGBS based SHGC cured at ambient temperature. The effect of sand content (0-40% by weight of the geopolymer binder) on the engineering properties of the composite is experimentally investigated by conducting flow table test, setting time test, drying shrinkage test, static compression test, and four-point bending test. The influence of sand content on the deflection-hardening behaviour of SHGC is particularly estimated and discussed including stress-deflection response, failure patterns and cracking, flexural strength, and flexural toughness and toughening mechanisms. Afterwards, the optimal sand content for developing SHGC is determined and used to prepare SHGC specimens for following chapters.

The results presented in this chapter were published as a journal article, with the following reference:

Yi Wang, Yansong Wang, Mingzhong Zhang, Effect of sand content on engineering properties of fly ash-slag based strain-hardening geopolymer composites, *Journal of Building Engineering*, 34 (2021) 101951.

3.2 Raw materials

Herein, low-calcium (equivalent to ASTM Class F) FA and GGBS were used as the precursors for producing geopolymer. The chemical compositions and particle size distribution of FA and GGBS are presented in Table 3-1 and Figure 3-1, respectively. FA and GGBS have average particle sizes of 53.60 μm and 14.77 μm, and specific gravity of 2.65 and 2.9, respectively. A mixture of sodium hydroxide (NaOH; SH) solution with molarity of 10 and sodium silicate (Na_2SiO_3; SS) solution with modulus (SiO_2/Na_2O ratio) of 2.0 (Na_2O: 15.35 wt%, SiO_2: 29.79 wt%, water: 54.86 wt%) was used as alkaline activator that was mixed with a SS/SH ratio of 2.0. It was prepared by dissolving the NaOH powder in the tap water, followed by the addition of Na_2SiO_3 solution. Then, the alkaline activator was stored in the cupboard overnight to allow the heat dissipation that was caused by the exothermic chemical reaction between NaOH and Na_2SiO_3 (Ling et al., 2019). The modified polycarboxylate-based superplasticiser (SP) was used to improve the workability of geopolymer composites. It was reported that the addition of such type of SP by 1 wt% of the geopolymer binder resulted in an increase in flow value of the composite by 41% though a sacrifice of compressive strength by up to 15% (Nematollahi and Sanjayan, 2014).

Table 3-1 Chemical compositions (wt%) of FA and GGBS

Oxide	SiO_2	Al_2O_3	CaO	MgO	K_2O	Fe_2O_3	TiO_2	Na_2O	SO_3	LOI
FA	49.80	25.08	4.65	1.67	3.30	11.67	1.24	0.66	1.35	0.58
GGBS	36.77	13.56	37.60	7.45	0.55	0.41	0.79	0.25	1.82	0.8

Note: LOI (loss on ignition)
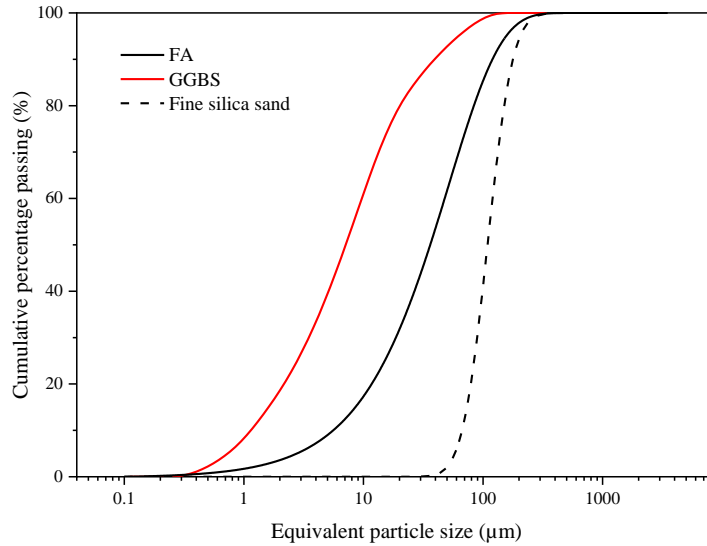
Figure 3-1 Particle size distribution of FA, GGBS, and sand

Fine silica sand sourced from a quarry in Cheshire, UK was used as the aggregate, which has a specific gravity of 2.65. As seen in Figure 3-1, the particle size distribution of sand has the maximum and average particle size of 250 µm and 148 µm, respectively. PVA fibre was used as reinforcement because of its higher tensile strength and elastic modulus (Ranjbar and Zhang, 2020). Moreover, PVA fibre supplied by Kuraray was applied because the fibre was coated with 1.2 wt% oil to reduce its hydrophilicity and control the interface properties of SHGC (Li et al., 2002). PVA fibre has a nominal diameter of 40 µm and a length of 12 mm. The tensile strength, elastic modulus and strain capacity of PVA fibre are 1600 MPa, 41 GPa and 6.0%, respectively.

3.3 Mix proportions

Five SHGC mixtures with 0%, 10%, 20%, 30%, and 40% (by weight) incorporation of fine silica sand were studied here, which were denoted as S0, S1, S2, S3, and S4, respectively. Table 3-2 shows the mix proportions of SHGC specimens, where the contents of precursors (FA and GGBS), alkaline activator, SPs and PVA fibre were determined based on previous studies on engineering properties of FA-GGBS based geopolymer composites cured at ambient temperature (Fang et al., 2018b, Fang et al., 2018a, Tu et al., 2019). Herein, the binder of SHGC mixtures is composed of FA and GGBS with a FA/GGBS ratio of 0.8/0.2. The activator/binder ratio was taken as 0.4. SPs with a weight ratio to binder of 1% were added to improve the workability of fresh SHGC specimen.

50

Short PVA fibre was incorporated with a volume fraction of 2% to the mixture. The above mix proportions were kept constant in all mixtures.

Table 3-2 Mix proportions of SHGC

Mix No.	Binder		Activator/binder	SP/binder	Fine silica sand/binder	Fibre (vol%)
	FA	GGBS				
S0	0.8	0.2	0.4	0.01	0	2
S1	0.8	0.2	0.4	0.01	0.1	2
S2	0.8	0.2	0.4	0.01	0.2	2
S3	0.8	0.2	0.4	0.01	0.3	2
S4	0.8	0.2	0.4	0.01	0.4	2

Note: SP – superplasticiser

3.4 Specimen preparation

All specimens were mixed using a Hobart HSM 10, and the mixing typically lasted around 8 min in total. Firstly, FA, GGBS and dry silica sand were added in the mixer and dry mixed for 1 min to obtain a homogeneous mix. Then, the alkaline activator was gradually added into the binder and mixed for 1 min, followed by the addition of SPs to enhance the flowability of the matrix and mixed for another 1 min. Subsequently, the PVA fibre was added gradually to avoid multifilament forms. After the mixing, the material was immediately poured into moulds and vibrated to allow the air bubble to escape and compact the SHGC. All specimens were then covered with cling film to prevent water evaporation and stored in the ambient environment for 24 h. Afterwards, the specimens were demoulded and then stored in a curing room with an average temperature of 20 ± 2 °C and relative humidity of $60 \pm 5\%$ until the age of testing.

3.5 Test methods

3.5.1 Flow table test

Flow table test was conducted in accordance with ASTM C1437-15 (ASTM, 2015) to determine the flowability of SHGC by measuring the spread diameter of fresh mortar immediately after mixing. The truncated mould with an upper diameter of 70 mm, a lower diameter of 100 mm ($D_0 = 100$ mm) and a depth of 50 mm was filled with fresh SHGC on the wet flow table. The mould was lifted upwards, and the table was dropped 25 times in 15 s. Four measurements of the diameter of each mixture were taken to obtain the average flow value, D (mm). The flow (F) of the fresh SHGC specimen can be calculated

by following equation.

$$F = (D - D_0)/D_0 \times 100\% \hspace{4cm} (3\text{-}1)$$

3.5.2 Setting time test

Setting time test was carried out according to ASTM C191-08 (ASTM, 2019b) by measuring the penetration depth of fresh SHGC immediately after mixing using CONTROLS Vicamatic 4417 with a needle diameter of 1.13 mm. The penetration of the Vicat needle was recorded with the intervals of 5 min. The Vicat needle time was added to the duration of initial mixing and the first Vicat recording and considered as the setting time. The initial setting time was interpreted by the time to reach the penetration depth of 25 mm, and the final setting time was recorded when the penetration measurement did not mark the specimen surface with a complete circular impression. One measurement of each mixture was used to represent the setting time.

3.5.3 Drying shrinkage test

Drying shrinkage test was carried out on SHGC prisms with a dimension of 280 x 50 x 50 mm (length x width x height) as per ASTM C490 (ASTM, 2017) on a daily basis. The prisms were exposed to the environment with a temperature of 20 ± 2 °C and relative humidity of 60 ± 5%. The change of length of specimens was obtained using a digital gauge with an accuracy of ± 0.01 mm. The average value of three specimens were used as drying shrinkage.

3.5.4 Static compression test

Static compression test was carried out on 50×50×50 mm cubic SHGC specimens in accordance with ASTM C109-16 (ASTM, 2020a) at curing ages of 1, 7, and 28 d using a CONTROLS C4600/FR with a maximum loading capacity of 2000 kN. The loading rate of 1200 N/s was used for all specimens. For each curing age of the mixtures, three specimens were tested, and the average value was used.

3.5.5 Four-point bending test

Four-point bending test was conducted to determine the flexural strength and evaluate the deflection hardening behaviour of SHGC according to ASTM C1609-05 (C1609, 2005) using an Instron 3345 with a maximum loading capacity of 5 kN. The average values of flexural strength of three 400×100×20 mm prismatic specimens at 7 and 28 d of curing

were obtained. The loading rate during the test was 1.6 mm/min, and the deflection was automatically recorded at an interval of 0.5 s. The test terminated when one of the following failure criteria was met: (1) the load reached 4900 N, the loading capacity of the machine, (2) the deflection reached 105 mm, the deformation limitation of the machine, and (3) the load dropped by 150 N to ensure flexural failure while avoiding specimen crush. After the test terminated, specimens were still loaded so that microcracks were not closed. Dino-Lite digital microscope was then used to capture the status of fibres in the specimens and the image of cracks for determining the microcrack number and widths.

Figure 3-2 shows a typical load-deflection curve of SHGC, where point A denotes the first-crack load where the slope of the curve is zero and the deflection value at point A is δ. The curve of SHGC specimens may display stable deflection hardening behaviour due to the formation of multiple microcracks, and therefore the turning point could be difficult to be identified. In this case, the limit of proportionality (FLOP) is used instead. The first-crack strength (or limit of proportionality) and flexural strength of SHGC were calculated by following equations (C1609, 2005).

$$\sigma_{fc} = \frac{P_A l}{bd^2} \tag{3-2}$$

$$\sigma_f = \frac{P l}{bd^2} \tag{3-3}$$

where σ_{fc} and σ_f represent the first-crack strength (MPa) and ultimate flexural strength (MPa) of the specimen respectively, P_A and P stand for the first-crack load (N) and ultimate load (N) of the specimen respectively, l is the span of the specimen (300 mm), b is the width of the specimen (100 mm), and d is the depth of the specimen (20 mm).

Toughness measures the energy absorbed by the material during plastic deformation. Low toughness materials tend to present brittle failure pattern, whereas high toughness materials are prone to exhibit prolonged plastic failure (Noushini et al., 2018). The flexural toughness T_{150}^D, defined in ASTM C1609 (C1609, 2005), was calculated as the area enclosed beneath the load-deflection curve up to the point of net deflection of L/150 (i.e. 2 mm).
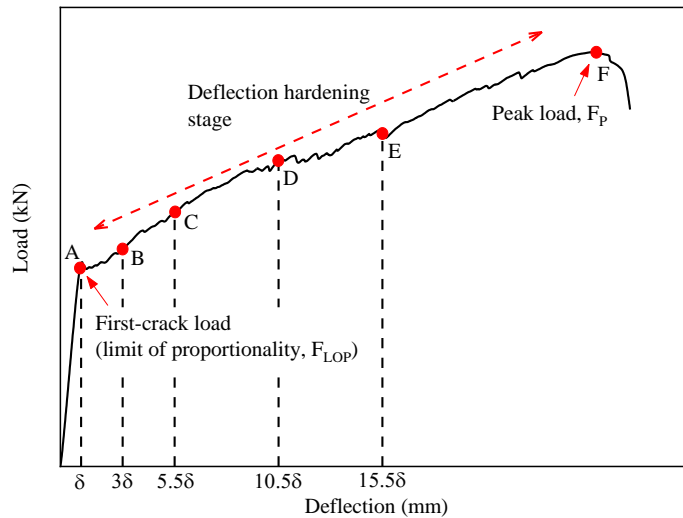
Figure 3-2 Typical load-deflection curve for SHGC under bending

3.6 Results and discussion

3.6.1 Flowability

Flowability was used to represent the workability of fresh SHGC mixtures. The SHGC mixture with higher flowability reflects better fluidity and workability and is easier for casting and compacting. Figure 3-3 shows the flow values of fresh SHGC mixtures with various sand content. It can be observed that the addition of fine silica sand resulted in a gradual reduction in the flow of SHGC specimens. The SHGC paste without fine silica sand (S0) had a flow of 68.3%. The increase of sand content by 10 wt% (S1), 20 wt% (S2), 30 wt% (S3), and 40 wt% (S4) gradually reduced the flow of fresh SHGC mixtures by 7.0%, 19.5%, 41.5%, and 45.5%, respectively. A similar trend in workability influenced by sand content was also reported by Alrefaei and Dai (Alrefaei and Dai, 2018). According to their study, the SHGC paste without sand had better workability than the SHGC mortar containing 30 wt% sand, and a drop of 23% in workability of SHGC mortar incorporated with 30 wt% sand was observed as compared with its counterpart paste. The reduction in flowability of SHGC mixtures with the increase of sand content can be ascribed to the higher shear resistance of SHGC mixtures to flow. In addition, while adding alkaline activator into the dry mix, part of water would be restrained by sand as the adsorption layer water, resulting in the reduced content of alkaline activator solution and activator-to-binder ratio (Wang et al., 2003, Huseien et al., 2018, Fang et al., 2018a). On the other hand, the total surface area of the sand in fresh SHGC increased with the increase

of sand content (Khan et al., 2016), and required more water as the adsorption layer water, which led to the decrease of workability of SHGC mixtures with higher sand content. It should be noted that the addition of fine silica sand in SHGC specimens caused difficulties in mixing, casting, and vibration.
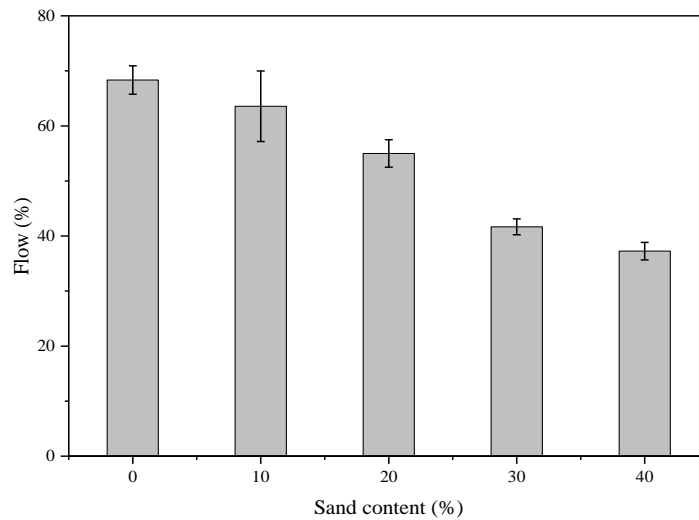
Figure 3-3 Effect of sand content on flowability of fresh SHGC specimens

3.6.2　Setting time

Setting time is one of the important properties of SHGC, which comprises of initial setting time and final setting time depending on the rigid level of the material. Setting time was used to verify the feasibility of SHGC mixtures for engineering application, because the mixture that had short setting time could lead to difficulties in casting and compaction. Figure 3-4 illustrates the change in setting time against sand content. The inclusion of sand had a marginal reduction effect on the setting time of SHGC mixtures. The SHGC paste without sand (S0) had initial and final setting time of 85 min and 155 min, respectively. Compared to S0, the increase of sand content by 10 wt% (S1), 20 wt% (S2), 30 wt% (S3), and 40 wt% (S4) reduced the initial setting time by 9.7%, 12.1%, 28.3%, and 19.1%, respectively, as well as the final setting time by 8.2%, 21.8%, 15.5%, and 22.0%, respectively. This can be attributed to the decrease of alkaline activator to binder ratio with increasing sand content. Moreover, the reduction of alkaline activator-to-binder ratio further caused the insufficient alkaline activator for dissolution of geopolymer binder and then the reduced level of geopolymerisation (Siyal et al., 2016, Fang et al., 2018a, Temuujin et al., 2010). However, the reaction between sodium hydroxide and micrometric

particles of silica sand generally requires external conditions such as heating and pressurisation, therefore can be negligible in this study (Aldabsheh et al., 2018).
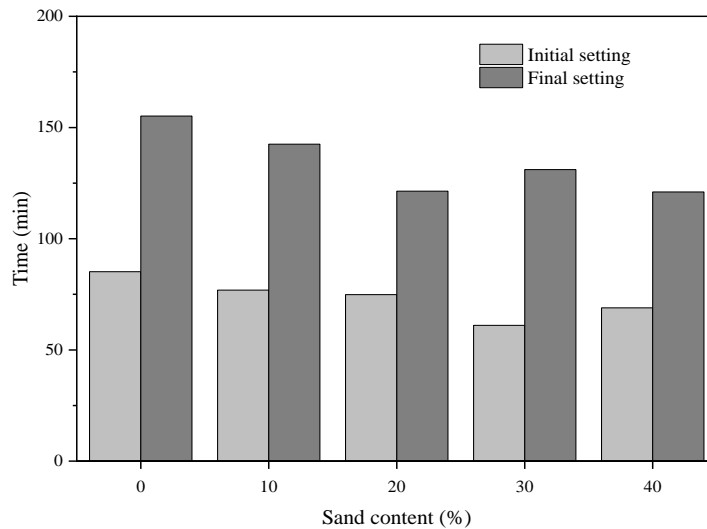
Figure 3-4 Effect of sand content on setting time of SHGC specimens.

3.6.3 Drying shrinkage

Drying shrinkage is the net volumetric contraction caused by the high capillary pressures generated by the loss of water, which could result in cracking in the microstructure (Kuenzel et al., 2012, Scherer, 1990). Figure 3-5 shows the drying shrinkage of SHGC specimens with various sand content ranging from 0% to 40% by weight of the geopolymer binder. The drying shrinkage of SHGC specimens was effectively reduced with the increase of sand content. At the early ages, the SHGC specimens without sand (S0) exhibited the most rapid drying shrinkage rate. The incorporation of sand up to 40 wt% gradually reduced the drying shrinkage rate of SHGC specimens with the lowest drying shrinkage rate observed in SHGC with 40 wt% sand (S4). A similar finding was reported in a previous study (Yang et al., 2017). The rapid drying shrinkage rate of SHGC specimens at early ages can be associated with the rapid reduction of internal relative humidity due to the loss of water from the surface of specimens, which was freshly formed (Yang et al., 2017). At 28 d, the SHGC specimens without sand (S0) showed the highest drying shrinkage. When the sand content was increased by 10 wt% (S1), 20 wt% (S2), 30 wt% (S3), and 40 wt% (S4), the drying shrinkage of SHGC specimens dropped by 10.4%, 19.5%, 26.5%, and 56.1%, respectively. This is because fine silica sand as the aggregate in SHGC specimens had a restraining effect on drying shrinkage due to the

56

excellent stability in shape, and thus controlled the volume stability of samples as the skeleton in SHGC specimens (Mastali et al., 2018a).
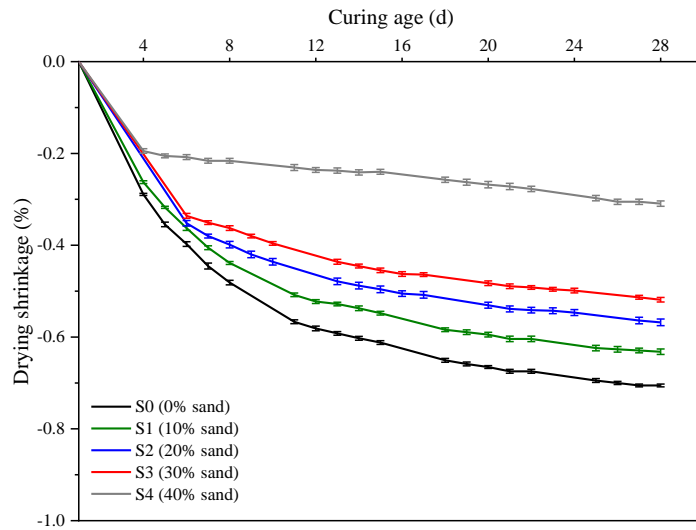
Figure 3-5 Effect of sand content on drying shrinkage of SHGC specimens

3.6.4 Compressive strength

Figure 3-6 shows the typical failure pattern of SHGC specimen at 28 d along with the loading direction. The red line indicates the cut plane perpendicular to the loading direction after uniaxial compression test, which will be explained in detail below. When the peak load was reached, all SHGC specimens remained the original cubic shape while a series of microcracks can be observed on the surface of specimens. These findings are consistent with those reported in other studies (Alrefaei and Dai, 2018, Lee et al., 2012). Noticeable vertical macrocrack parallel to the loading direction appeared on the specimen. The propagation of microcracks and sliding of matrix were limited by fibres incorporated in SHGC specimens due to the bridging effect, which also constrained the lateral expansion of specimens subjected to compressive load.
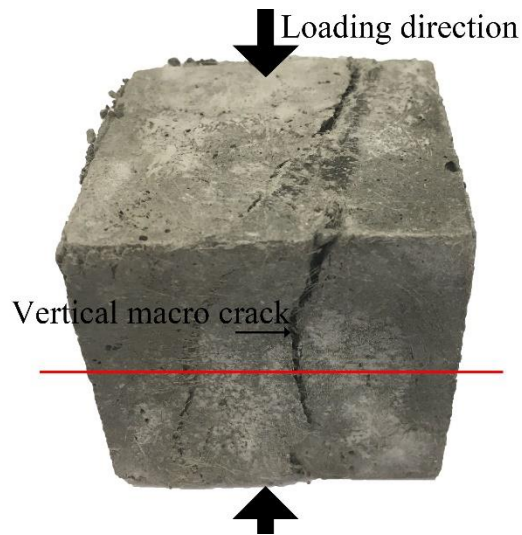
Figure 3-6 Typical failure pattern and loading direction of SHGC specimen at 28 d

Figure 3-7 displays the compressive strength of SHGC specimens with various sand content ranging from 0% to 40% by weight. The inclusion of fine silica sand resulted in a drop of the compressive strength of SHGC specimens. At 1 d, SHGC paste without sand (S0) had a compressive strength of 18.73 MPa. The increase of sand content up to 40 wt% (S4) gradually reduced the compressive strength of SHGC specimens by 35.7%. Compared to S0, when the sand content was increased by 10 wt% (S1) and 20 wt% (S2), there existed a negligible reduction (1.2% and 5.8%, respectively) in compressive strength of SHGC specimens. When the sand content was increased by 30 wt% (S3) and 40 wt% (S4), the reduction trend was more pronounced, showing a decrease in compressive strength by 22.0% and 35.7%, respectively. Compared to 1 d, the compressive strength of SHGC paste without sand (S0) had an increase of 77.7% at 7 d, reaching the value of 33.28 MPa. At 7 d, compared to S0, the addition of 10 wt% sand led to a drop in compressive strength of SHGC specimens by 12.0%, but the further increase of sand content by 20 wt% (S2), 30 wt% (S3), and 40 wt% (S4) marginally reduced the compressive strength of SHGC specimens by 17.5%, 16.3%, and 19.5%, respectively. At 28 d, the compressive strength of SHGC0 was further developed to 42.89 MPa. Compared to SHGC0, the incorporation of 10 wt% sand (S1) resulted in a slight increase in compressive strength by 7.8%, but the further increase of sand content by 20 wt% (S2), 30 wt% (S3), and 40 wt% (S4) effectively reduced the compressive strength of SHGC specimens by 27.6%, 20.4%, and 33.4%, respectively.
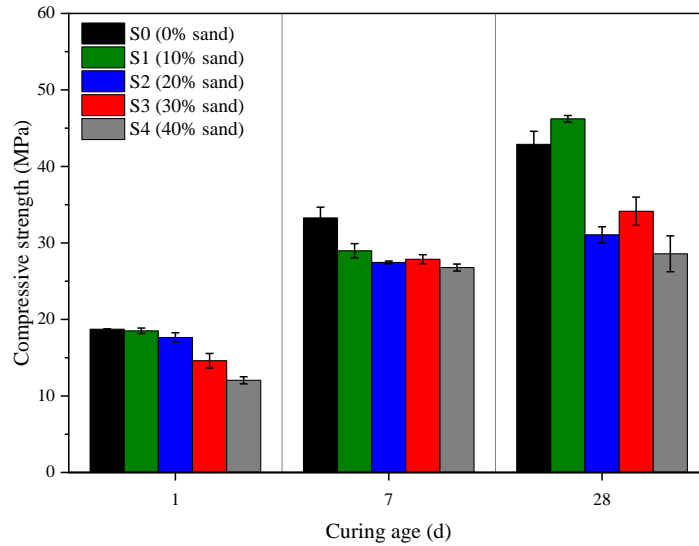
Figure 3-7 Effect of sand content on compressive strength of SHGC specimens

Generally, the inclusion of fine silica sand into the pure geopolymer paste could result in an increase in compressive strength of the paste (without fibre), but for SHGC specimens (with fibres), the incorporation of sand altered the trend, indicating the reduced compressive strength. This is because the additional sand in SHGC specimens could influence the distribution and orientation of fibres as well as the entrapped voids. The size and distribution of voids could influence the initiation of cracks, and the distribution and orientation of fibres could influence the propagation of cracks. The synergistic effect of fibres and voids could affect the compressive strength of specimens.

To examine the distribution and orientation of fibres as well as the voids, the microstructure of SHGC was investigated. After the static compression test, SHGC specimens were cut perpendicular to the loading direction along the red line indicated in Figure 3-6. Images of cross-sections captured using Dino-Lite digital microscope were converted into binary images to show features of fibres and voids (see Figure 3-8). The blue area represents the matrix, while the white area stands for fibres in SHGC specimens.

59
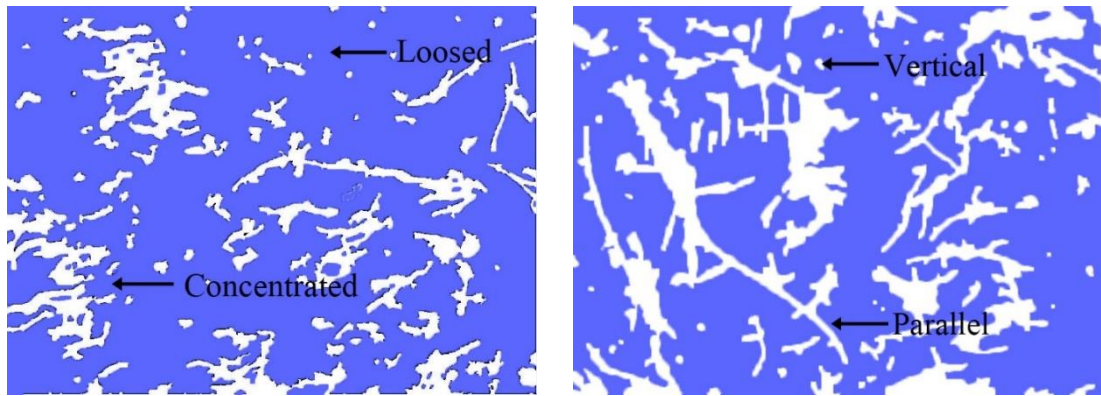
(a) Fibre distribution (S4)

(b) Fibre orientation (S4)
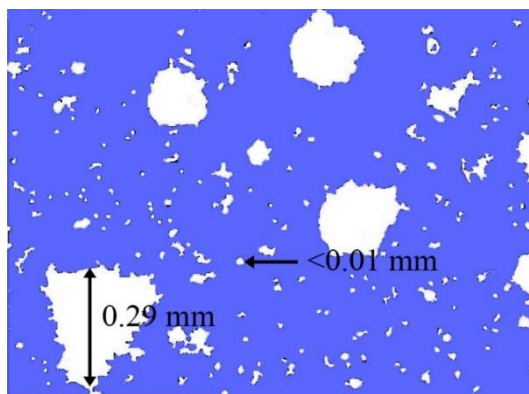
(c) Voids distribution and size (S0)

Figure 3-8 Typical features of fibres and voids over the cross-section of SHGC specimens.

As seen in Figure 3-8a, fibres distributed randomly, as more fibres were densely distributed in bottom-left while less fibres were loosely distributed in top-right of the figure. Compared with loosely distributed fibres, densely distributed fibres tended to better resist the crack propagation while the fibres were prone to corrugation, which could impair the effect of fibres. As shown in Figure 3-8b, the fibre orientation was also random with both parallel and vertical directions to the cross-section displayed as the white lines and the white dots, respectively. Since fibres were randomly incorporated into SHGC specimens during the mixing process, the distribution and orientation of fibres were both random over the cross-section of SHGC specimens. The bridging effect was mainly functioned by fibres oriented vertically to the propagation direction of microcracks. The uneven fibre dispersion further resulted in an increase in the total porosity of SHGC specimens, as the air bubbles were difficult to escape during the vibration process and thus voids were formed (Nematollahi et al., 2016a, Akkaya et al., 2000). The white area over

the cross-section of SHGC specimen in Figure 3-8c represents the voids. Most voids in SHGC specimens were tiny with a diameter of less than 10 μm, and few macro voids had a diameter of around 300 μm. Furthermore, the weak interfacial transition zone also led to the reduction in compressive strength of SHGC specimens.

3.6.5 Flexural behaviour

Flexural behaviour of SHGC specimens is discussed below in terms of stress-deflection response, failure patterns and cracking, flexural strength, and flexural toughness and toughening mechanisms. Table 3-3 summarises the flexural properties of SHGC specimens at 28 d under four-point bending.

Table 3-3 Flexural properties of SHGC specimens at 28 d

Mix No.	Average ultimate flexural strength (MPa)	Average ultimate flexural deflection (mm)	Flexural toughness (J)	Crack number	Average crack width (μm)
S0	6.48	24.20	0.48	93	68.2
S1	8.64	27.36	0.69	132	58.6
S2	8.97	24.80	0.93	98	80.0
S3	8.85	26.87	0.87	89	91.9
S4	7.55	22.74	0.83	50	124.1

3.6.5.1 Stress-deflection response

Figure 3-9 shows the stress-deflection curves of all SHGC specimens with various sand content under four-point bending at 7 d and 28 d. All SHGC specimens exhibited deflection hardening behaviour, and the stress-deflection curves were marginally affected by the addition of fine silica sand. For each SHGC mixture, the stress-deflection curve mainly consisted of two stages. The first stage of the stress-deflection curve was a linear elastic line until the first crack initiated. In the second stage, the stress-deflection curve continued with a higher rate in deflection until reaching the ultimate load capacity of the specimen, and then the specimen failed. During the second stage, the stress-deflection curve contained serrated lines, which were corresponding to the initiation and propagation of microcracks. As the load increased, the number and width of cracks increased and can be more clearly observed. Table 3-3 presents the average ultimate flexural deflection of specimens, which was marginally influenced by the inclusion of fine silica sand. The SHGC paste without sand (S0) had an average flexural deflection of 24.20 mm. The SHGC specimens with sand content of 10 wt% (S1) and 30 wt% (S3) had a slightly larger

average flexural deflection of 27.36 mm and 26.87 mm, respectively, but the SHGC specimens with sand content of 20 wt% (S1) and 40 wt% (S3) had a slightly smaller average flexural deflection of 24.80 mm and 22.74 mm, respectively. Similar as the compressive strength, the influence of sand content on the flexural properties of SHGC specimens can be attributed to the random distribution and orientation of fibres and the formed voids.

Among all mixtures, S2 with 20% sand displayed the optimum deflection hardening behaviour, as illustrated in Figure 3-9c, which is used to explain the deflection hardening behaviour of SHGC at 7 and 28 d. Compared to 7 d, SHGC specimens presented higher first crack strength and ultimate flexural strength at 28 d. At 7 d, the first crack and ultimate flexural strengths of SHGC specimens were 2.90 MPa and 8.03 MPa, respectively. At 28 d, the first crack and ultimate flexural strengths of SHGC specimens were 3.92 MPa and 8.97 MPa, respectively. This is because the matrix strength was still developing, and the fibre-matrix interfacial bond strength also increased with the geopolymerisation process as the curing age increased (Altwair et al., 2012). However, the increase in strength in turn caused the reduction in flexural deflection of SHGC specimens at 28 d. For instance, the average flexural deflection of S2 was 32.03 mm and 24.8 mm at 7 d and 28 d, respectively. On the other hand, the slope of elastic region in the stress-deflection curves indicated the elastic modulus of SHGC specimens, which increased with the increase of curing age. At 7 d, the slope had an average value of 3.46, which was increased to 4.46 at 28 d, indicating that the SHGC specimens at 28 d became more brittle and therefore had a reduced flexural deflection capacity.

(a) S0 (0% sand)

(b) S1 (10% sand)

(c) S2 (20% sand)

63
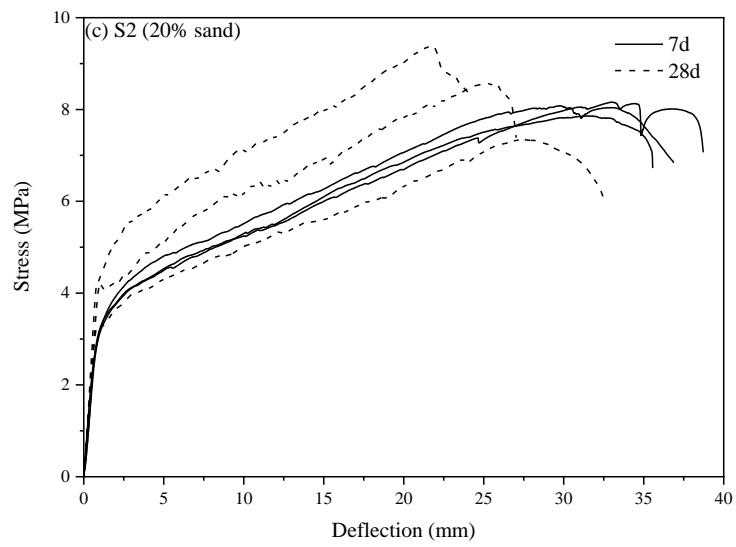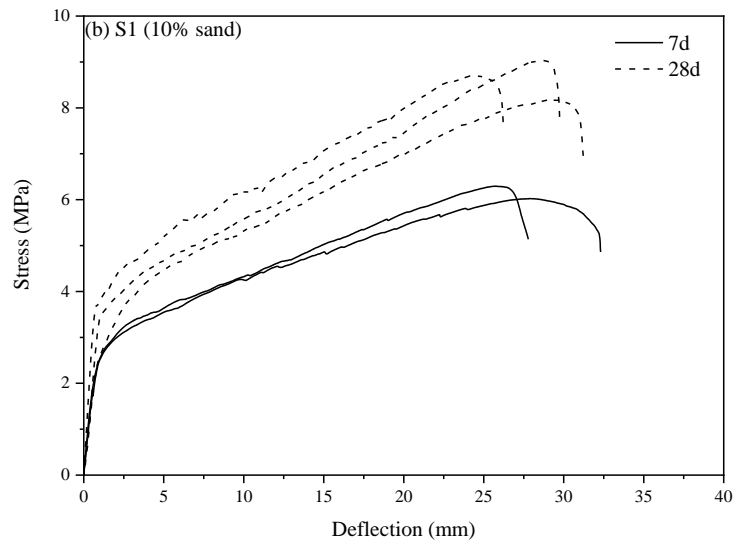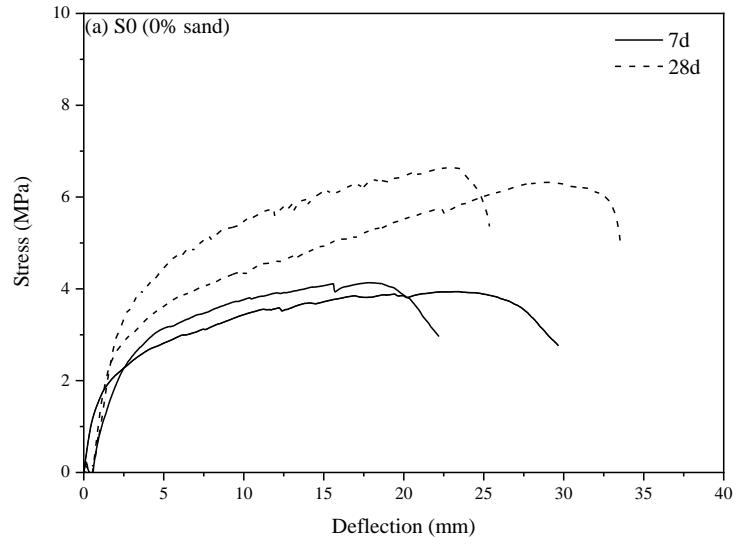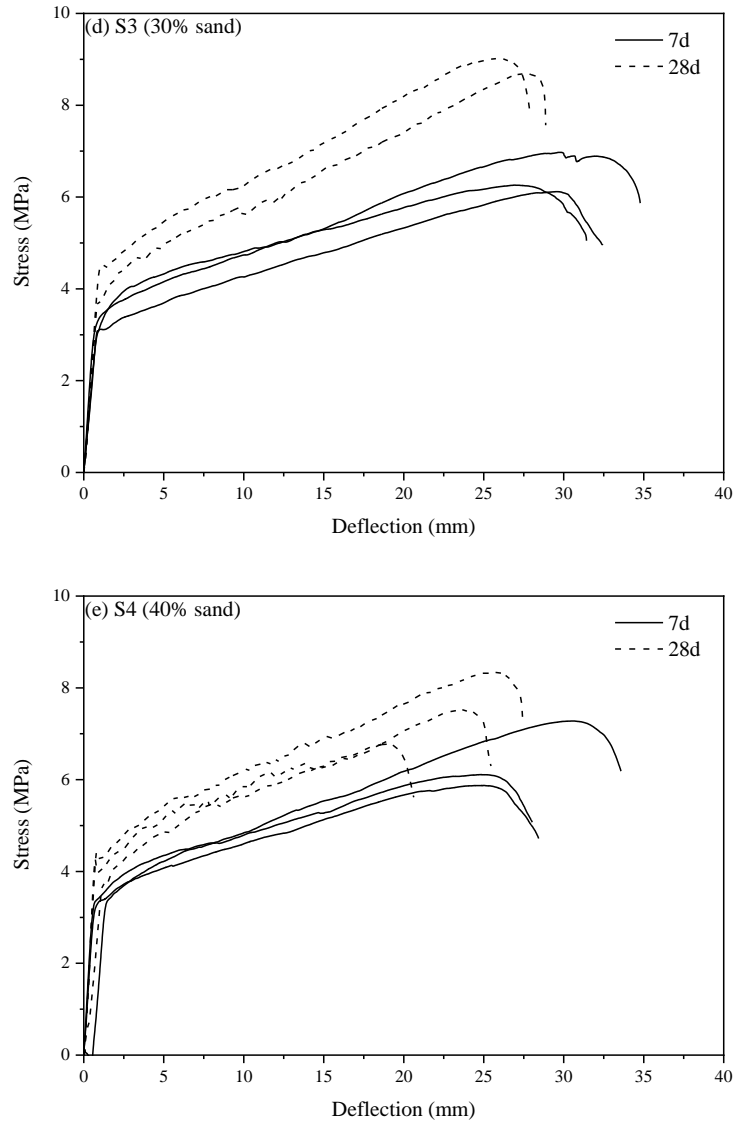
Figure 3-9 Typical stress-deflection curves of SHGC specimens with various sand

content at 7 and 28 d

3.6.5.2 Failure patterns and cracking

Figure 3-10 displays the typical failure pattern of SHGC specimens with a large deflection and multiple microcracks distributed over the tensile side of the specimen under four-point bending. During the bending test, the PVA fibres incorporated into the SHGC specimens can help them resist the tensile stress and release the strain energy due to fibre bridging effect. Hence, the SHGC specimens behaved like a bendable slab rather than failed suddenly after the ultimate flexural strength was reached. The SHGC specimens failed until a clear macro-crack appeared due to insufficient bridging effect of fibres.
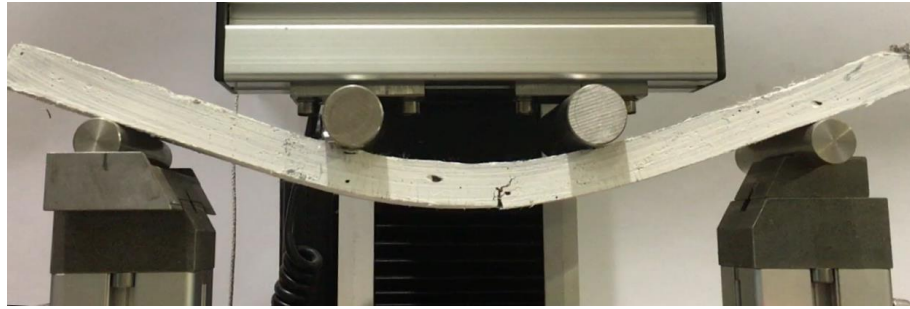
(a) Typical failure pattern of the specimen
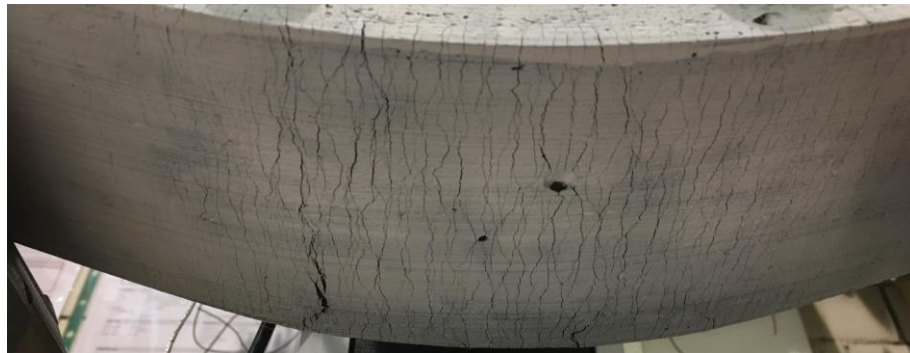
(b) Bottom view of microcracks
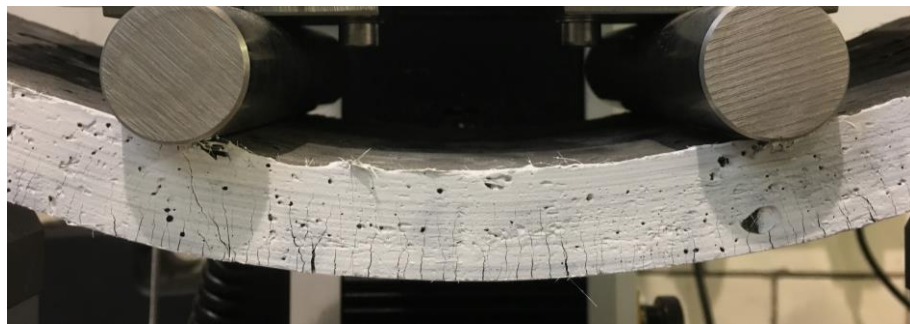
(c) Front view of microcracks

Figure 3-10 Typical failure mode and microcracks formed over the tensile side of SHGC specimen under four-point bending

Cracks were captured immediately after the test stopped and before unloading, because many microcracks generated during the test completely closed after unloading, which made it difficult to detect cracks fully on the surface of unloaded specimens (Nematollahi et al., 2016a, Nematollahi et al., 2015b). Crack number and average crack width of SHGC are listed in Table 3-3. Generally, the inclusion of fine silica sand resulted in a drop in the crack number but an increase in the average crack width of SHGC. Apart from SHGC paste without sand (SHGC0) that had an average crack number of 93 and average crack width of 68.2 μm, SHGC mortar with 10 wt% sand (S1) had 132 cracks and an average crack width of 58.60 μm. Compared to S1, the further incorporation of sand up

to 40 wt% (S4) led to a reduction in the crack number by 62.1% but an increase in the average crack width by 111.8%. The excessive incorporation of sand would adversely affect the interaction between matrix and fibres in the SHGC specimens and further reduce the fibre bridging effect, as a result of which the fracture resistance and defection hardening behaviour were reduced (Akkaya et al., 2000).
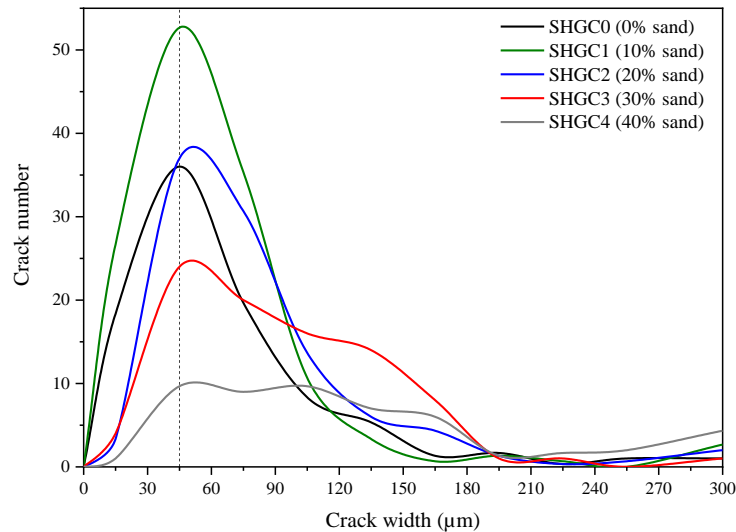
Figure 3-11 Effect of sand content on crack number and crack width of SHGC specimens under four- point bending

Figure 3-11 demonstrates the effect of sand content on the crack number and crack width distribution of SHGC specimens. The microcracks of SHGC specimens had widths of less than 300 μm. Among them, in S0, 58.4% of microcracks distributed in the crack width range from 0 μm to 45 μm. The addition of fine silica sand by 10 wt% (S1) resulted in a slight increase in the number of microcracks that distributed in the width range of no more than 45 μm, which took 59.2% of the total crack number. However, when the sand content further increased by 20 wt% (S2), 30 wt% (S3), and 40 wt% (S4), the percentage of microcracks with the width of no more than 45 μm was reduced to 40.6%, 31.5%, and 20.6% of the total crack number of SHGC specimens. With the increase of sand content, the SGHC specimens tended to have cracks with larger widths, which was associated with the brittleness of the geopolymer matrix.

3.6.5.3 Flexural strength

Figure 3-12 shows the effect of sand content on the flexural strength of SHGC specimens at 7 d and 28 d. At both 7 d and 28 d, the flexural strength of SHGC specimens increased

with the increase of sand up to 20 wt% (S2), but further adding sand up to 40 wt% (S4) led to a decrease in flexural strength of SHGC specimens. At 7 d, SHGC paste without sand (S0) had a flexural strength of 4.04 MPa. The increase of sand content up to 20 wt% (S2) significantly increased the flexural strength of SHGC specimens by 99.0% compared to S0, but the further increase of sand content decreased the flexural strength of SHGC specimens by 20.1% compared to S2. At 28 d, SHGC paste (S0) had the lowest flexural strength of 6.48 MPa. Compared to S0, the flexural strength was enhanced by 38.4% due to the incorporation of sand up to 20 wt% (S2). However, SHGC specimens containing 30 wt% (S3) and 40 wt% (S4) sand indicated a reduction in flexural strength by 1.3% and 15.8%, respectively, compared to S2, which can be ascribed to the fibre corrugation caused by the interaction between matrix and fibre (Akkaya et al., 2000). Overall, the flexural strength of SHGC specimen increased over time with geopolymerisation during the curing process. The increase of flexural strength resulted from the development of matrix strength and the bond strength between fibre and matrix. Moreover, PVA fibre is hydrophilic and the chemical bond between PVA fibre and geopolymer matrix can be developed during the curing process, which would also contribute to the development of flexural strength of SHGC. This may be the main reason why the number of microcracks became less with the increase of curing age.
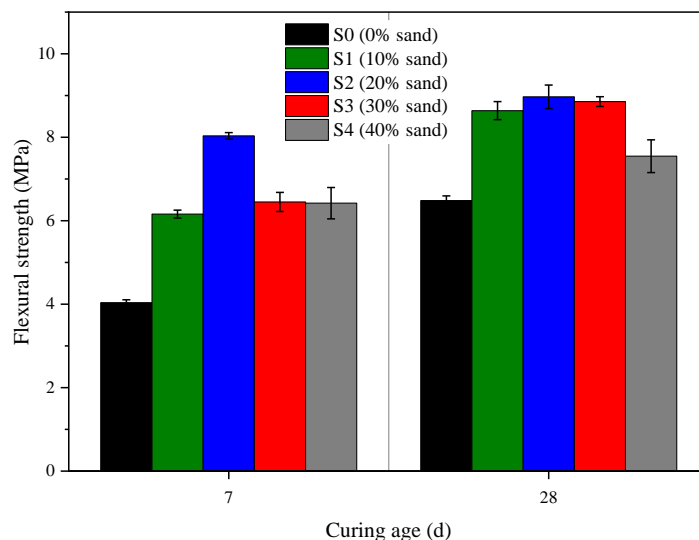
Figure 3-12 Effect of sand content on flexural strength of SHGC specimens at 7 d and 28 d

3.6.5.4 Flexural toughness and toughening mechanisms

Figure 3-13 shows the influence of fine silica sand on the flexural toughness of SHGC specimens at 7 d and 28 d. At 7 d, the SHGC paste without sand (S0) had a flexural toughness of 0.29 J, which was increased by 171.9% with the increase of sand content up to 40 wt%. However, at 28 d, the influence of sand content on the flexural toughness of SHGC specimens was different. S0 (0 wt% sand) had a flexural toughness of 0.48 J. S1 and S2 containing 10 wt% and 20 wt% sand showed a 44.1% and 94.0% respectively higher flexural toughness compared to SHGC0. Unlike 7 d, S3 and S4 containing 30 wt% and 40 wt% sand had a 6.8% and 10.8% respectively lower than S2. As discussed for the stress-deflection curves and flexural strength of SHGC specimens, the improvement of flexural toughness of SHGC specimens can be attributed to the increase of first-crack flexural strength, which was induced by the increased fracture toughness of the matrix due to the added sand and the developed strength of the matrix. However, the further addition of sand would result in the reduction in flexural strength due to the weakened interfacial transition zone between fibre and matrix.
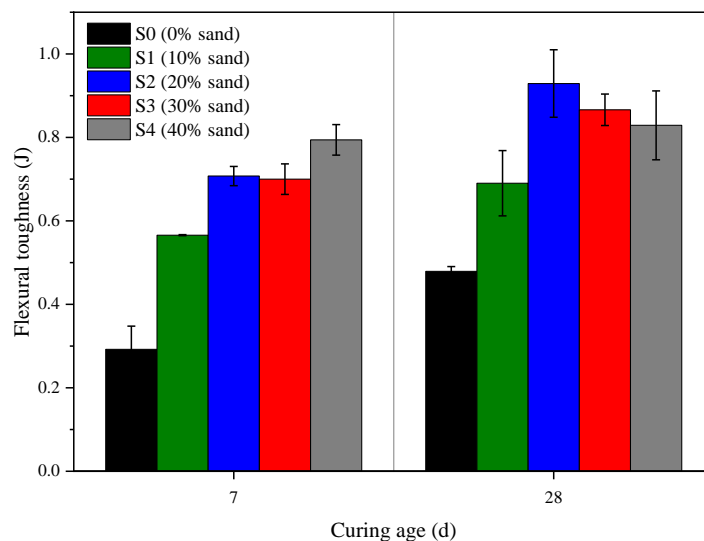
Figure 3-13 Effect of sand content on flexural toughness of SHGC specimens at 7 d and 28 d

Figure 3-14a-d demonstrate the toughening mechanisms of SHGC, including fibre rupture, fibre pull-out, and fibre bridging. Crack deflection and branching can also be observed in samples (see Figure 3-14e-f), which can be attributed to fibre corrugation.

Primarily, the development of deflection hardening behaviour of SHGC specimens can be ascribed to fibre bridging effect that limited the crack propagation within SHGC specimens under four-point bending. Once the crack initiated, the flexural stress was transferred to other parts of the specimens due to fibre bridging effect and prevent the sudden failure at the crack region. When the fibre at the crack region cannot resist the flexural stress, fibre rupture occurred, while fibre pull-out occurred when the flexural stress exceeded the bond strength between fibre and matrix. The increase of fine silica sand content resulted in fibre corrugation and crack branching, which adversely influenced the deflection hardening behaviour of SHGC specimens in terms of both flexural strength and flexural toughness (Noushini et al., 2018, Ranjbar et al., 2016b, Bhutta et al., 2017, Xu et al., 2017).
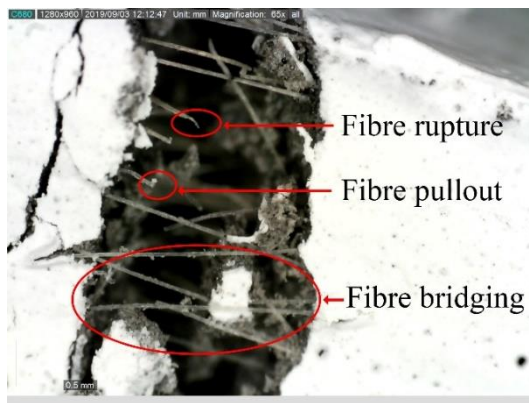
(a) Fibre toughening mechanism
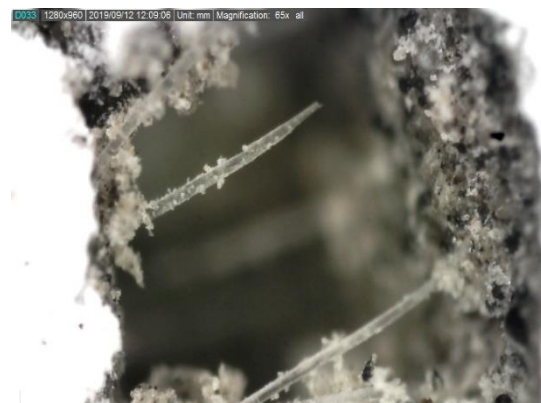
(b) Fibre rupture

(c) Fibre pullout
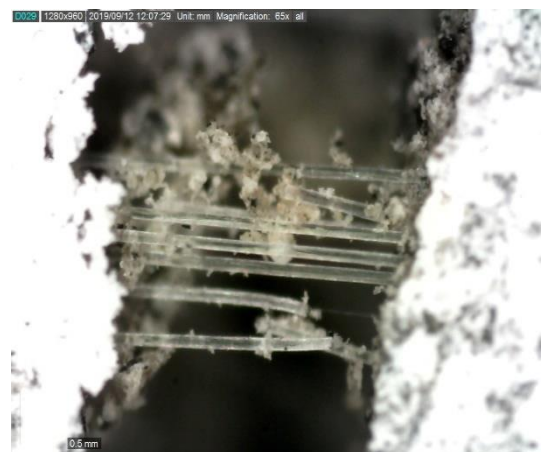
(d) Fibre bridging
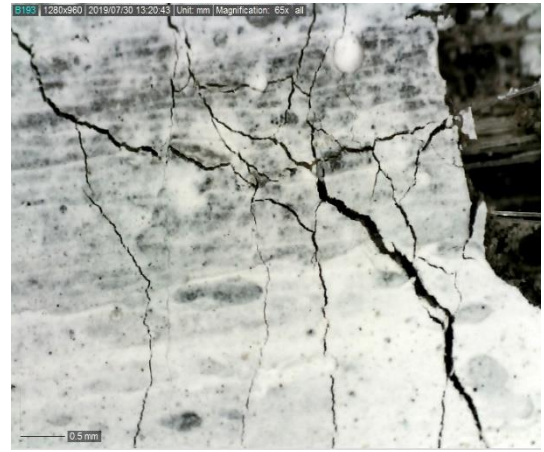
| (e) Fibre corrugation | (f) Crack deflection and branching |

Figure 3-14 Toughening mechanisms of SHGC specimens

3.7 Concluding remarks

This chapter developed the FA-GGBS based SHGC cured at ambient temperature, i.e. bendable geopolymer composites, and experimentally investigated its engineering properties considering various fine silica sand content (0%, 10%, 20%, 30%, and 40% by weight of the geopolymer binder). Fresh and hardened properties of SHGC specimens including flowability, setting time, drying shrinkage, compressive strength, and flexural strength were investigated. Deflection hardening behaviour of SHGC specimens was explored in terms of stress-deflection response, failure pattern and cracking, flexural strength, and flexural toughness and toughening mechanisms. Based on the results, the main conclusions can be drawn as follows:

- The incorporation of sand up to 40 wt% resulted in a reduction in workability of SHGC specimens for around 45% with the flow ranging from 68.3% to 37.3%. The increase of sand content up to 40 wt% marginally reduced the initial and final setting time of SHGC specimens by approximately 20%.

- The drying shrinkage of SHGC specimens was significantly decreased with the increase of sand content because of the restraining effect. The addition of 40 wt% sand reduced the drying shrinkage of SHGC specimens by 56.1% compared to SHGC paste.

- The compressive strength of SHGC was decreased with the increase of sand content. The incorporation of sand up to 40 wt% resulted in a decrease in compressive strength of SHGC specimens by 35.7%, 19.5%, and 33.4%, at 1 d, 7 d, and 28 d, respectively.

Under uniaxial compression, all SHGC specimens preserved almost the cubic shape at failure because of the fibre bridging effect.

- All SHGC specimens exhibited deflection hardening behaviour with large deflection and multiple microcracks distributed over the tensile side of the specimens under four-point bending. The SHGC specimens containing 10 wt% sand presented the largest value in crack number but the smallest value in average crack width, i.e. 132 microcracks and 58.6 μm, respectively. The increase of sand content resulted in the increased number of microcracks that had larger crack width. SHGC specimens with a longer curing age tended to have a higher flexural but lower flexural deflection.

- The flexural strength and flexural toughness of SHGC specimens were increased with the increase of curing age. At 28 d, compared to S0, adding sand up to 20 wt% resulted in the increase in flexural strength and flexural toughness by 38.4% and 94.0%, respectively, but the further increase of sand content reduced the flexural strength and flexural toughness. The changes in flexural strength and toughness were governed by fibre toughening mechanisms, including fibre rupture, fibre pull-out, and fibre bridging.

- The incorporation of 20 wt% fine silica sand can be suggested as the optimal mixture of FA-GGBS based SHGC considering the engineering properties.

Chapter 4 Micromechanics-based Design and Strain-hardening Behaviour of SHGC

4.1 Introduction

Based on the analysis in Chapter 3, the deflection hardening behaviour of SHGC, i.e. bending capacity, depends on the tensile properties of the material. Li et al. (Li, 1993, Li and Leung, 1992) developed the micromechanical modal that uses the pseudo strain-hardening (PSH) criteria as the design basis of SHCC, which requires a steady-state crack opening under tension. According to the literature review in Chapter 2, the occurrence of PSH in SHGC reinforced with random short fibres requires the two criteria to be met, including the strength-based criterion and energy-based criterion. Hence, this chapter mainly aims to experimentally investigate the micromechanical parameters of SHGC reinforced with 2% PVA fibre and validate the strength-based criterion and energy-based criterion for PSH criteria. Uniaxial tension test, single-crack tension test, and three-point bending test were conducted to obtain the micromechanical parameters, including the first cracking strength, maximum fibre bridging strength, crack tip toughness, and the maximum complementary energy.

4.2 Raw materials

Due to the limited quantity of raw materials used in Chapter 3, a group of raw materials sourced from different companies is used in Chapter 4 to analyse the micromechanical parameters of SHGC. Meanwhile, to ensure consistency of the following investigations, the same raw materials are used throughout Chapters 4-6.

Geopolymer was synthesised using low-calcium FA (equivalent to ASTM Class F (ASTM, 2012)) and GGBS as precursors, the chemical compositions and particle size distribution of which are presented in Table 4-1 and Figure 4-1, respectively. The specific gravities of FA and GGBS are 2.19 and 2.90, and their average particle sizes are 19.58 μm and 9.78 μm, respectively. A mixture of 10 M sodium hydroxide (SH) solution and sodium silicate (SS) solution with modulus ($SiO_2:Na_2O$ ratio) of 2.0 was used as alkaline activator. The SH solution was prepared by dissolving the SH powder in tap water and

then stored in the cupboard until its temperature became ambient. This allows the heat dissipation caused by the exothermic chemical reaction in the mixed solution (Ling et al., 2019). Based on the preliminary test, the SH solution and SS solution were added separately during the mixing to avoid the rapid setting of the SHGC specimens. As per a previous study (Wang et al., 2020a), the modified polycarboxylate-based superplasticiser (SP) (Sika ViscoFlow 3000) was added to improve the workability of SHGC and ensure a uniform fibre dispersion in SHGC.

Fine silica sand was used as aggregates, which has a specific gravity of 2.66 and a maximum and mean particle size of 250 μm and 130 μm, respectively. The particle size distribution of fine silica sand is also shown in Figure 4-1. The sand was used in surface saturated dry (SSD) condition with an absorption rate of zero, according to a preliminary absorption test. SHGC was reinforced with oil coated PVA fibre, which was supplied by Kuraray, Japan. The physical and mechanical properties of PVA fibre are presented in Table 4-2.

Table 4-1 Chemical compositions (wt%) of fly ash (FA) and ground granulated blast-furnace slag (GGBS).

Oxide	SiO_2	Al_2O_3	CaO	MgO	K_2O	Fe_2O_3	TiO_2	Na_2O	SO_3	LOI
FA	57.02	32.35	2.88	0.58	2.07	3.01	1.26	0.03	0.41	0.39
GGBS	31.85	17.31	41.20	6.13	0.33	0.34	0.62	0.03	1.78	0.41

Note: LOI (loss on ignition)

Table 4-2 Physical and mechanical properties of polyvinyl alcohol (PVA) fibre.

Fibre ID	Length (mm)	Nominal diameter (μm)	Aspect ratio	Density (g/cm^3)	Tensile strength (MPa)	Elastic modulus (GPa)
PVA	12	40	300	1.3	1600	41
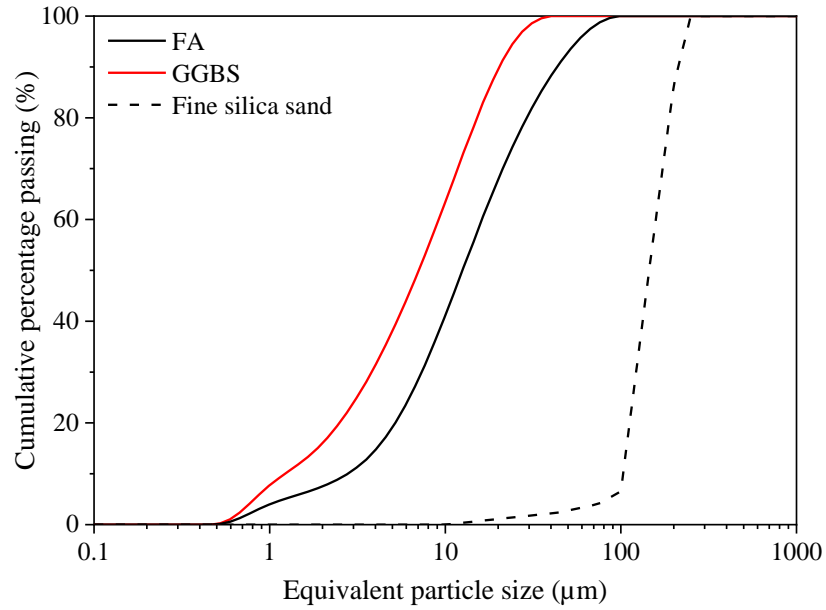
Figure 4-1 Particle size distribution of FA, GGBS and fine silica sand.

4.3 Mix proportions

Table 4-3 shows the mix proportions of SHGC. Based on a previous study (Wang et al., 2020a), the geopolymer binder was prepared with the FA/GGBS ratio of 0.8:0.2, SS/SH solution ratio of 2.0, and sand/binder ratio of 0.2. To ensure the flowability of the mix, the alkaline activator/binder ratio and SPs/binder ratio were determined as 0.45 and 0.01, respectively, where the activator/binder ratio denotes the weight ratio of alkaline activator composed of SH and SS solution to geopolymer binder consisting of FA and GGBS. No additional water was added. Herein, the studied parameter was the content of PVA fibre. For the mixture labels given in Table 4-3, "P" represents PVA fibre, and the denoted number stands for the fibre content, where P2 denotes the mixture containing 2% PVA fibre.

Table 4-3 Mix proportions of SHGC

Mix No.	Binder		Activator/binder	Sand/binder	SPs/binder	PVA (vol%)
	FA	GGBS				
P2	0.8	0.2	0.45	0.2	0.01	2.0

4.4 Specimen preparation

All SHGC specimens were prepared using a 10 L Hobart mixer, following the preparation steps described in previous chapter. The entire mixing process typically lasted approximately 8 min and 30 s. Firstly, all solid ingredients (FA, GGBS, and sand) were

added to the mixer and dry mixed for 1.5 min until a homogeneous mix was obtained. Then, the SH solution was added gradually into the dry mixture and mixed for 1 min, followed by the very slow addition of SS solution, which lasted around 2 min to avoid the rapid setting of the mixture. Afterwards, SPs were added to achieve an appropriate flowability and mixed for another 1 min. PVA fibres were then slowly incorporated into the mixture by rubbing and separating fibres to reduce the multifilament forms, followed by the mixing of the whole mixture for another 1min. The fresh SHGC was poured into the moulds immediately after the mixing and then vibrated to allow the air bubble to escape and compact the SHGC. All specimens were covered with cling film to prevent moisture loss after casting and stored in the ambient temperature (20 ± 2 °C) for 24 h. Then, the specimens were demoulded and stored in a standard curing room at an average temperature of 20 ± 2 °C and relative humidity of 95% until testing.

4.5 Test methods

Micromechanics-guided design is based on the determination of micromechanical parameters including the matrix and fibre bridging properties. The properties of the matrix include the first cracking strength (σ_{fc}) and the crack-tip toughness ($J_{tip} = K_m^2/E_m$), while the fibre bridging properties are the maximum fibre bridging strength (σ_0) and the maximum available complementary energy (J_b'). In this chapter, the uniaxial tension test, single-crack tension test, and three-point bending test were carried out to determine the micromechanical parameters.

4.5.1 Uniaxial tension test

Uniaxial tension test was performed according to JSCE Recommendations (Rokugo et al., 2009a) using a universal testing machine WDW-50E with a maximum loading capacity of 50 kN to determine the tensile properties and evaluate the strain-hardening behaviour of SHGC specimens. The uniaxial tensile loading with the displacement control at a rate of 0.5 mm/min was imposed on the dog-bone shaped specimens at 28 d of curing, the dimension of which is displayed in Figure 4-2. Two LVDTs (linear variable displacement transducers) were used and attached on both sides of the testing specimen, as illustrated in Figure 4-3. The mean values of tensile strength and strain capacity of three specimens were obtained, and the cracking characteristics of specimens were captured to explore the

fracture mechanism after the uniaxial tension test.
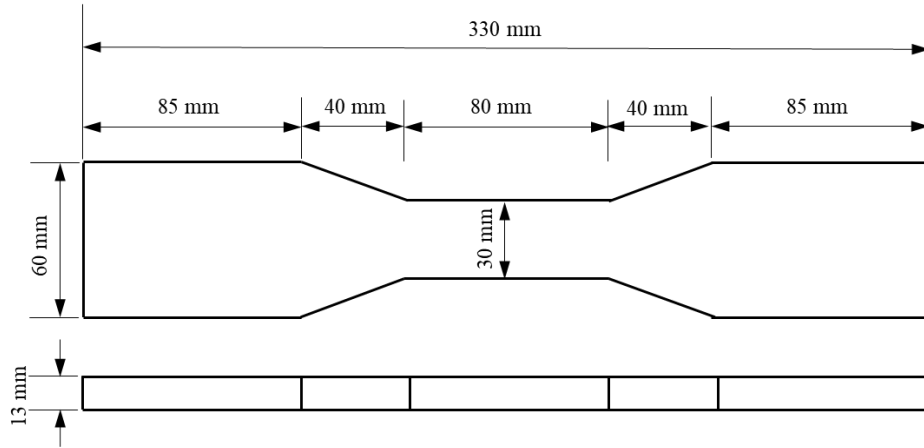
Figure 4-2 Dimensions of the dog-bone shaped specimen for the uniaxial tension test.
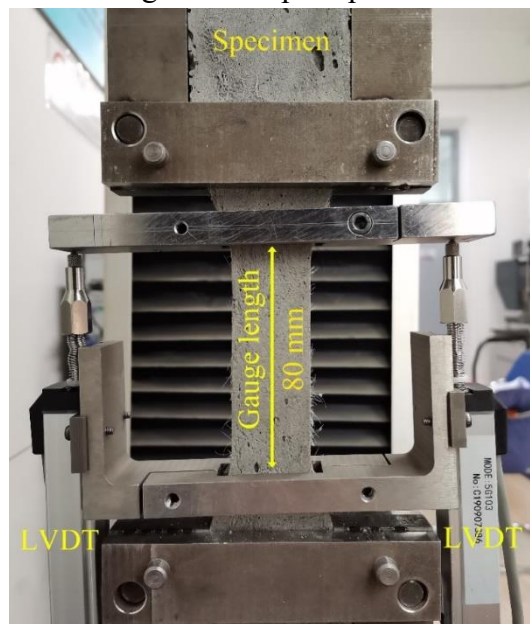
Figure 4-3 Setup of the uniaxial tension test.

4.5.2 Single-crack tension test

Single-crack tension test was conducted on dog-bone shaped specimens using a universal testing machine WDW-50E with a maximum loading capacity of 50 kN to determine the maximum fibre bridging strength (σ_0) and the maximum available complementary energy (J_b') (Kan et al., 2020a, Yu et al., 2017, Ohno and Li, 2018). The dimensions of the specimens and the setup of the single-crack tension test were the same as those shown in Figure 4-2 and Figure 4-3, respectively. Two LVDTs were used and attached on both sides of the testing specimen to measure the crack opening. Prior to testing, all specimens were cut with a diamond saw on the four faces in the centre to create a notch with a depth of 6.5 mm and 2 mm, respectively, as illustrated in Figure 4-4, where the shaded and unshaded

areas denote the remained area and the notched area, respectively. This was prepared to facilitate the formation of the single crack of specimens (Yu et al., 2017). It is worth noting that the thickness of the notch was less than 0.6 mm (Yu et al., 2017, Kan et al., 2020a). The mean values of three specimens at 28 d of curing were obtained.
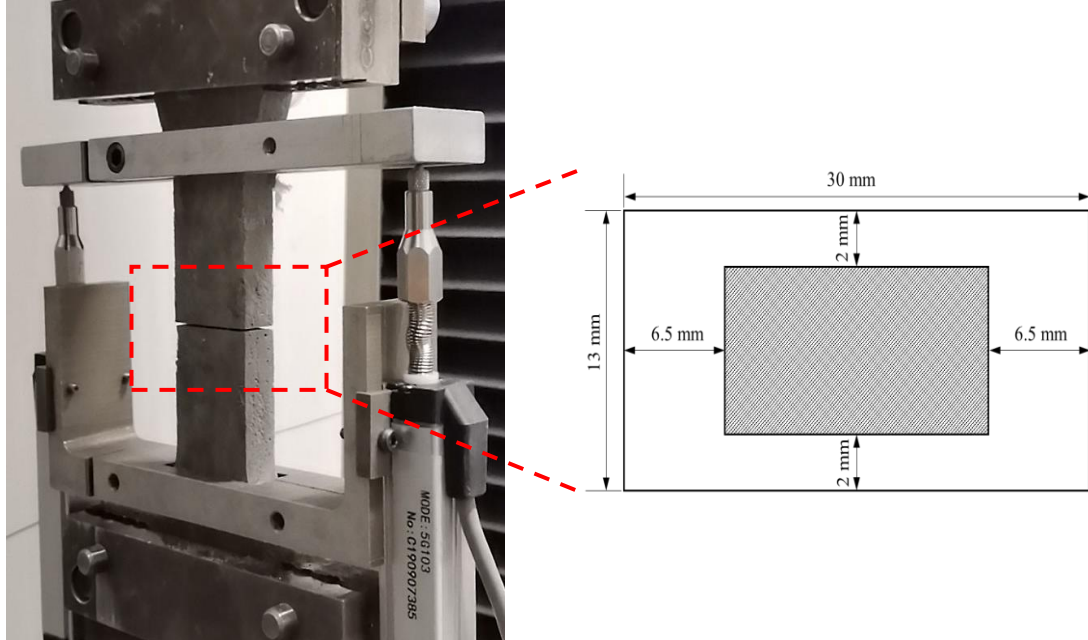
Figure 4-4 Setup and schematic illustration of the notched specimen for the single-crack tension test.

4.5.3 Three-point bending test

Three-point bending test was carried out to evaluate the fracture toughness and crack tip toughness of the matrix according to ASTM E399 (ASTM, 2020b) using a universal testing machine WDW-50E with a maximum loading capacity of 50 kN. Figure 4-5 shows the setup of three-point bending test. Three specimens of geopolymer mortar without fibres were used to prepare the single-edge notched prisms with a dimension of 40 × 40 × 160 mm and test after 28 d of curing. Prior to testing, a diamond cutting saw was used to create a notch of 16 mm in depth at the centre of the bottom surface. The relative notch depth ratio α (α = a/W) was kept as 0.4 for all specimens (hereby a = 16 mm, W = 40 mm). The clear span of specimens was 90 mm. The load was applied in displacement control at a rate of 0.5 mm/min during the test. The ultimate loads were recorded, based on which the fracture toughness (K_m) and crack tip toughness (J_{tip}) of the matrix can be calculated using the peak load as follows (Zhang et al., 2020):

$$K_m = \frac{1.5 P_{max} S \sqrt{\pi a}}{BW^2} \times f(\alpha)$$

<div align="right">(1)</div>

$$f(\alpha) = \frac{(0.68 - 0.744\alpha)}{(1 - 2.155\alpha + 1.161\alpha^2)} + 0.36 - 2.088\alpha + 4.611\alpha^2 - 6.499\alpha^3 + 4.232\alpha^4$$

<div align="right">(2)</div>

$$J_{tip} = K_m^2 / E_m$$

<div align="right">(3)</div>

Where P_{max} is the peak load B is the specimen width (mm), W is the specimen depth (mm), S is the loading span (mm), and a is the notch depth.
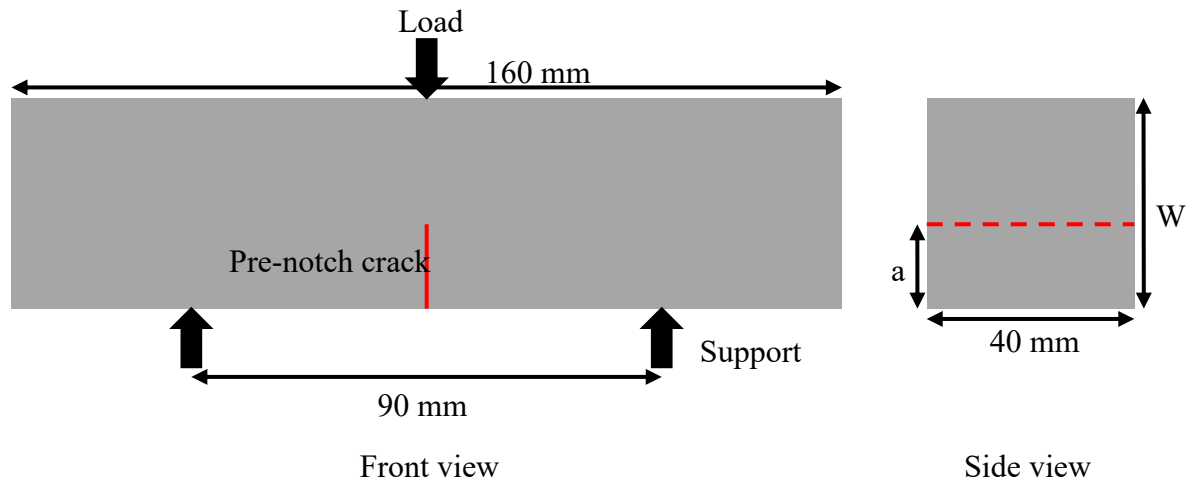
Figure 4-5 Schematic illustration of three-point bending test setup (notch depth a = 16 mm, specimen depth W = 40 mm).

4.6 Test results

4.6.1 Uniaxial tensile performance

Figure 4-6 displays the stress-strain curves of SHGC specimens reinforced with 2% PVA fibre. The uniaxial tensile performance characterised by first-crack strength (σ_{fc}), ultimate tensile strength (σ_{ult}), ultimate tensile strain (ε), and average crack width is summarised in Table 4-4. It can be observed that SHGC specimens reinforced with 2% PVA fibre all exhibited strain-hardening behaviour. For the curve of each specimen, the tensile stress increased linearly with the increase of tensile strain until it reached the first-crack strength. Then, the stress-strain curves became non-linear, and the slope of the curve decreased significantly, indicating that the specimens entered the strain-hardening stage. Finally, the maximum tensile stress of the specimen was reached, and the specimen failed.

SHGC specimens reinforced with 2% PVA fibre had an average first-crack strength, ultimate tensile strength, and ultimate tensile strain capacity of 2.68 MPa, 4.45 MPa, and 4.91%, respectively. The elastic modulus of SHGC specimens under uniaxial tension load was 4.34 GPa. The average crack width was 85.39 μm.
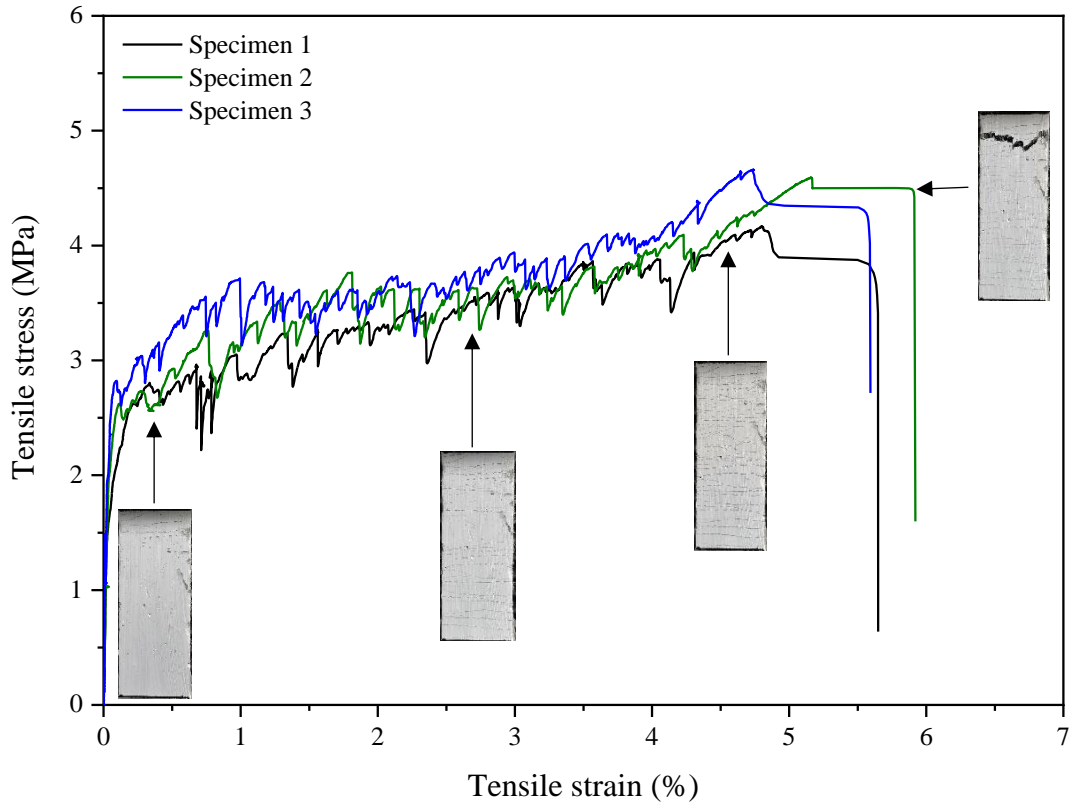
Figure 4-6 Uniaxial tensile stress-strain curves of SHGC specimens with 2% PVA fibre

Table 4-4. Uniaxial tensile performance of SHGC specimens with 2% PVA fibre.

Mix No.	Fist-crack strength (MPa)	Ultimate tensile strength (MPa)	Tensile strain capacity (%)	Elastic modulus (GPa)	Average crack width (μm)
P2	2.68	4.45	4.91	4.34	85.39

4.6.2 Fibre-matrix interface properties

Figure 4-7 shows the stress-crack opening curves of the SHGC specimens reinforced with 2% PVA fibre obtained from the single-crack tension test, which were used to calculate the fibre bridging complementary energy J_b' as follows:

$$J_b' = \sigma_o \delta_o - \int_0^{\delta_o} \sigma(\delta)d\delta \tag{4-3}$$

The fibre-matrix interface properties in terms of specific peak stress (σ_o), the corresponding crack opening (δ_o), and fibre complementary energy (J_b') are presented in

Table 4-5. It can be observed that the average value of the maximum fibre bridging strength of SHGC reinforced with 2% PVA fibre was 4.34 MPa. The crack opening width of SHGC specimens was 0.44 mm, and the complementary energy of SHGC specimens was 323.80 J/m^2.
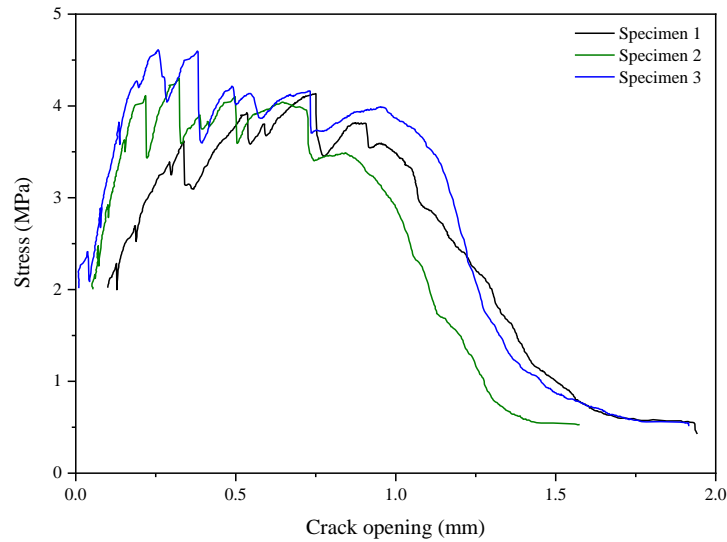
Figure 4-7 Stress-crack opening curves of the SHGC specimens obtained from the single-crack tension test

Table 4-5 Results of single-crack tension test (average value).

Mix No.	Peak stress (MPa)	Crack opening (mm)	Fibre complementary energy (J/mm^2)
P2	4.34	0.44	323.80

4.6.3 Matrix properties

The matrix properties were obtained by three-point bending test and characterised by fracture toughness (K_m) and crack tip toughness (J_{tip}), which were calculated by:

$$J_{tip} = K_m^2 / E_m \qquad (4\text{-}4)$$

The fracture toughness and crack tip toughness of the material were 0.329 $MPa \cdot m^{1/2}$ and 24.94 J/mm^2, respectively, as shown in Table 4-6.

Table 4-6 Matrix properties of SHGC

Mix No.	Fracture toughness (MPa· m$^{1/2}$)	Crack tip toughness (J/mm^2)
P2	0.329	24.94

4.7 Validation of micromechanics of SHGC

To achieve the desired strain-hardening behaviour with multiple microcracks, the developed SHGC should meet two criteria, including strength-based criterion and energy-

based criterion, which were explained in Chapter 2 and are validated in this section.

4.7.1 Strength-based criterion

The strength-based criterion requires that the first cracking strength of the matrix (σ_{fc}) shall not exceed the maximum fibre bridging strength (σ_0) to avoid exhausting fibre bridging capacity of the composite.

$$\sigma_{fc} \leq \sigma_0 \tag{4-5}$$

For SHGC reinforced with 2% PVA fibre, the first-crack strength of the matrix and the maximum fibre bridging strength were 2.68 MPa and 4.34 MPa, respectively, which met the strength-based criterion.

4.7.2 Energy-based criterion

The energy-based criterion indicates that the crack tip toughness of the matrix (J_{tip}) shall not exceed the fibre bridging complementary energy (J'_b), as expressed in the following equation, which aims to avoid Griffith-type crack propagation.

$$J_{tip} \leq \sigma_o \delta_o - \int_0^{\delta_o} \sigma(\delta) d\delta = J'_b \tag{4-6}$$

According to Kanda and Li (Kanda and Li, 1998), the saturation state of multi-cracking represents the state that no more multiple microcracks can initiate under the tensile load, and the saturation degree of multiple microcracks can be evaluated using the PSH index as follows:

$$PSH = J'_b / J_{tip} \tag{4-7}$$

It was demonstrated that the saturated multi-cracking can be achieved only when the PSH index of the composite exceeds 3.0 (Kanda and Li, 1998). The stable multi-cracking and strain-hardening behaviour of the composite can be easier to be achieved when the PSH value is larger (Kanda and Li, 2006b). The test results of SHGC reinforced with 2% PVA fibre indicate that the crack tip toughness of the matrix (J_{tip}) and the fibre bridging complementary energy (J'_b) were 24.94 J/mm^2 and 323.80 J/mm^2, respectively, and the corresponding PSH index (J'_b / J_{tip}) was 12.98 that met the energy-based criterion.

4.8 Concluding remarks

In this chapter, the micromechanical parameters of SHGC reinforced with 2% PVA fibre were obtained by conducting uniaxial tension test, single-crack tension test, and three-point bending test, and the PSH criteria including the strength-based and energy-based

criterion were validated. Based on the experimental results, the main conclusions can be drawn as follows:

- After 28 d curing, all specimens containing 2% PVA fibre exhibited strain-hardening behaviour with the average first-crack strength and ultimate tensile strength of 2.68 MPa and 4.45 MPa, respectively. Specimens reached a high tensile strain capacity of 4.91%, and the average crack width was 85.39 μm.

- The average value of the maximum fibre bridging strength was 4.34 MPa with the crack opening width of 0.44 mm. The maximum complementary energy was 323.80 J/m^2. The SHGC matrix had a fracture toughness of 0.329 $MPa \cdot m^{1/2}$ and crack tip toughness of 24.94 J/mm^2, respectively.

-

- The obtained micromechanical parameters showed that both the strength-based and energy-based criteria were fulfilled. The first-crack strength of the matrix (2.68 MPa) was smaller than the maximum fibre bridging strength (4.34 MPa), and the crack tip toughness of the matrix (24.94 J/mm^2) was smaller than the fibre bridging complementary energy (323.80 J/mm^2), which met both the strength-based and energy-based criteria. Hence, the micromechanical theory of SHGC was validated.

Chapter 5 Effect of PVA Fibre on Engineering Properties of SHGC

5.1 Introduction

The pseudo strain-hardening behaviour of SHGC has been validated in Chapter 4 by experimentally investigating the micromechanical parameters of SHGC reinforced with 2% PVA fibre. Both strength-based criterion and energy-based criterion were satisfied: (1) the first cracking strength of the matrix (2.68 MPa) was smaller than the maximum fibre bridging strength (4.34 MPa); and (2) the crack tip toughness of the matrix (24.94 J/mm^2) was smaller than the fibre bridging complementary energy (323.80 J/mm^2). Based on the validated SHGC, this chapter presents an experimental study on the effect of polyvinyl alcohol (PVA) fibre content (0%, 1%, 1.5%, and 2%) on engineering properties of FA-GGBS based SHGC cured at ambient temperature in terms of flowability, drying shrinkage and mechanical properties, with a special focus on strain-hardening behaviour and dynamic compressive behaviour. Single-crack tension test and three-point bending test were conducted to determine the micromechanical properties of SHGC.

The results presented in this chapter were published as a journal article, with the following reference:

Yi Wang, Hui Zhong, Mingzhong Zhang, Experimental study on static and dynamic properties of fly ash-slag based strain-hardening geopolymer composites, *Cement & Concrete Composites,* 129 (2022) 104481.

5.2 Raw materials, mix proportions, and specimen preparation

In this chapter, raw materials used to prepare specimens as well as the mix proportions of geopolymer matrix were the same to that used in Chapter 4, which were kept constant for all mixtures. The studied parameter was the content of PVA fibre. The mix proportions used in this chapter are given in Table 5-1, where "P" represents PVA fibre, and the denoted number stands for the fibre content. For instance, P0 represents the mixture without fibre, and P2 represents the mixture containing 2% PVA fibre. All specimens were prepared following the same procedure introduced in Section 4.4.

Table 5-1 Mix proportions of SHGC

Mix no.	Binder		Activator/binder	Sand/binder	SPs/binder	PVA (vol%)
	FA	GGBS				
P0	0.8	0.2	0.45	0.2	0.01	0
P1	0.8	0.2	0.45	0.2	0.01	1.0
P1.5	0.8	0.2	0.45	0.2	0.01	1.5
P2	0.8	0.2	0.45	0.2	0.01	2.0

5.3 Test methods

A series of tests including flow table test, drying shrinkage test, static compression test, uniaxial tension test, static splitting tenson test, and SHPB test were conducted to investigate engineering properties of SHGC. As the details about flow table, drying shrinkage and uniaxial tension tests have been introduced above, herein, only the static compression test, static splitting tension test, and SHPB test are described below.

5.3.1 Static compression test

Static compression test was carried out according to ASTM C109-16 (2020a) on specimens with a size of 50 × 50 × 50 mm. Given that the strength of concrete would be affected by the specimen size, many studies determined the dynamic increase factor (DIF) using the static and dynamic compressive strengths that were measured using the same specimen size (Ross et al., 1995, Zhang et al., 2007, Li et al., 2021b). Thus, cylindrical specimens with 100 mm diameter and 50 mm height were tested to estimate the DIF at various strain rates. All specimens were tested at 28 d using the machine CONTROLS C4600/FR with a maximum load capacity of 2000 kN. The loading rate was 1200 N/s. Three specimens were tested, and the mean value was considered as the compressive strength.

5.3.2 Static splitting tension test

Static splitting tension test was conducted to evaluate the static splitting tensile strength using cylindrical specimens with a diameter of 100 mm and height of 50 mm. For each mixture, the average value of three specimens was used. The static splitting tensile strength can be calculated by (Zhong and Zhang, 2021):

$$f_{st} = k \times 2F_p/\pi DB$$

(5-1)

where f_{st} is the splitting tensile strength of the specimen, k is the coefficient related to

the loading angle (0.95 for $2\alpha = 20°$), F_p is the peak load in the splitting tension test, D is the diameter of the specimen (100 mm), and B is the depth of the specimen (50 mm).

5.3.3   Split Hopkinson pressure bar (SHPB) test

Split Hopkinson pressure bar (SHPB) test was conducted to measure the dynamic compressive behaviour of SHGC at various strain rates. The SHPB machine used in this study was made of a superior alloy steel material and had a diameter of 100 mm, the lengths of bullet, incident, transmission, and absorbing bars of which were 600, 5000, 3500, and 1200 mm, respectively. Three cylindrical specimens with a diameter of 100 mm and a height of 50 mm were used to obtain the mean value of dynamic compressive properties of SHGC specimens at 28 d. The specimens were sandwiched between the incident and transmission bars before the SHPB test, as illustrated in Figure 5-1. At the beginning, the start button on the computer system was clicked, and then the bullet started to be propelled by the compressed nitrogen. The incident bar was then impacted by the 100 mm bullet and the impact velocity was measured by the speed detection device shown in Figure 5-1. Subsequently, an incident pulse $(\varepsilon_i(t))$ was generated and known as the incident wave. At the interface between the incident bar and the specimen, the incident wave was partially reflected from the specimen due to the impedance difference, which is known as reflected pulse $(\varepsilon_r(t))$ (Xiao et al., 2015). The remaining wave was transmitted through the specimen into the transmission bar called transmission pulse $(\varepsilon_t(t))$.These strain pulses were recorded using two strain gauges (see Figure 5-1) which were demonstrated in the form of strain against time. During the SHPB test, the pulse shaper with the size of 60 mm in diameter and 2 mm in height was mainly used to achieve the stress equilibrium to ensure the reliability and accuracy of SHPB test results (W. Chen and Song, 2011, Yu et al., 2021). Figure 5-2 displays an example of checking the stress equilibrium. It can be observed that the sum of incident pulse and reflected pulse has a good match with the transmission pulse, which confirms that the stress equilibrium along the specimen thickness has been reached. The time histories of stress $(\sigma_s(t))$, strain $(\varepsilon_s(t))$, and strain rate $(\dot{\varepsilon}_s(t))$ were determined using the following equations (W. Chen and Song, 2011):

$$\sigma_s(t) = \frac{E_0 A_0}{2A_s}[\varepsilon_i(t) + \varepsilon_r(t) + \varepsilon_t(t)]$$

(4)

$$\varepsilon_s(t) = \frac{C_0}{l_s}\int_0^t [\varepsilon_i(t) - \varepsilon_r(t) - \varepsilon_t(t)]\, dt$$

(5)

$$\dot{\varepsilon}_s(t) = \frac{C_0}{l_s}[\varepsilon_i(t) - \varepsilon_r(t) - \varepsilon_t(t)]$$

(6)

where E_0 is the elastic modulus of the bars (MPa), A_0 is the cross-sectional area of the bars (mm^2), A_s is the cross-sectional area of the tested specimen (mm^2), C_0 is the longitudinal wave velocity of the bars (m/s), and l_s stands for the thickness of the tested specimen (mm).

The dynamic compressive and splitting tensile behaviours of SHGC were investigated at different strain rates, which were produced by various impact velocities. Three groups of impact velocity were applied, including low impact velocity of around 6 m/s, medium impact velocity of about 8 m/s, and high impact velocity of approximately 10 m/s, which were used to differentiate the failure patterns of specimens from low strain rate to high strain rate. For each mixture at each impact velocity, three specimens were used to obtain the average value of dynamic compressive properties.
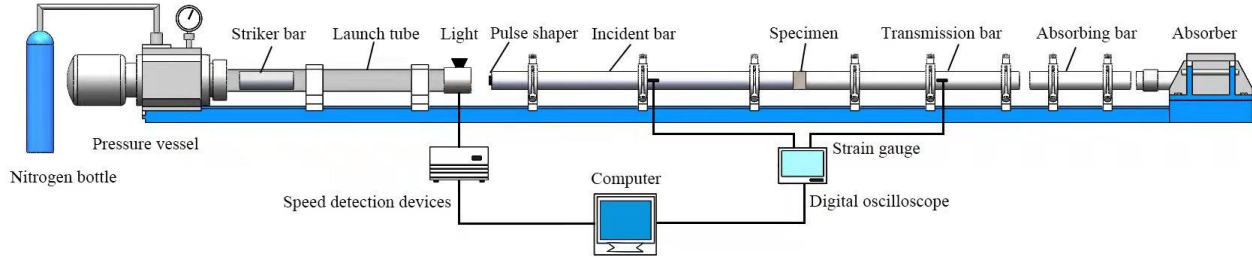
Figure 5-1 Schematic diagram of splitting Hopkinson pressure bar (SHPB) testing system (Chen et al., 2020).
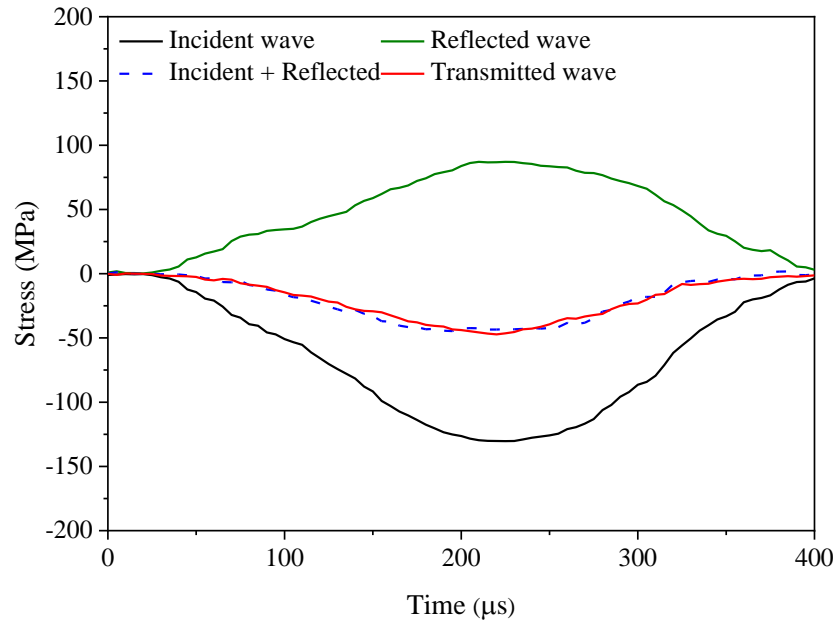
Figure 5-2 An example of checking the stress equilibrium.

5.4 Results and discussion

5.4.1 Flowability

Figure 5-3 shows the flow values of fresh SHGC mixtures with different fibre content. Better workability can be reflected by higher flow value, and therefore the mix can be easier for casting and compacting. As seen in Figure 5-3, the flow values of fresh SHGC mixtures reduced with the increase of fibre content. The geopolymer mortar without fibre (P0) had a flow value of 94.66%. Compared to P0, when the fibre content was increased to 1%, 1.5%, and 2%, the flow value of the fresh mixture was reduced by 13.73%, 22.89%, and 26.06%, respectively. The reduction in flowability of SHGC with the increase of fibre content agrees well with that presented in (Wang et al., 2020a, Zhong and Zhang, 2021, Farooq et al., 2019), which can be ascribed to the contact mechanism between PVA fibres in geopolymer mortar (Ranjbar and Zhang, 2020). Therefore, the overall movement of the fresh SHGC was confined, resulting in an increased shear resistance.
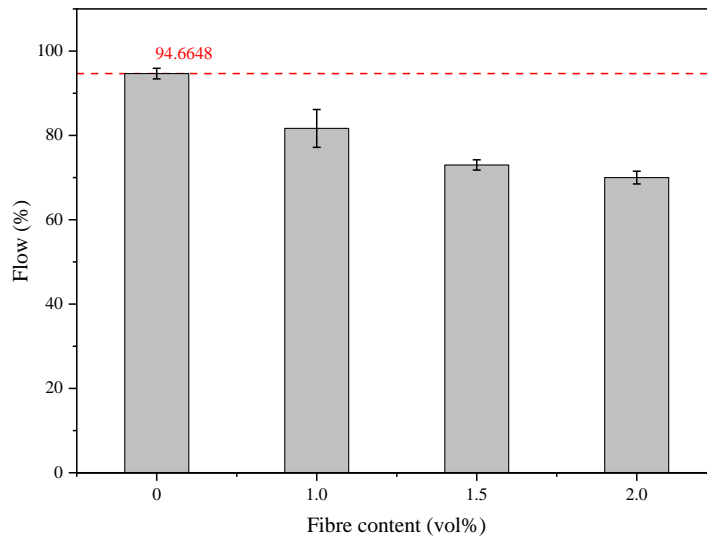
Figure 5-3 Flowability of fresh SHGC specimens with various fibre content

5.4.2 Drying shrinkage

Figure 5-4 shows the drying shrinkage of all mixtures with various fibre content. Overall, all specimens exhibited a sharp drop in shrinkage at early ages due to the evaporation of capillary water from internal (with higher relative humidity) to external environment (with lower relative humidity) through pore network of SHGC (Yang et al., 2017). With the increase of curing age, the drying shrinkage reduced, which can be ascribed to the resistance of volume deformation of hardened SHGC induced by the rigid zeolite structure formed during geopolymerisation (Yang et al., 2017, Mastali et al., 2018b).

Overall, the drying shrinkage of SHGC specimens at 28 d was decreased with the increase of fibre content, as seen in Figure 5-4. The geopolymer mortar without fibre (P0) had a 28 d drying shrinkage of -0.77%. Compared with P0, the incorporation of PVA fibre by 1%, 1.5%, and 2% resulted in the reduction of drying shrinkage by 31.33%, 57.25%, and 48.84%, respectively. The addition of PVA fibre up to 1.5% resulted in a decrease in drying shrinkage because of the restriction effect by PVA fibre. As the fibre content increased from 1.5% to 2.0%, a rise in drying shrinkage of SHGC can be observed, which can be ascribed to the fibre corrugation and weak fibre-matrix interface due to the poor compaction of the composites and weak interaction between fibre and matrix. The weak interaction could lead to debonding by expanding the gap between fibre and its surrounding matrix, which curtailed the stress transfer in SHGC specimens and reduced the resistance to shrinkage (Ranjbar et al., 2016b). Moreover, the excessive addition of PVA

fibre can result in poor compaction and higher porosity of SHGC, where the formed pore network allows the moisture to move towards the surface of specimens (Afroughsabet and Teng, 2020, Zhong et al., 2019, Ranjbar and Zhang, 2020).
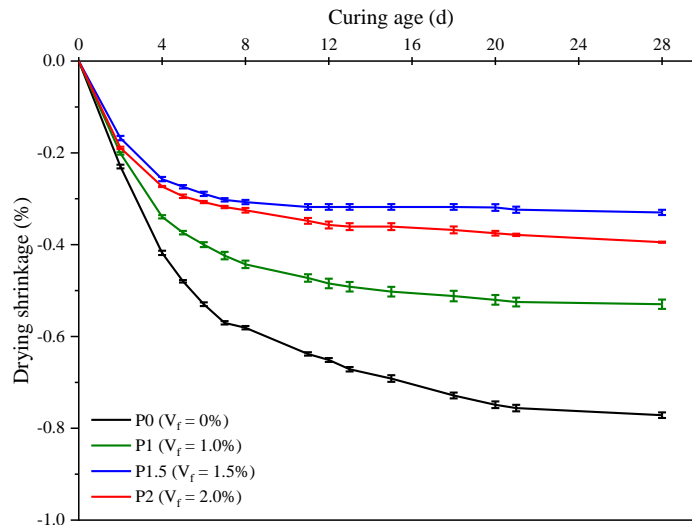
Figure 5-4. Drying shrinkage of SHGC specimens with various fibre content.

5.4.3 Strain-hardening behaviour

This section presents the results of the static uniaxial tension test on SHGC specimens with various fibre content, including stress-strain response, failure patterns, tensile strength, and micromechanical analysis. Table 5-2 summarises the uniaxial tensile properties of all mixtures.

Table 5-2 Uniaxial tensile performance of all mixtures (average values).

Mix No.	Fist-crack strength (MPa)	Ultimate tensile strength (MPa)	Tensile strain capacity (%)	Average crack width (μm)
P0	-	1.04	0.03	-
P1	1.13	2.61	3.75	142.86
P1.5	1.84	4.37	5.15	111.35
P2	2.68	4.45	4.91	85.39

5.4.3.1 Stress-strain response

Figure 5-5 displays the uniaxial tensile stress-strain curves of all mixtures. Due to the unexpected failure of one out of three specimens for P0 and P1 before test setup, the stress-strain response of two specimens is presented for them, while three specimens were adopted for P1.5 and P2. The reference mixture (P0) exhibited a brittle failure and failed immediately after the crack initiated in the specimen at the elastic stage, while all SHGC specimens demonstrated strain-hardening behaviour under uniaxial tension. For SHGC

89

specimens, the tensile stress increased linearly with the increase of tensile strain until it reached the first-crack strength. Then, the stress-strain curves became non-linear, and the slope of the curve decreased significantly, suggesting that the specimens entered the strain-hardening stage. Finally, the maximum tensile stress was reached, and the specimens failed.

As shown in Figure 5-5 and Table 5-2, P0 had an ultimate tensile strain of 0.03%, and the incorporation of fibres significantly enhanced the tensile strain capacity of the material. For SHGC specimens, the content of the incorporated PVA fibres had a significant influence on the stress-strain response of SHGC specimens in terms of first-crack strength, strain-hardening stage, and ultimate strain. SHGC specimens reinforced with 1% fibre had a first-crack strength of 1.13 MPa, and an ultimate strain of 3.75%. The strain-hardening stage experienced obvious serrated lines due to the continuous crack initiation and propagation up to failure, which represented wider cracks compared with P1.5 and P2 that had smoother lines. When the fibre content was increased to 1.5%, the first-crack strength and ultimate strain of SHGC specimens were increased by 62.30% and 37.30%, respectively. SHGC specimens with 2% fibre (P2) had a fist-crack strength of 2.68 MPa, which was 45.72% higher than that of P1.5, while its tensile strain was 4.89% lower than that of P1.5. As compared with P0, SHGC specimens reinforced with various fibre content resulted in the ultimate tensile strain capacity of 147-201 times that of P0, which can be attributed to the fibre-bridging effect.
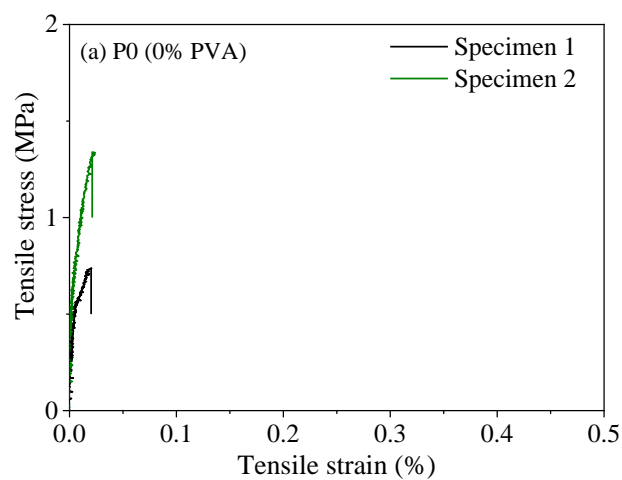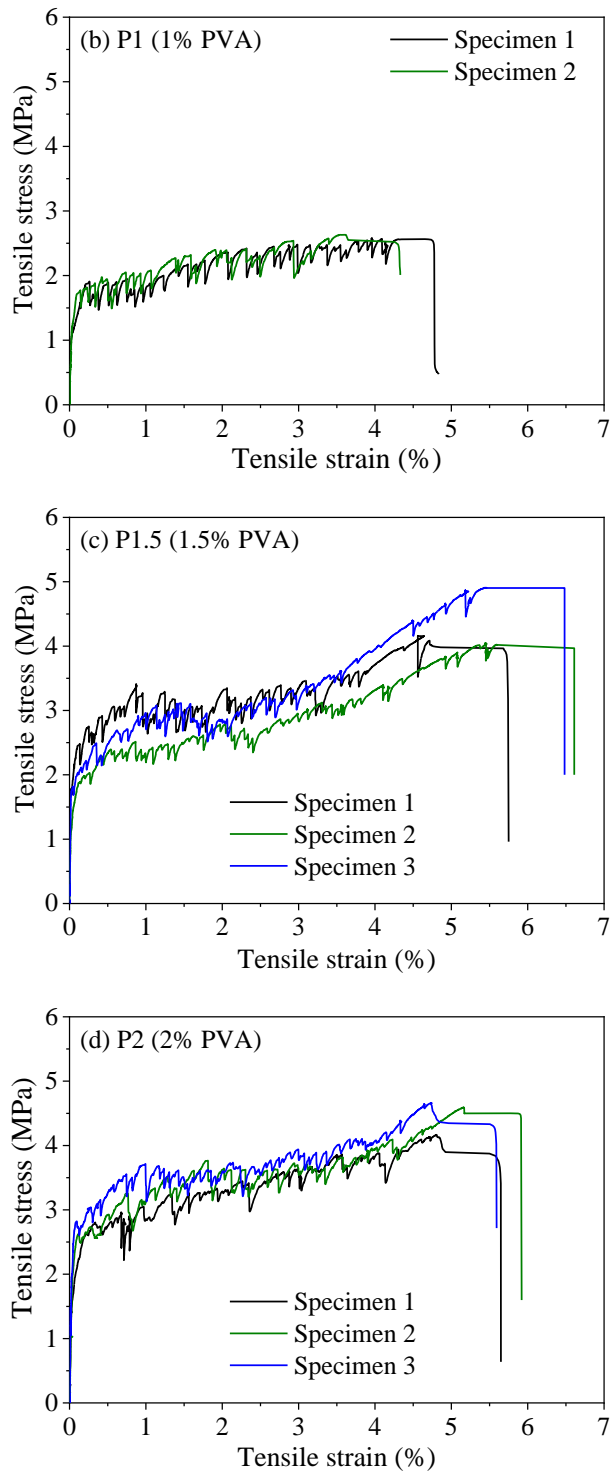
Figure 5-5 Tensile stress-strain curves of all mixtures.

5.4.3.2 Failure patterns

The cracking behaviour is critical for structural design, as the crack control ability of the material contributes to the serviceability and durability of the structures (Li, 2019). Figure 5-6 demonstrates the typical failure patterns of SHGC mixtures under uniaxial tension. All cracks were captured right before unloading to avoid difficulties of tracing the cracks due to the possible closure of microcracks when the load was removed (Nematollahi et al.,

2015a). Here, only the tested area within the gauge length (30 × 80 mm) was presented. As expected, all SHGC specimens exhibited multiple micro-cracking behaviour under uniaxial tension, leading to strain-hardening behaviour, while the microcrack features varied with the fibre content in SHGC, which is consistent with the stress-strain curves of the corresponding mixtures shown in Figure 5-5. Among them, P1 showed the least crack number but wider crack width (142.86 μm) due to the less efficient fibre bridging effect. When the fibre content was increased to 1.5% and 2%, the crack number increased (see **Fig. 11**) while the crack width reduced to 111.35 μm and 85.39 μm, respectively (see **Table 4**), which can be attributed to the more significant fibre bridging effect induced by higher fibre content. Compared with P1.5, the tensile strain of P2 exhibited a marginal reduction of 4.89% on average, while the crack width of P2 dropped by about 23.31% due to the increased fibre bridging effect, leading to more microcracks in P2 under uniaxial tension.

| (a) P1 | (b) P1.5 | (c) P2 |
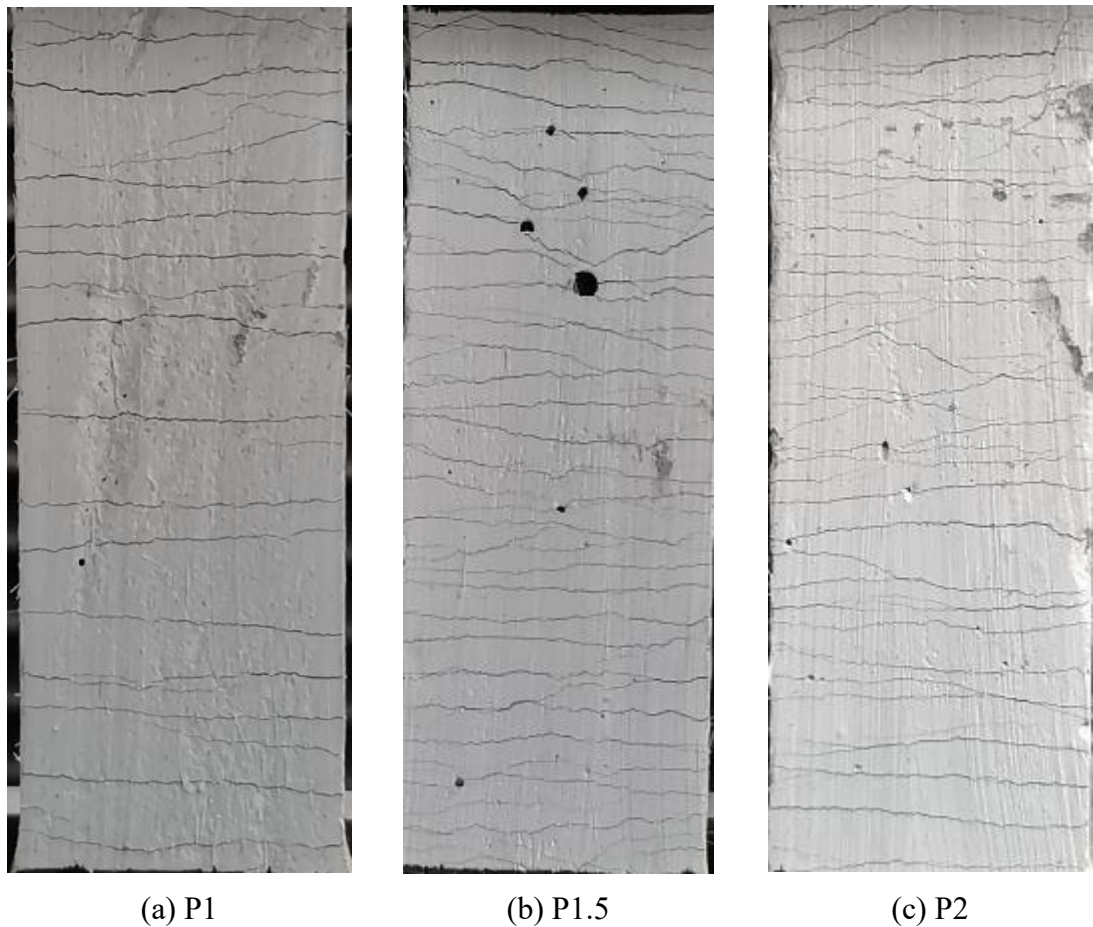
Figure 5-6 Typical failure patterns of SHGC mixtures.

5.4.3.3 Tensile strength

Figure 5-7 demonstrates the effect of fibre content on the ultimate tensile strength of all

mixtures, indicating that the increase of fibre content resulted in a significant enhancement of tensile strength. P0 had a tensile strength of 1.04 MPa, which was improved by 151.25%, 321.35%, and 331.07%, respectively, when adding 1%, 1.5%, and 2% PVA fibres. This agrees with the finding by a previous study (Zhong and Zhang, 2021) that over 100% increase in tensile strength of geopolymer mortar can be achieved by adding 2% PVA fibre. This can be ascribed to the fibre bridging effect, where the number of fibres that provide efficient bridging tends to increase when more fibres are added.

Figure 5-8 displays the toughening mechanisms of SHGC specimens, including fibre bridging, fibre rupture and fibre pull-out. Strain-hardening behaviour of SHGC can be attributed to the incorporation of PVA fibres, which limited the initiation and propagation of microcracks because of the fibre bridging effect. Once the bond strength between fibre and matrix was not enough to resist the tensile stress, the fibre pull-out occurred, while the fibre rupture happened when the tensile stress exceeded the tensile strength of PVA fibre.
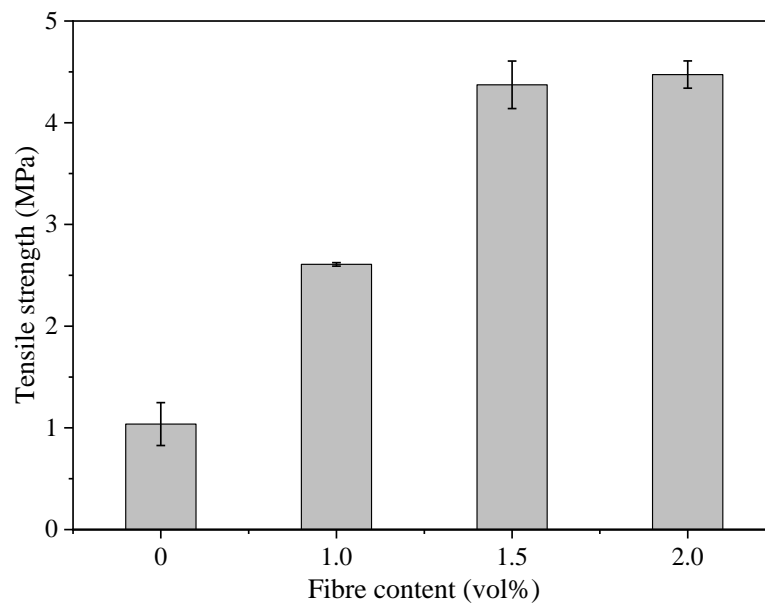
Figure 5-7 Effect of PVA fibre content on tensile strength of SHGC.
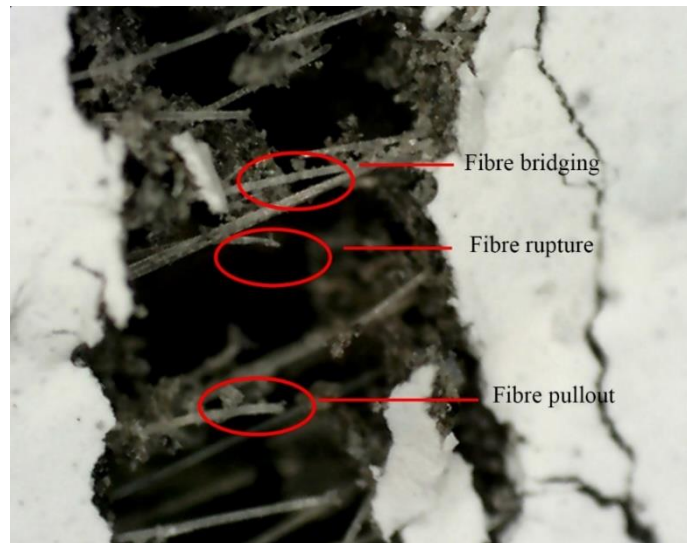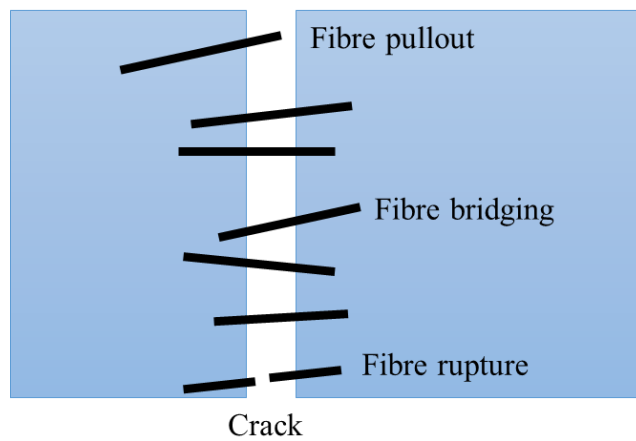
Figure 5-8 Toughening mechanisms of SHGC specimens: schematic and digital image.

5.4.3.4 Micromechanical analysis

As mentioned above, pseudo strain-hardening behaviour requires the satisfaction of two criteria, including strength-based and energy-based criteria. Micromechanical parameters of SHGC mixtures were obtained from uniaxial tension, single-crack tension, and three-point bending tests. Table 5-3 presents the single-crack tension test results and micromechanical parameters of P1, P1.5, and P2. It can be observed that the first-crack strength was smaller than peak stress for all mixtures, and the pseudo strain-hardening (PSH) index (J_b'/J_{tip}) of all SHGC specimens exceeds 3, indicating that all mixtures satisfied both the strength-based and energy-based criteria for SHGC (Kanda and Li, 1998). It was demonstrated that the strain-hardening behaviour along with saturated/stable multiple micro-cracking can be achieved only when the PSH index of the composite exceeds 3, and they can be easier to be achieved when the PSH value is larger (Zhong and Zhang, 2021).

Table 5-3 Results of single-crack tension test and micromechanical parameters of SHGC mixtures.

Mix No.	Single-crack tension test results			Micromechanical parameters		
	Peak stress (MPa)	Crack opening (mm)	Fibre complementary energy (J/mm^2)	First crack strength (MPa)	Crack tip toughness (J/mm^2)	PSH index
P1	3.21	0.34	219.19	1.13	24.94	8.79
P1.5	3.56	0.27	236.32	1.84	24.94	9.48
P2	4.34	0.44	323.80	2.68	24.94	12.98

5.4.4 Static compressive behaviour

Figure 5-9 shows the typical failure patterns of all cubes under static compression. The incorporation of PVA fibre altered the failure pattern of geopolymer composites from fragile to ductile mode. Geopolymer specimens without fibre failed following the typical fragile failure pattern of normal cementitious materials, i.e., two pyramid failure (Figure 5-9a), while SHGC specimens containing PVA fibre regardless of fibre content presented the shape integrity up to the end of the test, where a series of cracks can be observed (Figure 5-9b-d). The change of the failure pattern can be attributed to the bridging effect due to additional fibres, which resist sliding and propagation of cracks and constrain the lateral expansion subjected to compressive load (Choi et al., 2015, Wang et al., 2020b). Similar to cubes, failure patterns of cylinders were changed with the incorporation of PVA fibre. Geopolymer mortar without fibre failed suddenly in a brittle manner, while SHGC specimens showed crushing failure, where shape integrity was retained, and vertical cracks can be observed through specimens surrounding the inner core.

Figure 5-10 shows the typical failure patterns of all cylinders under static compression. Similar to cubes, failure patterns of cylinders are altered by the incorporation of PVA fibre. Geopolymer mortar (P0) failed with the two pyramid failure. SHGC specimens show crushing failure, where shape integrity was retained, and vertical cracks were observed through specimens surrounding the inner core.

Figure 5-11 displays the compressive strength of all mixtures obtained from cubes and cylinders. It should be mentioned that the compressive strength of all tested cylinders has multiplied a factor (0.82) when the aspect ratio (length-to-diameter ratio) of the specimen is less than 1.75 as per ASTM C39/39M-21 (ASTM C39/39M-21, 2021). For cubes, the addition of PVA fibre regardless of fibre content resulted in a reduction of compressive strength. The geopolymer mortar without fibre (P0) had a compressive strength of 45.67 MPa. As the PVA fibre content was increased by 1%, 1.5%, and 2%, the compressive

strength of geopolymer mortar was reduced by 21.82%, 17.01%, and 28.25%, respectively, which is in consistence with previous studies on geopolymer composites (Wang et al., 2020a, Zhong and Zhang, 2021, Xiao et al., 2021) and cementitious composites containing PVA fibres (Yu et al., 2020, Lin et al., 2020). As mentioned previously, incorporating PVA fibre can avoid the crack extension via bridging the micro-cracks, which improved the integrity of cubic specimens after the compressive failure (Figure 5-9). However, the compactness of the matrix can be reduced by the presence of fibres as the soft property of PVA fibre (low modulus) may induce more voids (Ranjbar and Zhang, 2020, Yu et al., 2020). This would lead to a higher extent of compressibility and the local fracture easily appeared around the fibres (Ranjbar and Zhang, 2020). Therefore, the compressive strength of SHGC composites is decreased. Meanwhile, the insufficient bond between fibre and matrix due to the poor fibre distribution and multifilament of PVA fibre in the geopolymer matrix (Figure 5-12) also results in reduced compressive strength of SHGC specimens. As seen in Figure 5-11, the compressive strength of SHGC ranged from 32.77 to 37.90 MPa and P1.5 achieved the highest compressive strength among all SHGC mixtures, while the trend of compressive strength was not consistent with the change of fibre content, which has also been reported in literature (Zhu et al., 2019, Ye et al., 2021). This can be attributed to the different fibre orientation which plays a crucial role in the mechanical properties of SHGC. When the fibres were orientated perpendicular to the cracks induced by compressive loading, the compressive strength tended to be higher. The compressive strength of cylindrical specimens was 5.66-78.98% higher than that of cubic specimens, which can be partially ascribed to the larger region restrained by the loading plate when cylindrical specimens with a 100 mm diameter were used (Yu et al., 2020). Besides, the aspect ratio of cylindrical specimens was small (i.e., 0.5) and most of the specimens was under a complex stress state instead of pure tension, resulting in a crushing failure (Wang et al., 2011b, Kim and Yi, 2002). Thus, the compressive strength was higher. For cylindrical specimens, P0 had a compressive strength of 48.25 MPa. When adding 1%, 1.5%, and 2% PVA fibre, the compressive strength was increased by 13.97%, 3.18%, and 21.54%, respectively. The fibre effect on the cylindrical specimens is different from that on the cubic specimens due to the different compressive failure modes. When the aspect ratio of the tested specimen was increased, the mid-portion of the specimen in

pure tension increased ([Wang et al., 2011b](#)). The cubic specimen had a slightly larger aspect ratio than the cylindrical specimen used in this study. Thus, the cubic specimen would fail due to the tensile failure of its mid-portion and the number of effective fibres within this part can significantly affect the final compressive strength of SHGC. Nevertheless, as mentioned early, the failure mode of the cylindrical specimens was different, and more fibres can contribute to influencing the compressive strength.

| (a) P0 | (b) P1 | (c) P1. 5 | (d) P2 |
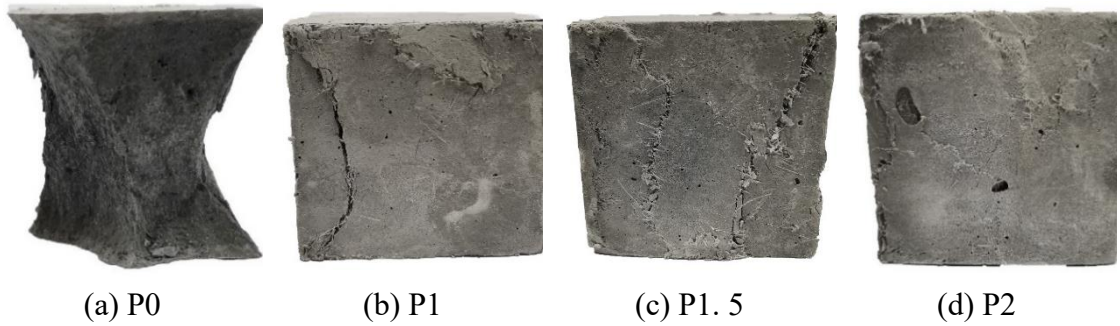
Figure 5-9 Typical failure patterns of SHGC cubes.

Mix No.	Top view	Side view
P0		
P1		
P1.5		

P2

Figure 5-10 Typical failure patterns of SHGC cylinders
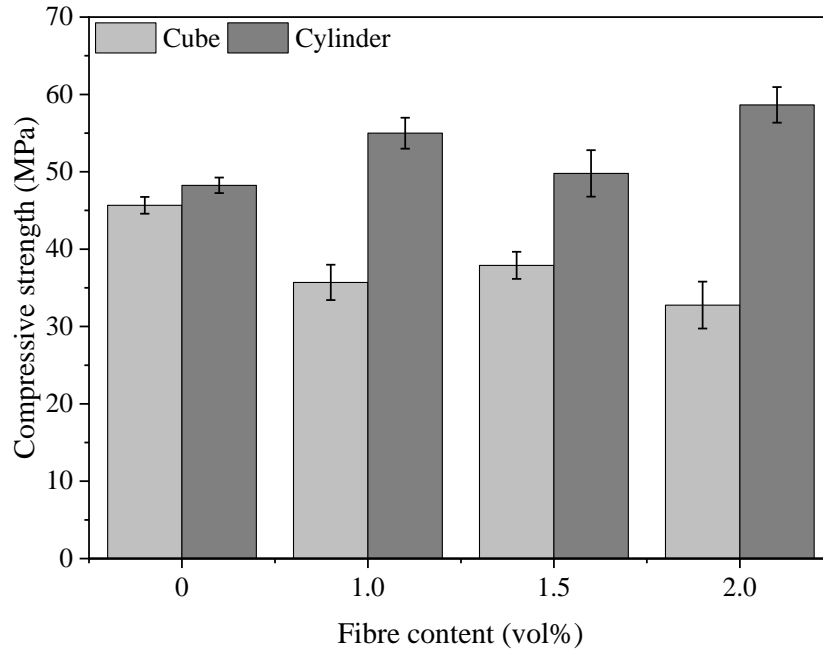
Figure 5-11 Compressive strength of SHGC cubes and cylinders with various fibre content.
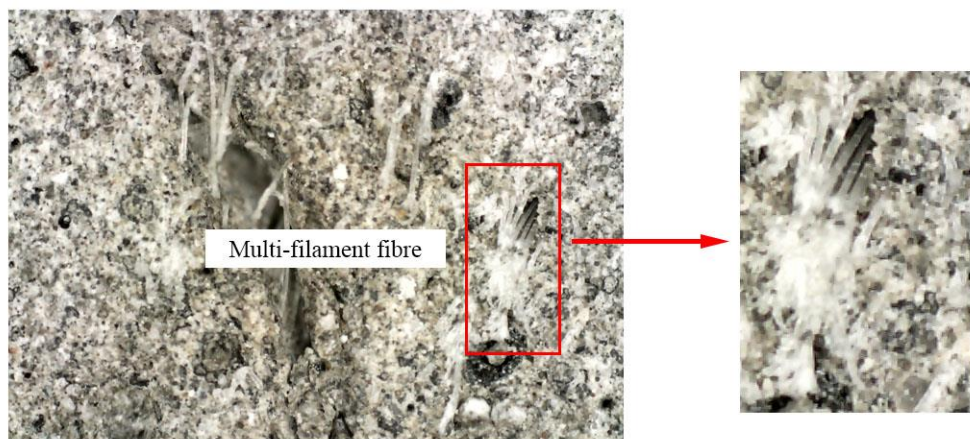
Figure 5-12 Multifilament PVA fibres in geopolymer matrix.

5.4.5 Static splitting tensile behaviour

Figure 5-13 shows the static splitting tensile strength of all mixtures. It can be observed that the increase of fibre content resulted in the increase of static splitting tensile strength.

The geopolymer without fibre (P0) had a static splitting tensile strength of 1.63 MPa. The increase of fibre content by 1%, 1.5%, and 2% resulted in the increase of splitting tensile strength by 80.67%, 178.18%, and 193.30%, respectively. The significant enhancement of static splitting tensile strength with the increase of fibre content can be ascribed to the fibre bridging effect across the fracture zone, which limited the crack growth and propagation.
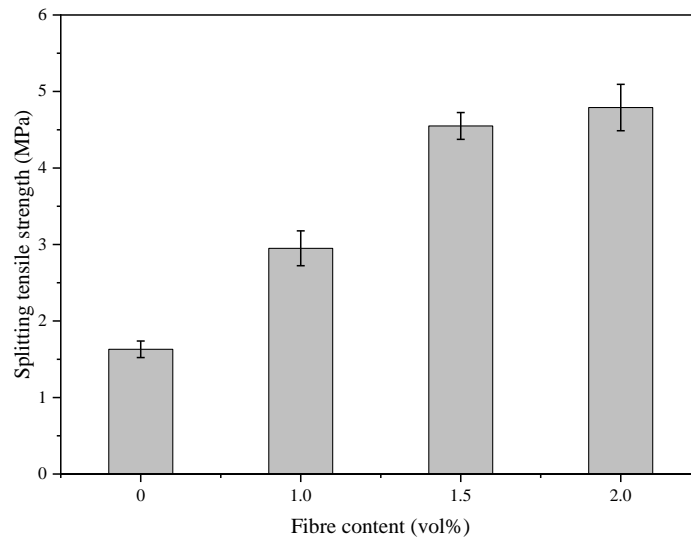
Figure 5-13 Static splitting tensile strength of all mixtures

5.4.6   Dynamic compressive behaviour

This section presents the results of dynamic compressive behaviour of all mixtures obtained from the SHPB test, including failure patterns, stress-strain response, dynamic compressive strength, DIF, and energy absorption capacity. The dynamic compressive properties of all mixtures in comparison with the corresponding static compressive properties are summarised in Table 5-4.

Table 5-4 Summary of static and dynamic properties of all mixtures obtained from SHPB test

Mix no.	Static compressive strength (MPa)		Average impact velocity (m/s)	Average strain rate (s⁻¹)	Maximum dynamic stress (MPa)	Strain at peak stress (με)	Ultimate strain (με)	DIF	Fracture energy (J)	Post-peak energy (J)	Total energy (J)
	Cubes	Cylinders									
P0	45.67	48.25	5.84	50.13	49.03	8813	17530	1.07	88.17	106.52	194.69
			7.42	97.55	53.61	19960	28270	1.17	294.18	114.45	408.63
			10.51	148.40	83.31	21290	39290	1.82	304.70	339.15	643.85
P1	35.70	54.99	5.88	51.79	40.06	7918	19160	1.12	57.20	131.02	188.22
			7.88	108.8	47.75	11180	30630	1.34	110.03	270.54	380.57
			10.78	174.6	56.72	23730	43320	1.59	256.98	285.64	542.62
P1.5	37.90	49.79	5.95	42.59	56.84	9117	15710	1.50	114.77	91.86	206.63
			8.34	105.50	70.43	13730	29480	1.86	193.81	297.2	491.01
			10.86	145.30	86.87	18930	37100	2.29	305.15	371.68	676.83
P2	32.77	58.65	5.92	58.14	45.05	8548	17780	1.37	95.70	109.43	205.13
			7.91	80.08	58.55	10780	24600	1.79	128.98	222.85	351.83
			10.46	133.80	67.45	16740	32780	2.06	193.54	308.62	502.16

5.4.6.1 Failure patterns

Figure 5-14 demonstrates the typical failure patterns of all mixtures containing various fibre content at three impact velocities, i.e., 6, 8, and 10 m/s that corresponded to the strain rates of around 50/s, 100/s, and 150/s, respectively. It can be observed that the damage of all mixtures became significant with the increase of strain rates. Geopolymer mortars without fibre (P0) showed a pulverised failure regardless of strain rates, which fractured into large pieces at low strain rates but crushed into fine fragments at high strain rates. The failure patterns of specimens changed with the addition of PVA fibres. At a low strain rate, only several small cracks can be observed on the surface of specimens. When the strain rate was increased to a medium level, the specimens experienced a vertical splitting failure with few visible major cracks through the specimens. At a high strain rate, all specimens including SHGC exhibited pulverised failure. The change of failure patterns with the increasing strain rate was also reported in literatures (Chen et al., 2013, Chen et al., 2019, Wang et al., 2012), which showed that more fragments with smaller sizes were generated when a higher strain rate was applied. Under the high velocity impact, there was very limited time for the cracks to propagate along the path with the lowest cracking resistance. The increased external energy caused by the high velocity impact was consumed by generating more cracks that required higher energy than the propagation of cracks (Chen et al., 2013, Khan et al., 2018).

Regarding the effect of fibre content, compared with P0, the incorporation of PVA fibre altered the failure patterns of specimens at low and medium strain rates, and reduced the damage level of specimens at a high strain rate. At low and medium strain rates, P0 experienced a pulverised failure, whereas the specimens containing PVA fibres displayed a good integrity until the end of the test with a series of cracks formed on specimens. Apart from the fibre effect, this can also be attributed to the reduced end friction confinement when the grease was applied to the specimens before the dynamic compression. Hence, the splitting vertical cracks occurred throughout the length of the specimen, which initiated from the outer layer (Wang et al., 2011b). At a high strain rate, although all specimens had a pulverise failure, P0 exhibited a large number of small and irregular broken fragments, while the PVA fibre reinforced SHGC specimens tended to

have larger fragments, suggesting that the incorporation of PVA fibre into geopolymer mortar can effectively resist the lateral deformation of specimens under dynamic compression (Wu et al., 2017). Besides, at a low strain rate, the specimens containing fibres were not fractured, resulting in a more complete failure pattern (Yu et al., 2021). When this happened, the dynamic compressive strength of the specimen tended to be smaller than the static compressive strength, which was also reported in previous studies (Chen et al., 2019, Zhang et al., 2012) for polymeric and steel fibre reinforced cementitious composites. This aspect will be explained in more detail below.

Mix No.	Strain rate (s⁻¹)		
	50	100	150

5.4.6.2 Stress-strain response

Figure 5-15 shows the dynamic compressive stress-strain curves of all mixtures containing various fibre content under dynamic compression at different strain rates. For all mixtures, the stress-strain curves showed an increasing branch up to the peak stress, followed by a descending branch until the ultimate strain. It is worth mentioning that fibres typically exhibit their bridging effects after the linear ascending stage and a large amount of energy is consumed to pull out or rupture the fibres during this stage (Yu et al., 2021, Hou et al., 2018). Besides, micro-cracks start to initiate during this stage and visible cracks can be identified along with the crack propagation and coalescence when the peak stress is exceeded (Ren et al., 2018). In addition, during this stage, fibres typically experience sliding to overcome the frictional bond or rupture immediately.
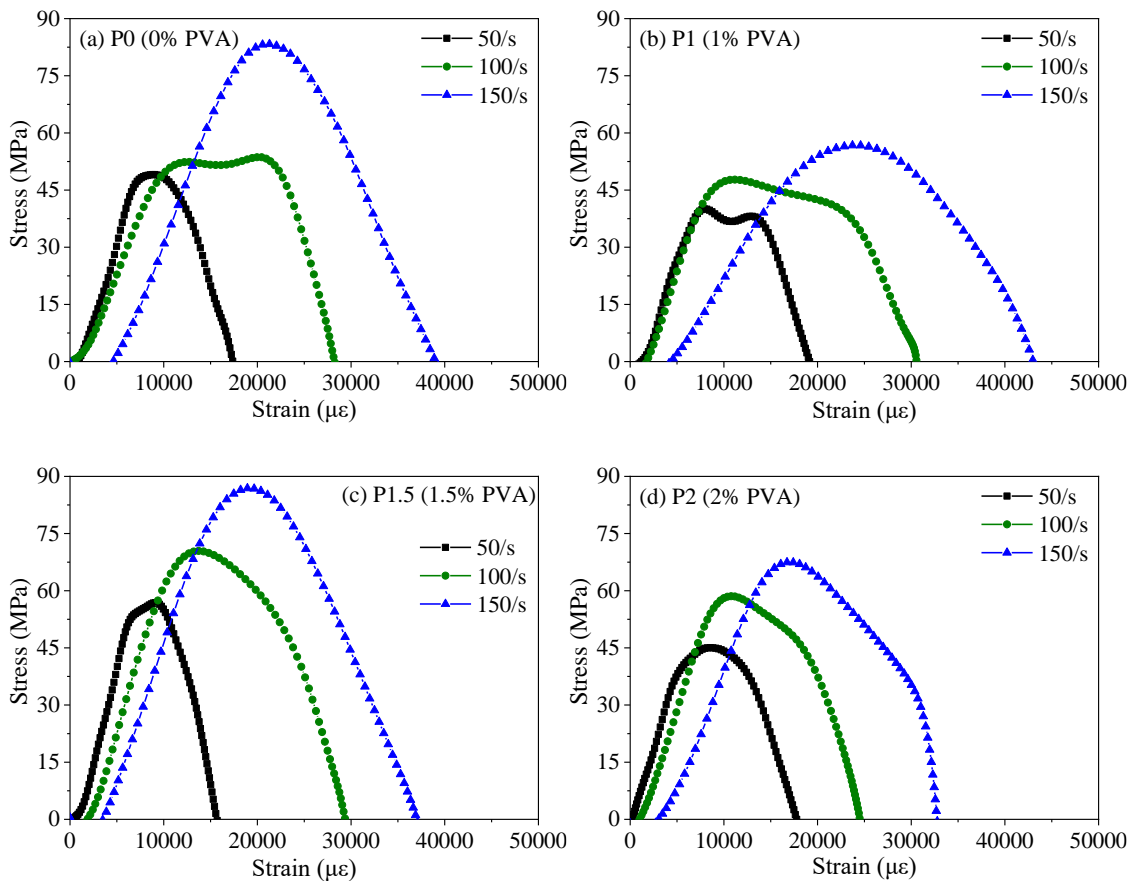
Figure 5-15 Dynamic compressive stress-strain curves of all mixtures at different strain rates.

5.4.6.3 Dynamic compressive strength

Figure 5-16 illustrates the effect of strain rate on the dynamic compressive strength of all

mixtures, i.e., the peak stress shown in Figure 5-15. As the increase of strain rate from a low level (50 s^{-1}) to a medium level (100 s^{-1}) and a high level (150 s^{-1}), the dynamic compressive strength of all mixtures was increased by 9.26-29.97% and 41.59-69.78%, respectively, suggesting that all specimens were sensitive to strain rate. This agrees well with the findings reported in (Zhang et al., 2018, Chen et al., 2019, Sun et al., 2018, Khan et al., 2018, Xiao et al., 2021). It can be associated with several factors including the structural effects (lateral inertia effect and end friction confinement effect) (Hao et al., 2013), viscous effect of free water in voids and pores (known as Stefan effect) (Rossi et al., 1992) and crack initiation and propagation effect (Yan and Lin, 2006). It was found that using the specimens with an aspect ratio of 0.5 can minimise the structural effects (Bertholf and Karnes, 1975) and applying the grease on the tested specimens can reduce the end friction effect (Li and Meng, 2003). In this study, all specimens for dynamic compression test had an aspect ratio of 0.5 and the grease was adopted to both surfaces of the specimens. Hence, the structural effects can be regarded as insignificant while the latter two factors would strongly affect the changes of peak stress with strain rate.
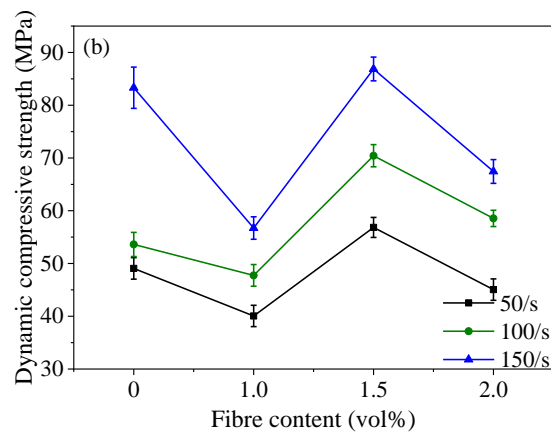
Figure 5-16 Dynamic compressive strength of all mixtures under dynamic compression at various strain rates.

Regarding the effect of PVA fibre on the dynamic compressive strength at different strain rates, increasing the PVA fibre content did not result in a consistent trend, similarly with that of static compressive strength for cubic specimens (Figure 5-11). P1.5 had the highest dynamic compressive strength, which was 15.83%, 31.37%, and 4.27% higher than that of P0 at strain rates of 50 s^{-1}, 100 s^{-1}, and 150 s^{-1}, respectively. Except P1.5, P1 and P2 exhibited lower compressive strengths than P0 at different strain rates. A similar

finding was reported in ([Xiao et al., 2021](#)) that the dynamic compressive strength of fly ash-slag based geopolymer was reduced by 16.45-89.42% when the PVA fibre content increased from 0% to 1.2%, which can be attributed to the increasing number of pores and micro-cracks with the increase of PVA fibre content. Additionally, previous studies also found that when the fibre content exceeded a certain value, the dynamic compressive strength of the mixture was weakened due to the increased porosity ([Chen et al., 2019](#), [Lai and Sun, 2009](#)). As mentioned previously, the dynamic compressive strength tended to be higher when more new cracks were generated rather than the propagation of existing cracks, as the initiation of new cracks would consume more energy. Thus, if more existing cracks appear inside the specimen, the dynamic compressive strength would be reduced. Thus, adding appropriate fibre content is important to avoid fibre clumping or balling, minimise the significant increase of pores and voids, and achieve a better fibre orientation ([Ranjbar and Zhang, 2020](#)). Similar to static mechanical properties, the fibre orientation is also crucial for dynamic mechanical properties ([Wu et al., 2017](#), [Zhang et al., 2018](#)), which can vary depending on the fresh properties, e.g., flowability and rheology ([Yang et al., 2009](#)). Under a good fibre orientation, fibres can effectively bridge the existing cracks and slow down the crack propagation. Thus, more new cracks would initiate in other areas. Besides, when the strain rate is higher, it requires more energy to fracture the bridging action of fibres as there is no sufficient time for the cracks to grow along the weak paths and thus the dynamic compressive strength would be higher. Based on results of drying shrinkage and static mechanical properties, it seems that P1.5 exhibited better fibre orientation and therefore showed a higher dynamic compressive strength under various strain rates. It should be mentioned that when the strain rate was equal to or smaller than 100 s^{-1}, the dynamic compressive strength of P1 was about 13.17-27.15% smaller than its static compressive strength (54.99 MPa), which can support the previous discussion on the failure patterns (Section 3.5.1) that the specimens were not completely fractured. A similar phenomenon was observed for P2 when the strain rate was around 50 s^{-1}.

Table 5-4 presents the strain at the peak stress, i.e., peak strain, which can reflect the deformation capacity of the specimens ([Li and Xu, 2009](#)). Consistent with the dynamic compressive strength, the peak strain of all mixtures was increased considerably with the

increasing strain rate. For instance, the peak strain for P0 was increased by 126.48-141.57% when the strain rate changed from 50 s^{-1} to higher levels, and it did not show a clear change trend with PVA fibre content. When the strain rate was in the range of 100-150 s^{-1}, P0 exhibited a higher peak strain, while at low strain rates, the peak strain was comparable for all mixtures ranging from 7918 με to 9117 με. All these indicated that the peak strain was sensitive to strain rate instead of fibre content, which is in good agreement with previous studies (Ren et al., 2018, Wu et al., 2017, Khan et al., 2018, Zhang et al., 2018).

5.4.6.4 Dynamic increase factor (DIF)

DIF is defined as the ratio of dynamic compressive strength to the static compressive strength of the mixture, which has been widely used to evaluate the effect of strain rate on the material properties (Xiao et al., 2015, Ren et al., 2018, Yu et al., 2021). In this study, the DIF was calculated as the ratio of dynamic compressive strength to static compressive strength of cylindrical specimen. According to Table 5-4, the DIF values of all cubic specimens in this study were higher than 1, indicating that the dynamic compressive strength of all mixtures was higher than the static compressive strength. Nevertheless, at some strain rates, P1 and P2 exhibited DIF values less than 1. The possible reasons for this were provided in the previous sections. On the other hand, previous studies indicated that the DIF increases with the log10 of strain rate linearly for quasi-brittle materials, like concrete (C. Allen Ross and Steven, 1995, Chen et al., 2013, Tedesco et al., 1997), which can also be observed in this study as illustrated in Figure 5-17a that there existed a linear relationship between DIF and strain rate for all mixtures. It can be described using $DIF = b + c \log_{10}(\dot{\varepsilon}_s)$, where b and c are constants and summarised in Table 5-5. The reliability of the fitting curves for all mixtures can be assessed by the correlation coefficient (R^2), where the equations for all SHGC specimens with various fibre content showed high reliability with R^2 close to 1, whereas the fitting linear equation for pure geopolymer mortar had slightly less reliability ($R^2 = 0.72$).

The slope (c) of the equation in Table 5-5 can reflect the increasing rate of dynamic compressive strength as the increase of strain rate when the intercept (b) is similar. It can be observed that as the strain rate raised, the increasing rates of dynamic compressive

strength for P0 and P1.5 were higher than those for P1 and P2. Unlike traditional cementitious materials, the water in the alkaline activator is not reactant and acted as a medium inside the geopolymer mixture (Ma and Ye, 2015). Thus, more free water is available in pores and voids, which would generate a meniscus at the crack tip limiting the crack propagation and thus the dynamic compressive strength would be enhanced (Fu et al., 2021). In addition, it was reported that the increasing rate of dynamic compressive strength was higher for concrete with lower quality (Bischoff and Perry, 1991). As seen in Figure 5-11, the static compressive strength of P0 (cylindrical specimen) was the lowest, which may explain why the increase of DIF was more sensitive to the strain rate (considering the definition of DIF). For P1.5, although the free water may be reduced due to the hydrophilic behaviour of PVA fibre, the good fibre orientation can provide an effective bridging action, as discussed previously, and thus more energy would be needed to fracture this bridging behaviour along with the generation of more new cracks, resulting in an increased DIF. These can be also seen in Figure 5-17b that P1.5 had the highest DIF values at different strain rates, ranging from 1.14-1.74. The results of DIF are consistent with that of dynamic compressive strength.

Table 5-5 Fitted equations of DIF against strain rate for all mixtures.

Mix No.	Fitted equation of DIF	Correlation coefficient (R^2)
P0	$DIF = 1.360 \log_{10}(\dot{\varepsilon}_s) - 1.377$	0.721
P1	$DIF = 0.611 \log_{10}(\dot{\varepsilon}_s) - 0.320$	0.965
P1.5	$DIF = 1.219 \log_{10}(\dot{\varepsilon}_s) - 0.957$	0.957
P2	$DIF = 0.793 \log_{10}(\dot{\varepsilon}_s) - 0.580$	0.999
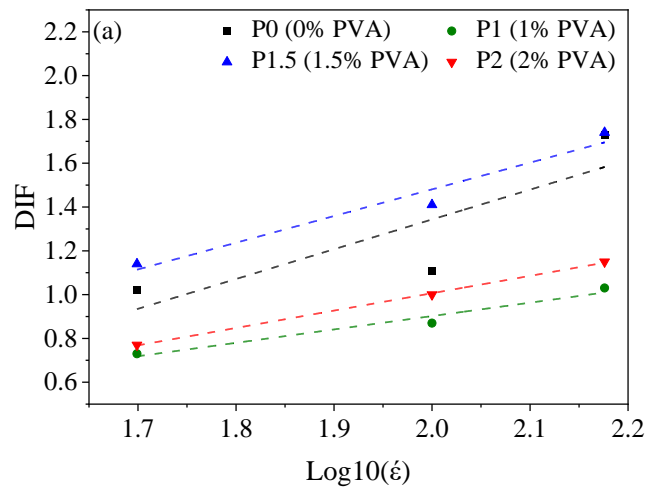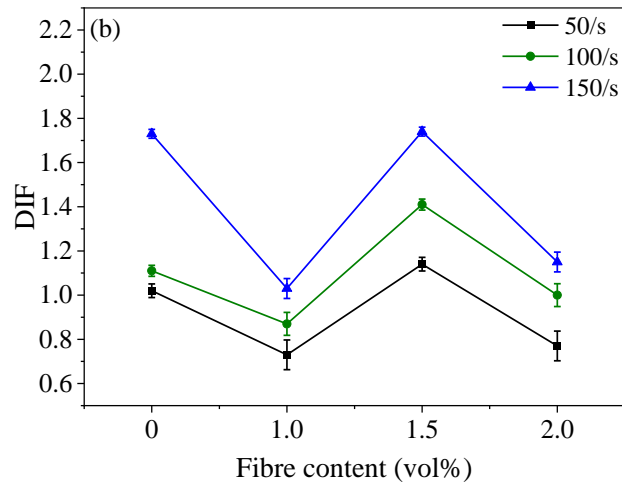
Figure 5-17 DIF of all cubes under dynamic compression at various strain rates.

5.4.6.5 Energy absorption capacity

The energy absorption capacity of all mixtures was characterised by pre-peak energy and post-peak energy, which are defined as the energy absorbed by the specimen up to the peak stress during the SHPB test and the energy absorbed by the specimen in the post-peak region, respectively (Yu et al., 2021, Chen et al., 2019). Figure 5-18 shows the fracture energy and post-peak energy of all mixtures calculated based on stress-strain curves presented in Figure 5-15. Similar to dynamic compressive strength and DIF, both fracture energy and post-peak energy of all mixtures were enhanced significantly by 7.44-349.27% with the increasing strain rate from 50 s^{-1} to 150 s^{-1}, which can be associated with the effects of crack initiation and propagation.

As discussed in Section 3.5.2, the ascending part of the stress-strain curve referred to the initiation of micro-cracks and the fibre pull-out or rupture process, while the descending part related to the crack propagation and complete pull-out or rupture of fibres. This can explain why the post-peak energy of SHGC was mostly higher than the pre-peak energy, suggesting that a large amount of energy was dissipated to pull out or rupture the fibres. For instance, at various strain rates, the post-peak energy of P1.5 was about 11.15-145.88% higher than its pre-peak energy. It is worth noting that when the strain rate was 150 s^{-1}, the difference between them was reduced (only 11.15%) as the high velocity impact may damage the fibres immediately rather than pulling the fibres out. A very big portion of the energy can be absorbed during the pull-out process of fibres. Regarding P0, the difference between the pre-peak energy and the post-peak energy was very small,

ranging from 11.31% to 61.10%. Typically, the pre-peak energy of the mixtures containing fibres should be higher than that without fibres, as reported in (Khan et al., 2018, Chen et al., 2019). However, the pre-peak energy of SHGC was mostly lower than that of geopolymer mortar (except P1.5), as seen in Figure 5-18a. Xiao et al. (Xiao et al., 2021) observed that the PVA fibre reinforced geopolymers exhibited lower energy absorption capacity than geopolymer mortars due to the significant reduction in dynamic compressive strength induced by the incorporation of PVA fibre. A similar finding was reported in (Zhang et al., 2018) that the energy absorption capacity of PP fibre reinforced concrete dropped when the PP fibre content exceeded a certain value. The energy absorption capacity can be affected by both dynamic compressive strength and peak strain. As presented in Table 5-5, the fibres did not have an obvious effect on the peak strain and P0 exhibited higher peak strain at strain rates, which can be ascribed to the increased cumulative strain when more cracks were generated (Li et al., 2021b), as confirmed by Figure 5-14. As seen in Figure 5-18b, the post-peak energy of all SHGC mixtures was mostly larger than that of geopolymer mortar when the strain rate exceeded 50 s^{-1} owing to the extra part of the energy required to pull out or rupture the fibres. Nevertheless, due to the reduced dynamic compressive strength, the total absorbed energy (sum of pre-peak energy and post-peak energy) of P1 and P2 was still lower than that of P0. Consistent with dynamic compressive strength and DIF, P1.5 outperformed P0 in terms of total absorbed energy at different strain rates, with an improvement of 6.13-20.16%.
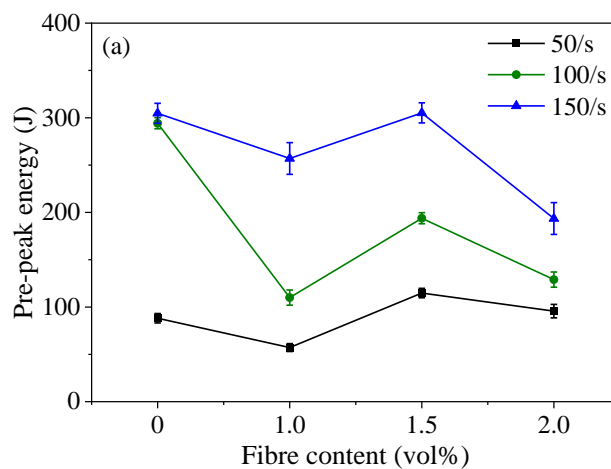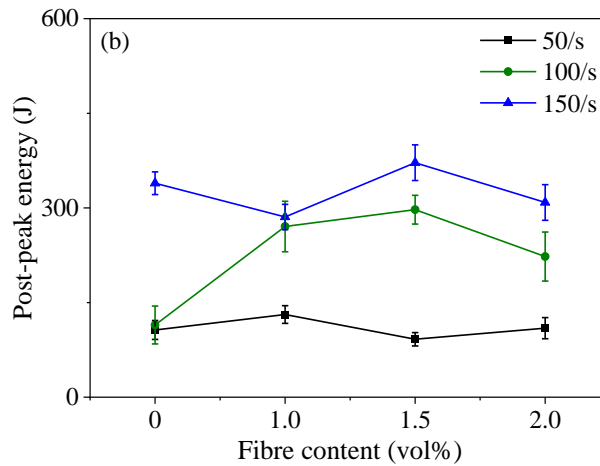
Figure 5-18. Energy absorption capacity of all mixtures under dynamic compression at different strain rates: (a) pre-peak energy and (b) post-peak energy.

5.4.7 Dynamic splitting tensile behaviour

This section provides results of dynamic splitting tensile behaviour of SHGC specimens with various fibre content, including failure patterns and dynamic splitting tensile strength.

5.4.7.1 Failure patterns

Typical failure patterns of all mixtures are shown in Figure 5-19. Due to the heterogeneity of concrete, the strain rate resulted from the same impact velocity on the same mixture could be different, and therefore the levels of impact velocity are used to analyse the dynamic splitting tensile behaviour (Chen et al., 2020). As seen in Figure 5-19, geopolymer mortar without fibre (P0) had a pulverised failure at all impact velocity as no fibre was added to limit the growth of the crack. For SHGC specimens containing PVA fibre, specimens failed with a straight crack along the surface of specimens, where P1 were broken into two parts due to the insufficient fibre bridging effect, while P1.5 and P2 remained the integrity because of increased fibre bridging effect. At medium and high impact velocity, all SHGC specimens were broken into two or three parts, and the formed crack along the surface was not straight. Triangular crush at both ends of the specimen, where impact load was applied, was observed, which could be attributed to the cracks appearing before the stress equilibrium state was reached (Chen et al., 2016), and the increased friction at the interface between the specimen and loading points (Feng et al., 2018).

110

Mix	Impact velocity (m/s)		
No.	6	8	10
P0			
P1			
P1.5			
P2			

Figure 5-19 Failure patterns of all mixtures at different impact velocity

5.4.7.2 Dynamic splitting tensile strength

Figure 5-20 shows the dynamic splitting tensile strength of all mixtures under different impact velocities. It can be observed that the dynamic splitting tensile strength was increased with the increase of strain rates in all mixtures. When the impact velocity increased from 6 m/s to 8 m/s and 10 m/s, the dynamic splitting tensile strength of geopolymer mortar without fibre (P0), SHGC specimens reinforced with 1% (P1), 1.5%

(P1.5), and 2% (P2) PVA fibre was increased by 8.65%-23.20%, 102.21%-122.92%, 95.33%-102.07%, and 84.15%-122.22%, respectively.

On the other hand, the dynamic splitting tensile strength of SHGC specimens exhibited similar trend at different impact velocity. In general, the increase of fibre content resulted in the increase of dynamic splitting tensile strength, and the trend was more pronounced at medium and high impact velocity. At low impact velocity, all mixtures had splitting tensile strength of approximately 7 MPa, and the effect of fibre content could be ignored. At medium impact velocity, P0 had a dynamic splitting tensile strength of 8.00 MPa, when adding PVA fibre by 1%, 1.5%, and 2%, the dynamic splitting tensile strength was increased by 70.27%, 75.78%, and 79.97%, respectively. At high impact velocity, the dynamic splitting tensile strength of P0 was 9.07 MPa, and the addition of PVA fibre by 1%, 1.5%, and 2% led to the enhancement of dynamic splitting tensile strength by 65.54%, 60.36%, and 91.52%, respectively. This can be ascribed to the increased fibre bridging effect.
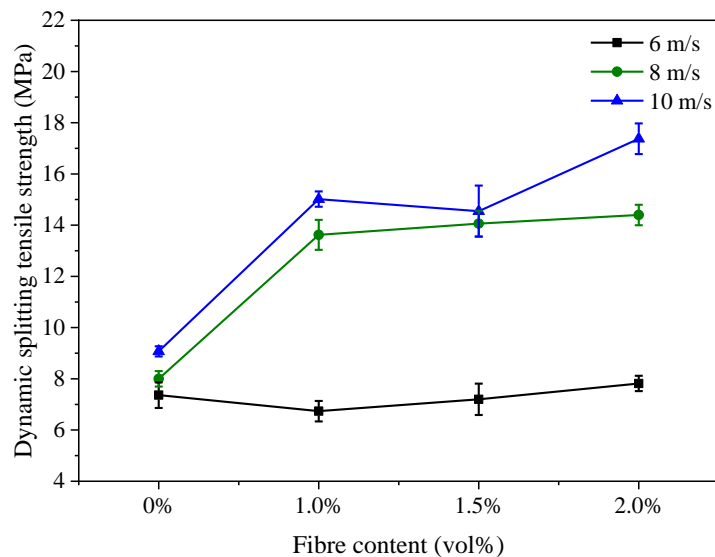
Figure 5-20 Effect of fibre content on dynamic splitting tensile strength of all mixtures under different strain rates

5.5 Concluding remarks

This chapter presents a systematic experimental study on the effect of PVA fibre content (0%, 1%, 1.5%, and 2% by volume) on engineering properties of FA-GGBS based SHGC, including flowability, drying shrinkage, tensile properties, and compressive properties, focusing on the tensile strain-hardening behaviour and dynamical compressive behaviour.

Based on the experimental results, the main conclusions can be drawn as follows:

- Compared to pure geopolymer mortar, the PVA fibre reinforced SHGC specimens had a lower flowability. The addition of up to 2% PVA fibre resulted in a reduction in flowability of fresh mixtures by 26.06% due to the increased shear resistance. The drying shrinkage of SHGC specimens at 28 d declined with the incorporation of fibre content, except for P1.5 (1.5% PVA) that had a smaller drying shrinkage than P2 (2% PVA) due to the relatively weaker fibre-matrix interfacial bond and higher porosity of geopolymer matrix in P2.

- The pure geopolymer mortar exhibited a brittle failure, while all SHGC specimens containing PVA fibre presented a strain-hardening behaviour along with multiple micro-cracking. The addition of 2% PVA fibre resulted in an increase of ultimate tensile strength by 331.07%. The ultimate tensile strain of P1.5 and P2 was approximately 200 times that of P0, which can be ascribed to the fibre bridging effect. All specimens reinforced with PVA fibre fulfilled both the strength-based and energy-based criteria for SHGC, as indicated by the pseudo strain-hardening (PSH) index that ranged from 8.79 to 12.98, exceeding the required PSH index of 3.

- For both cubic and cylindrical SHGC specimens, the failure patterns of them changed with addition of PVA fibre while the integrity was mostly remained. With the increase of fibre content to up to 2%, the static compressive strength of cubic specimens reduced by 28.25%, while that of cylindrical specimens went up by 21.55%, which can be ascribed to their different failure patterns. Compared to cubic specimens, cylindrical specimens had a 5.66-78.98% higher compressive strength owing to the larger region restrained by the confinement and complex stress distribution under loading.

- The strain rate had a significant influence on the compressive behaviour of SHGC. With the increasing strain rate from a low level (50 s^{-1}) to a medium level (100 s^{-1}) and a high level (150 s^{-1}), the dynamic compressive strength of SHGC was increased by 9.26-29.97% and 41.59-69.78%, respectively. The dynamic impact factor (DIF) and energy absorption capacity of all mixtures were also enhanced with the increase of strain rate. There existed a linear relationship between DIF and log10 of strain rate.

The dynamic compressive behaviour of SHGC was strongly associated with the fibre content and fibre distribution. P1.5 outperformed other mixtures in terms of dynamic compressive strength, DIF and energy absorption capacity.

- Dynamic splitting tensile behaviour also changed with the increase of the impact velocity. When the impact velocity increased from low level to medium and high levels, the dynamic splitting tensile strength of geopolymer mortar without fibre (P0), SHGC specimens reinforced with 1% (P1), 1.5% (P1.5), and 2% (P2) PVA fibre was increased by 8.65%-23.20%, 102.21%-122.92%, 95.33%-102.07%, and 84.15%-122.22%, respectively. On the other hand, the increase of fibre content also resulted in the increase of dynamic compressive strength, especially at medium and high impact velocities, due to the enhanced fibre bridging effect.

- SHGC containing 1.5% PVA fibre can be regarded as the optimal mixture considering the static and dynamic properties.

Chapter 6 Effect of Hybrid PVA-RTS Fibres on Engineering Properties of SHGC

6.1 Introduction

Recycled tyre steel (RTS) fibre has been increasingly used as an alternative to manufactured steel fibres to enhance sustainability of fibre reinforced composites. This paper presents an experimental study on the effect of hybrid polyvinyl alcohol (PVA) and RTS fibres on engineering properties of FA-GGBS based SHGC cured at ambient temperature in terms of flowability, drying shrinkage, and mechanical properties, with a special focus on strain-hardening behaviour and dynamic compressive behaviour. Four mixtures with various volume fractions of hybrid PVA and RTS fires, including 1.5% PVA, 2% PVA, 1.75% PVA + 0.25% RTS, and 1.5% PVA +0.5% RTS were considered.

The results presented in this chapter were submitted as two journal articles in Journal of Construction and Building Materials (one published and one currently under review) with the following references:

Yi Wang, Choi Lin Chan, Si Hang Leong, Mingzhong Zhang, Engineering properties of strain-hardening geopolymer composites with hybrid polyvinyl alcohol and recycled steel fibres, *Construction and Building Materials*, 261 (2020) 120585.

Yi Wang, Mingzhong Zhang, Static and dynamic properties of strain-hardening geopolymer composites reinforced with hybrid polyvinyl alcohol and recycled steel fibres, *Construction and Building Materials*, under review (Manuscript Number: CONBUILDMAT-D-22-00981).

6.2 Experimental program

In this chapter, the raw materials used to prepare specimens were the same to those used in Chapter 5, including FA, GGBS, SS, SH, SP, and silica sand. PVA and RTS fibres were used to produce SHGC, the properties and images of which are displayed in Table 6-1 and Figure 6-1, respectively. PVA fibres were supplied by Kuraray, Japan, and coated by 1.2 wt% oil to control fibre-matrix interface properties. The RTS fibres had different lengths ranging from 1 mm to more than 100 mm, which cannot be directly applied due

to the potential adverse effect. Thus, RTS fibres were manually sieved before use to obtain a nominal length of 12 mm.

Table 6-1 Physical and mechanical properties of polyvinyl alcohol (PVA) and recycled tyre steel (RTS) fibres.

Fibre ID	Length (mm)	Nominal diameter (μm)	Aspect ratio	Density (g/cm³)	Tensile strength (MPa)	Elastic modulus (GPa)
PVA	12	40	300	1.3	1600	41
RTS	12	220	80	7.8	2165	200

Figure 6-1 Images of (a) polyvinyl alcohol (PVA) and (b) recycled tyre steel (RTS) fibres.

The mix proportions of FA, GGBS, SS, SH, SP, silica sand were also same to that used in Chapter 5 and were kept constant for all mixtures, as shown in Table 6-2. The geopolymer binder was prepared with the FA/GGBS ratio of 0.8:0.2, SS/SH solution ratio of 2.0, sand/binder ratio of 0.2, and SP/binder ratio of 0.01. The alkaline activator/binder ratio was calculated by the weight ratio of alkaline activator composed of SH and SS solution to geopolymer binder consisting of FA and GGBS, which was determined as 0.45 to ensure the flowability of fresh mixtures. In Table 6-2, "P" and "R" refer to PVA and RTS fibres, and the denoted numbers after "P" and "R" stand for the content of PVA and RTS fibres, respectively. For instance, P1.5 represents the mixture reinforced with 1.5% mono PVA fibre, while P1.5R0.5 denotes the mixture containing 1.5% PVA fibre and 0.5% RTS fibre.

All SHGC mixtures were prepared using a 10 L Hobart mixer, following the preparation steps described in previous chapter. The entire mixing process typically lasted approximately 8 min and 30 s. Firstly, all solid ingredients (FA, GGBS, and sand) were

added in the mixer and dry mixed for 1.5 min until a homogeneous mix was obtained. Then, the SH solution was added gradually into the dry mixture and mixed for 1 min, followed by the very slow addition of SS solution, which lasted around 2 min to avoid the rapid setting of the mixture. Afterwards, SPs were added to achieve an appropriate flowability and mixed for another 1 min. The PVA fibres were then evenly incorporated into the mixture to avoid the multifilament forms, followed by the addition of RTS fibres, and the whole mixture was mixed for another 1min. The fresh SHGC was poured into the moulds immediately after the mixing and then vibrated to allow the air bubble to escape and compact the SHGC. All specimens were covered with cling film to prevent moisture loss after casting and stored in the ambient temperature (20 ± 2 °C) for 24 h. Then, the specimens were demoulded and stored in a standard curing room with an average temperature of 20 ± 2 °C and relative humidity of 95% until testing.

Table 6-2 Mix proportions of SHGC.

Mix No.	Binder		Activator/binder	Sand/binder	SPs/binder	PVA (vol%)	RTS (vol%)
	FA	GGBS					
P1.5	0.8	0.2	0.45	0.2	0.01	1.5	0
P2	0.8	0.2	0.45	0.2	0.01	2.0	0
P1.75R0.25	0.8	0.2	0.45	0.2	0.01	1.75	0.25
P1.5R0.5	0.8	0.2	0.45	0.2	0.01	1.5	0.5

Engineering properties of SHGC reinforced with hybrid PVA-RTS fibres were investigated by flow table test, drying shrinkage test, uniaxial tension test, static compression test, static splitting tension test, and split Hopkinson pressure bar test (SHPB). Test methods were the same to those described in Section 5.3.

6.3 Results and discussion

6.3.1 Flowability

Figure 6-2 shows the flow values of all mixtures with various hybrid fibre content. A higher flow value indicates better workability, allowing easier casting and compaction. As seen in Figure 6-2, the flow values of fresh SHGC mixtures decreased with the increase of PVA fibre content, the addition of RTS fibre, and the partial replacement of PVA fibre with RTS fibre. SHGC reinforced with 1.5% PVA fibre (P1.5) had a flow value

of 73%. When the PVA fibre content was increased to 2%, the flow value reduced by 4.11%. With the addition of 0.5% RTS fibre into P1.5, the flow value of fresh SHGC dropped by 8.68%. This decreasing trend of SHGC with a higher amount of PVA fibre or additional RTS fibre can be attributed to the rising shear resistance in the fresh mixtures, which is in good agreement with the previous studies (Wang et al., 2020a, Zhong and Zhang, 2020). However, previous studies showed a significant decrease in flow value when increasing PVA fibre content or adding RTS fibre in SHGC with 1.5% mono PVA fibre. This can be attributed to the different material preparation approach applied in the current study. In (Wang et al., 2020a), the activator/binder ratio was 0.4, and SH and SS were mixed together before adding to the mixer. However, in this study, the activator/binder ratio was 0.45, and SH and SS were added into the mixer separately to avoid rapid setting. The higher activator/binder ratio and different preparation steps can both lead to varying performance of fresh SHGC mixtures.

The partial replacement of PVA fibre with increasing RTS fibre content resulted in a slight drop in the flow value of fresh SHGC mixtures. Compared with P2, the replacement level of PVA fibre with RTS fibre by 0.25% and 0.5% led to a slight decrease of flow value by 2.50% and 4.76%, respectively, while the same replacement levels resulted in a significant reduction by 21.9% and 39.8%, respectively, as reported in (Wang et al., 2020a). This discrepancy can be ascribed to the different quality of RTS fibres used. Herein, RTS fibres were sieved with a target fibre length of 12 mm to ensure they have a good length distribution and thus improve the homogeneity of mixtures, while the applied RTS fibres in (Wang et al., 2020a) were not sieved before adding to the mixture, and therefore the shape and geometry of them were highly random. The non-uniform shape and geometry can cause more random fibre balling and agglomeration in the mixing process and thus further increase the contact network between fibre and geopolymer matrix, which allows the fresh geopolymer matrix to take extra loads and therefore reduce the flowability of SHGC (Farhan et al., 2018a, Martinie et al., 2010, Farhan et al., 2018b).
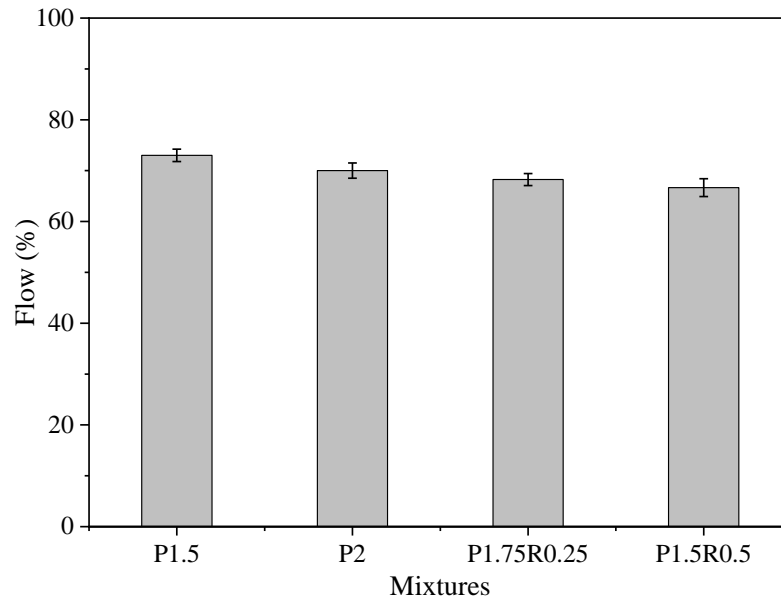
Figure 6-2 Flowability of fresh SHGC specimens with various hybrid fibre content

6.3.2 Drying shrinkage

Figure 6-3 illustrates the drying shrinkage of all SHGC mixtures with various hybrid PVA and RTS fibre content. Overall, the drying shrinkage of all mixtures decreased regardless of fibre content at early ages, while the decreasing rate gradually declined. This was because the capillary water lost rapidly at early ages, and therefore the internal relative humidity reduced quickly. With the geopolymerisation of matrix, the interfacial bond between fibre and matrix developed progressively, which restricted drying shrinkage, resulting in a relatively slow reduction in drying shrinkage (Yang et al., 2017, Noushini et al., 2018, Bernal et al., 2010). The drying shrinkage of SHGC reinforced with mono PVA fibre became stable after 10 d, while that of specimens containing hybrid PVA and RTS fibres flattened after 4 d. The different progress can be ascribed to the restriction effect of RTS fibre that has high elastic modulus and strong interaction with the geopolymer matrix because of the hydrophilic nature and large surface area (Ranjbar et al., 2016b, Ranjbar et al., 2016a).

At 28 d, the drying shrinkage of SHGC reinforced with mono-PVA fibre rose by 19.68% when the fibre content was increased from 1.5% to 2%, which is consistent with the findings presented in (Wang et al., 2020a) as the weak interaction between fibre and matrix can lead to debonding and reduced resistance to shrinkage (Ranjbar et al., 2016b). Moreover, the increasing fibre content can cause poor compaction and higher porosity of

119

mixtures, which allows moisture to move outwards the surface of specimens (Ranjbar and Zhang, 2020, Zhong et al., 2019, Afroughsabet and Teng, 2020). On the other hand, when adding 0.5% RTS fibre into P1.5, the drying shrinkage exhibited an obvious drop by 58.84% at 28 d due to the high elastic modulus of RTS fibre and strong fibre-matrix bond induced by the hydrophilic nature and large surface area of RTS fibre (Ranjbar et al., 2016b, Ranjbar et al., 2016a). The partial replacement of PVA fibre with RTS fibre resulted in an evident decreasing trend. Compared with SHGC containing 2% mono-PVA fibre, the drying shrinkage was decreased by 58.37% and 65.61%, respectively, when PVA fibre was partially replaced by RTS fibre at a replacement level of 0.25% and 0.5%, which is in good agreement with a previous study (Wang et al., 2020a). Thus, the incorporation of RTS fibre is an effective approach to control the drying shrinkage of SHGC.
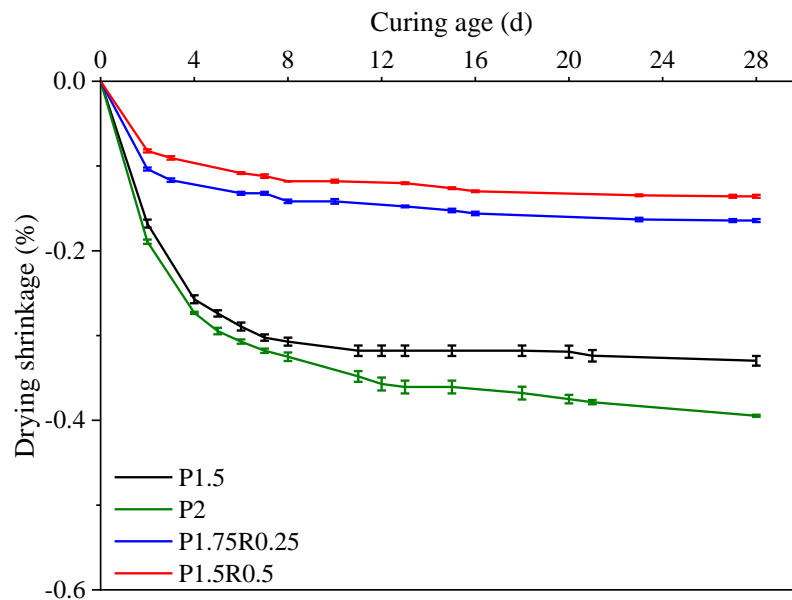
Figure 6-3 Drying shrinkage of SHGC specimens with various hybrid fibre content.

6.3.3 Strain-hardening behaviour

This section discusses the uniaxial tensile behaviour of SHGC specimens in terms of stress-strain response, failure patterns, tensile strength, and strain-hardening behaviour. The uniaxial tensile properties of all mixtures are summarised in Table 6-3.

6.3.3.1 Stress-strain response

Figure 6-4 displays the uniaxial tensile stress-strain curves of all SHGC specimens. All specimens exhibited strain-hardening behaviour under uniaxial tension, where the tensile stress increased linearly with the increase of tensile strain until it reached the first-crack

strength. Then, the stress-strain curves became nonlinear, and the slope of the curve decreased sharply, indicating that the specimens entered the strain-hardening stage. Finally, the maximum tensile stress was reached, and the specimens failed. As shown in Table 6-3 and Figure 6-4, P1.5 had an ultimate tensile strain of 5.15%, while the increase of PVA fibre by 0.5% and the addition of RTS by 0.5% resulted in the reduction of ultimate tensile strain by 4.89% and 15.95%, respectively. In comparison with P2, the partial replacement of PVA fibre with RTS fibre by 0.25% led to a slight increase of ultimate tensile strain by 0.39%, whereas replacing 0.5% PVA fibre with RTS fibre resulted in the reduction of ultimate tensile strain by 11.63%, which can be mainly attributed to the different characteristics of PVA and RTS fibres in terms of elastic modulus and interaction with geopolymer matrix.

Table 6-3 Uniaxial tensile properties of all SHGC mixtures.

Mix No.	Fist-crack strength (MPa)	Ultimate tensile strength (MPa)	Tensile strain capacity (%)	Average crack width (μm)
P1.5	1.84	4.37	5.15	111.35
P2	2.68	4.45	4.91	85.39
P1.75R0.25	2.52	4.70	4.92	78.72
P1.5R0.5	2.13	3.03	4.33	72.17
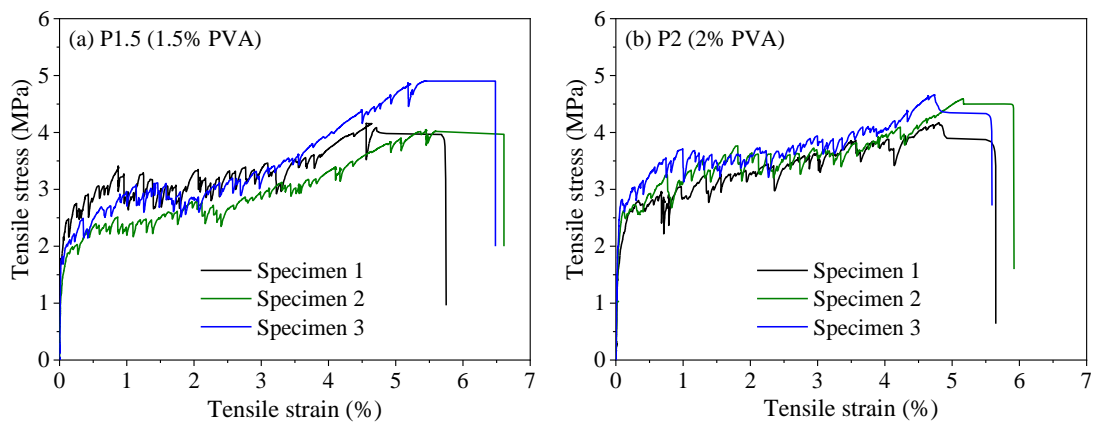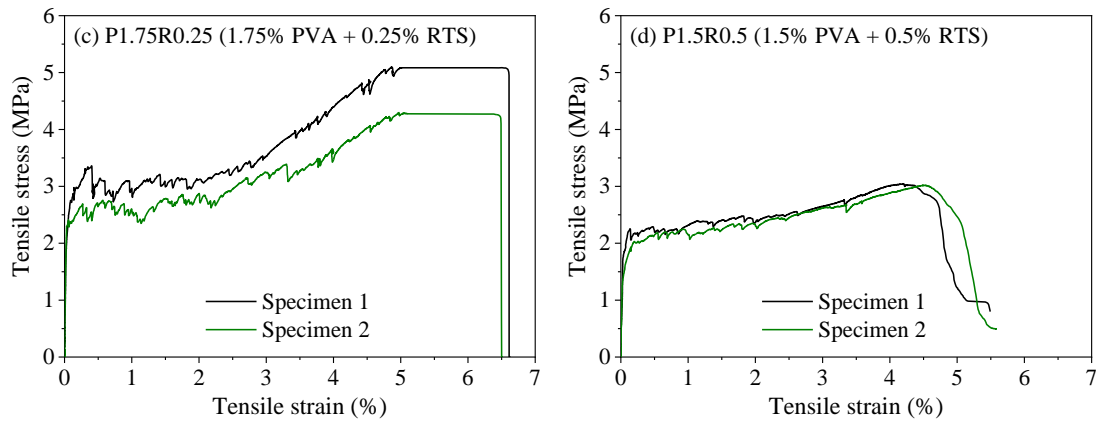
Figure 6-4 Tensile stress-strain curves of all SHGC mixtures.

6.3.3.2 Failure patterns

Figure 6-5 illustrates the typical failure patterns of SHGC mixtures under uniaxial tension. All cracks were captured right before unloading to avoid difficulty in tracing the cracks due to the possible closure of microcracks when the load was removed (Nematollahi et al., 2015a). Here, only the tested area within the gauge length (30 × 80 mm) is presented. As expected, all SHGC specimens demonstrated multiple microcracks under uniaxial tension, leading to strain-hardening behaviour. SHGC reinforced with mono PVA fibre indicated wider crack width and space between cracks (Figure 6-5a, b), whereas SHGC reinforced with hybrid PVA and RTS fibres showed tighter crack width and space between cracks (Figure 6-5c, d). These microcrack features are consistent with those observed from the stress-strain curves presented in Figure 6-4. Compared to mono PVA fibre reinforced SHGC, specimens containing RTS fibre had smaller average crack width (see Table 6-3 and Figure 6-5) due to the higher elastic modulus of RTS fibre than PVA fibre.

(a) P1.5　　　　　　(b) P2　　　　　　(c) P1.75R0.25　　　　(d) P1.5R0.5
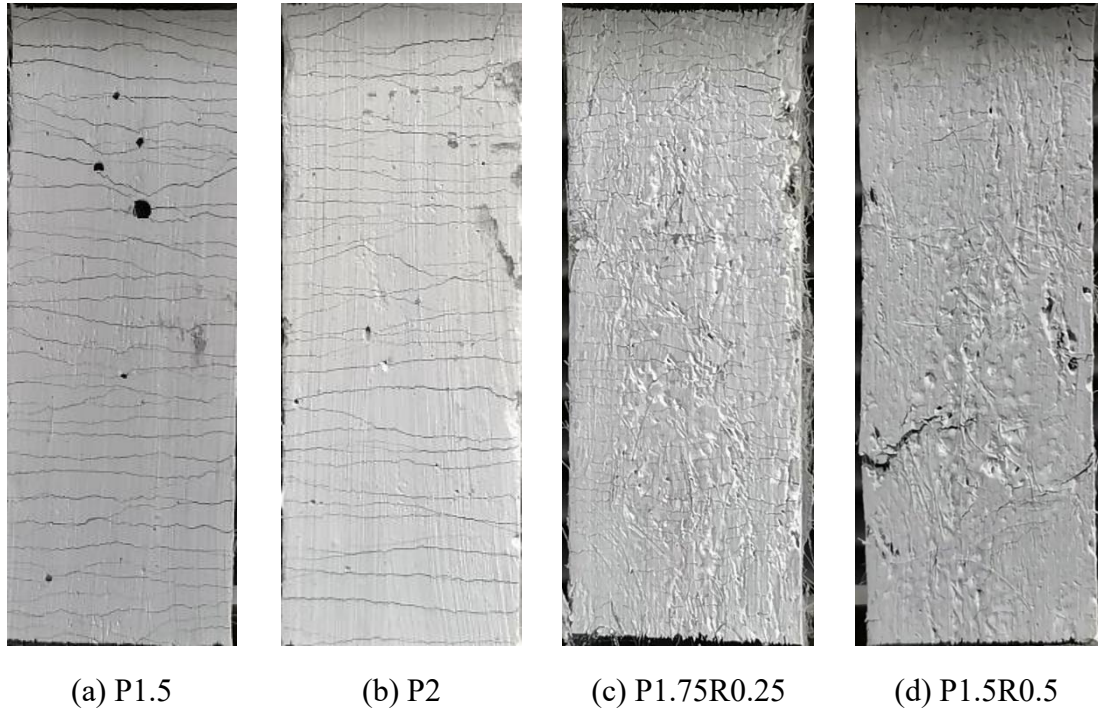
Figure 6-5 Typical failure patterns of SHGC mixtures under uniaxial tension.

6.3.3.3 Tensile strength

The effects of PVA fibre and hybrid PVA and RTS fibre content on tensile strength of SHGC are shown in Figure 6-6. It can be observed that the addition of PVA fibre and RTS fire resulted in opposite trends in tensile strength of SHGC specimens. Compared with P1.5, the increase of PVA fibre content by 0.5% resulted in a slight increase in ultimate tensile strength by 2.31%, which can be attributed to the fibre bridging effect, because the efficient bridging tends to be provided by increased number of fibres. However, when 0.5% RTS fibre was added into P1.5, the tensile strength of SHGC specimens was greatly dropped by 30.72%. The significant decline in tensile strength can be ascribed to the excessive addition of RTS fibre, leading to fibre-balling effect, which was also reported in previous studies (Mohammed et al., 2018, Wang et al., 2020a).

Regarding the partial replacement of PVA fibre with RTS fibre, the tensile strength of SHGC specimens was enhanced with the increase of replacement level by up to 0.25%, but further increase the replacement level by 0.5% resulted in the decline of tensile strength. Compared with P2.0, when PVA fibre was replaced with RTS fibre by 0.25%, the tensile strength was enhanced by 11.06%. This can be mainly ascribed to the better fibre-bridging effect provided by RTS fibre, because RTS fibre has higher elastic modulus than PVA fibre, and stronger bond between fibre and geopolymer matrix due to its

hydrophilic nature and large surface area (Ranjbar et al., 2016b, Ranjbar et al., 2016a). However, further increase of the replacement level up to 0.5%, a significant decrease of tensile strength by 32.30% was observed, which can be attributed to the poor fibre distribution caused by fibre balling effect.
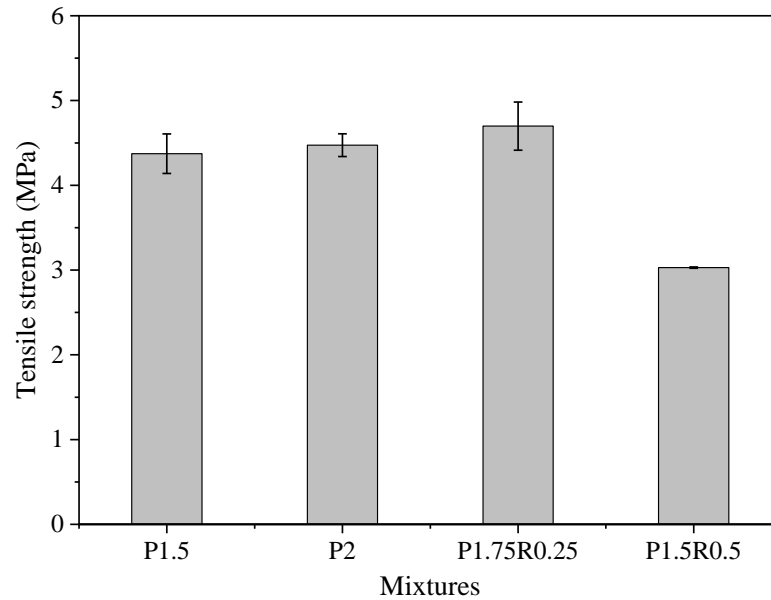
Figure 6-6 Effect of hybrid PVA-RTS fibre content on tensile strength of SHGC.

6.3.4   Static compressive behaviour

Figure 6-7 exhibits the typical failure patterns of SHGC cubes under uniaxial compression. All specimens failed while remaining their original shapes with tensile cracks formed over specimens. The propagation of tensile cracks was prevented by fibres that provided extra energy for resisting tensile stress in the cube, and thus helped to avoid the typical brittle failure mode (Jenq and Shah, 1986).

(a) P1. 5   (b) P2   (c) P1. 75R0.25   (d) P1.5R0.5
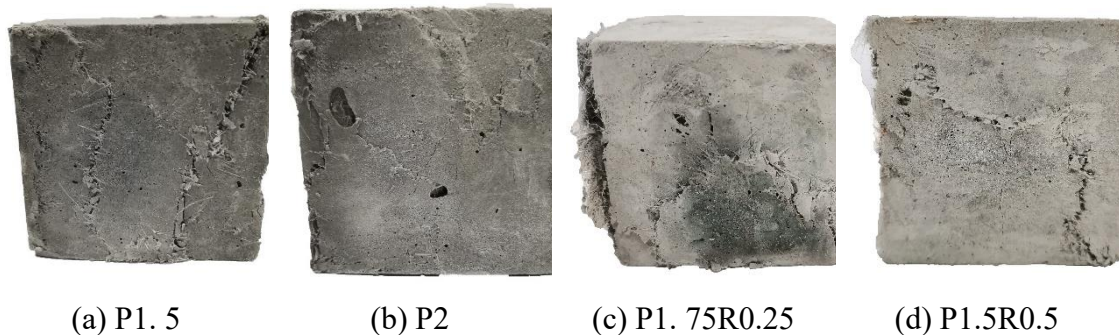
Figure 6-7 Typical failure patterns of SHGC cubes.

The effect of hybrid fibre content on the static compressive strength of SHGC cubes and cylinders is presented in Figure 6-8. In general, increasing the PVA fibre content and

adding RTS fibre led to different changing trends in compressive strength. SHGC specimens containing 1.5% mono-PVA fibre (P1.5) had a static compressive strength of 37.9 MPa. When the PVA fibre content was increased to 2%, the compressive strength was reduced by 13.54%, whereas the addition of 0.5% RTS fibre resulted in an increase of compressive strength by 13.02%. The different trend caused by increasing PVA fibre content and adding RTS fibre was in agreement with our previous observation (Wang et al., 2020a). This is caused by different properties of PVA and RTS fibres, as RTS fibre has higher stiffness and hydrophilicity nature, and therefore can absorb more energy and provide stronger fibre-matrix interaction (Ranjbar and Zhang, 2020, Ranjbar et al., 2016b, Fang and Zhang, 2020). Regarding the partial replacement of PVA with RTS fibre, the increase of replacement level resulted in an increase of compressive strength. Compared with P2, the compressive strength was increased by 8.04% and 30.72%, when PVA fibre was replaced with RTS fibre by 0.25% and 0.5%, respectively. The increase of compressive strength with a higher amount of RTS fibre can be ascribed to its hydrophilicity nature and higher stiffness than PVA fibre.

As seen in Figure 6-8, the compressive strengths obtained from cylinders were 60.20%-118.27% higher than those from standard cube specimens. The higher compressive strength of cylinders than that of cubes agrees with a previous observation that cylinder specimen with a diameter of 77 mm and height of 38 mm had 50-85% higher static compressive strength than cube specimens with a length of 100 mm (Wang et al., 2011b). This is because the height of the cylinder was smaller than its diameter, and therefore the confinement zone extends through the specimen, which resulted in crushing failure instead of cracking failure (Kim and Yi, 2002).
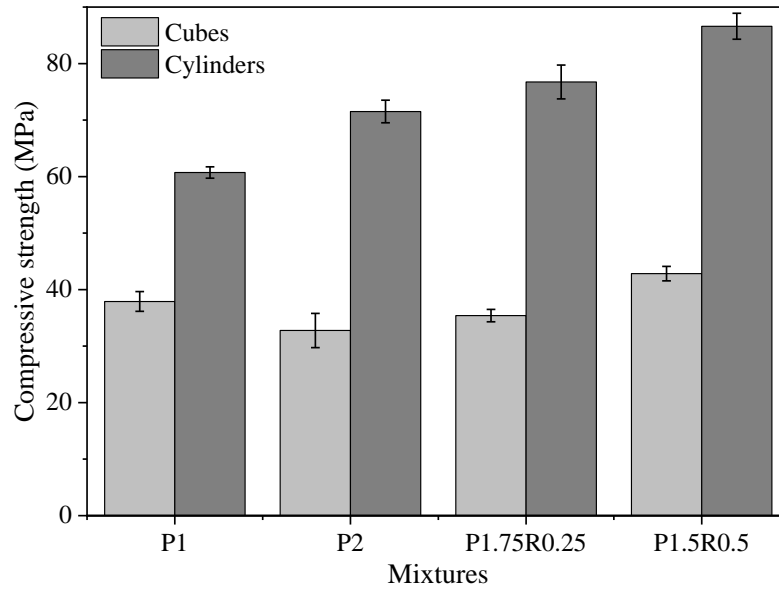
Figure 6-8 Compressive strength of SHGC cubes and cylinders with various hybrid fibre content.

6.3.5 Static splitting tensile behaviour

Figure 6-9 shows the static splitting tensile strength of all mixtures. Compared with P1.5, the increase of PVA fibre content by 0.5% and the addition of RTS fibre by 0.5% resulted in slight increase of splitting tensile strength by 5.44% and 11.32%, respectively. Regarding the partial replacement series, when replacing PVA fibre with RTS fibre by 0.25%, the splitting tensile strength had 0.40% reduction, whereas the replacement of PVA fibre with RTS fibre by 0.5% led to a slight increase of splitting tensile strength by 5.58%.
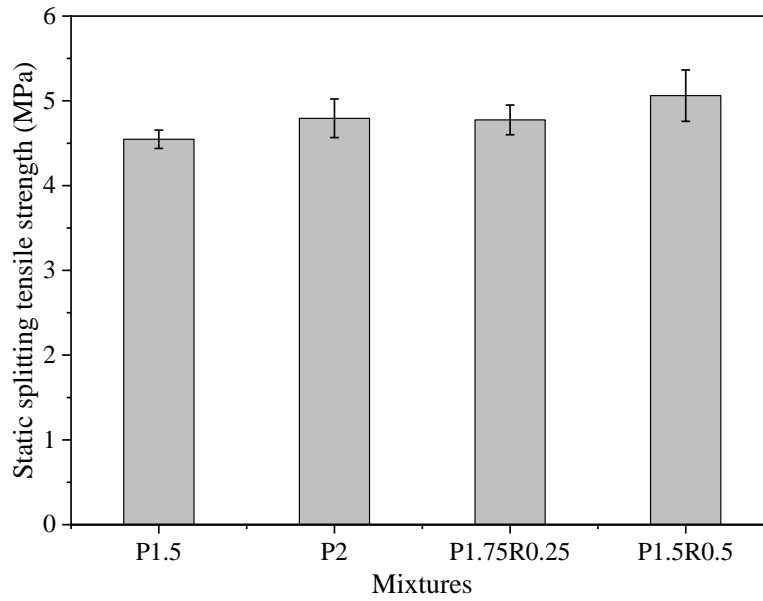
Figure 6-9 Static splitting tensile strength of all mixtures

6.3.6 Dynamic compressive behaviour

This section presents the results of dynamic compressive behaviour of SHGC specimens with various hybrid fibre content, including failure patterns, stress-strain response, dynamic compressive strength, dynamic increase factor (DIF), and energy absorption capacity. Table 6-4 summarises the dynamic compressive properties of SHGC, in comparison with the corresponding static compressive properties.

Table 6-4. Summary of static and dynamic properties of SHGC specimens with various hybrid fibre content obtained from SHPB test.

Mix no.	Static compressive strength (MPa)		Average impact velocity (m/s)	Average strain rate (s^{-1})	Maximum dynamic stress (MPa)	Strain at peak stress (µε)	Ultimate strain (µε)	DIF		Fracture energy (J)	Total energy (J)
	Cubes	Cylinders						Cubes	Cylinders		
P1.5	37.90	60.72	5.95	42.59	56.84	9117	15710	1.50	0.94	114.77	206.63
			8.34	105.50	70.43	13730	29480	1.86	1.16	193.81	491.01
			10.86	145.30	86.87	18930	37100	2.29	1.43	305.15	676.83
P2	32.77	71.52	5.92	58.14	45.05	8548	17780	1.37	0.63	95.70	205.13
			7.91	80.08	58.55	10780	24600	1.79	0.82	128.98	351.83
			10.46	133.80	67.45	16740	32780	2.06	0.94	193.54	502.16
P1.75R0.25	35.40	76.74	6.10	54.03	49.94	8986	18040	1.41	0.65	106.95	216.94
			8.34	107.00	55.68	11720	30610	1.57	0.73	135.40	455.27
			10.85	181.60	74.62	24080	45210	2.11	0.97	305.48	699.38
P1.5R0.5	42.83	86.60	5.92	49.46	49.85	7082	17270	1.16	0.58	71.69	217.89
			8.24	126.60	53.05	15740	32600	1.24	0.61	210.12	447.90
			10.56	178.4	66.07	19990	43050	1.54	0.76	281.30	669.72

6.3.6.1 Failure patterns

Figure 6-10 demonstrates the typical failure patterns of all mixtures containing various hybrid fibre content at three impact velocities, i.e., 6, 8, and 10 m/s, corresponding to the strain rates of around 50/s, 100/s, and 150/s, respectively. With the increase of strain rate, the damage level of all SHGC mixtures increased, and the failure patterns of all mixtures changed from splitting failure to pulverise failure. As displayed in Figure 6-10, only several small cracks can be observed on specimens under a low level of impact velocity and strain rates. When the impact velocity and strain rate were increased to a medium level, the specimens exhibited splitting failure with major cracks formed on specimens. Pulverise failure occurred when the specimens were subjected to a high level of impact velocity and strain rate. The change of failure patterns can be ascribed to the very limited time for microcracks to propagate but to generate more cracks under high impact velocity (Zhang et al., 2018, Chen et al., 2019).

At the high level of impact velocity, all specimens showed a pulverise failure, and the broken fragments of specimens had different sizes with various hybrid fibre content. The incorporation of RTS fibre mitigated the damage of specimens. SHGC specimen reinforced with mono PVA fibre had many fragments that were small and irregular, whereas SHGC specimens containing both PVA and RTS fibres had relatively larger major fragments. This agrees with the previous findings that the addition of steel fibre restricted the transverse deformation of specimens (Wu et al., 2017).

Mix No.	Strain rate (s⁻¹)		
	50	100	150
P1.5			

129

P2

P1.75R0.2
5

P1.5R0.5
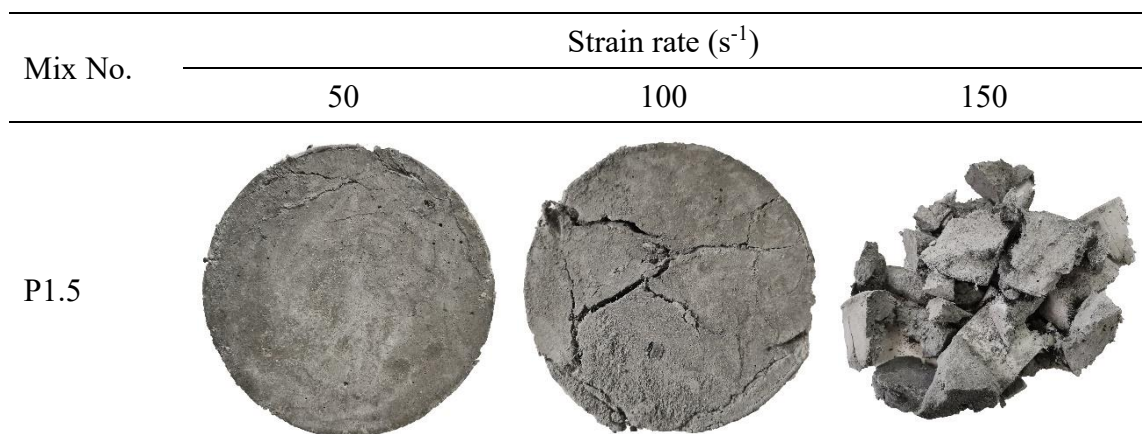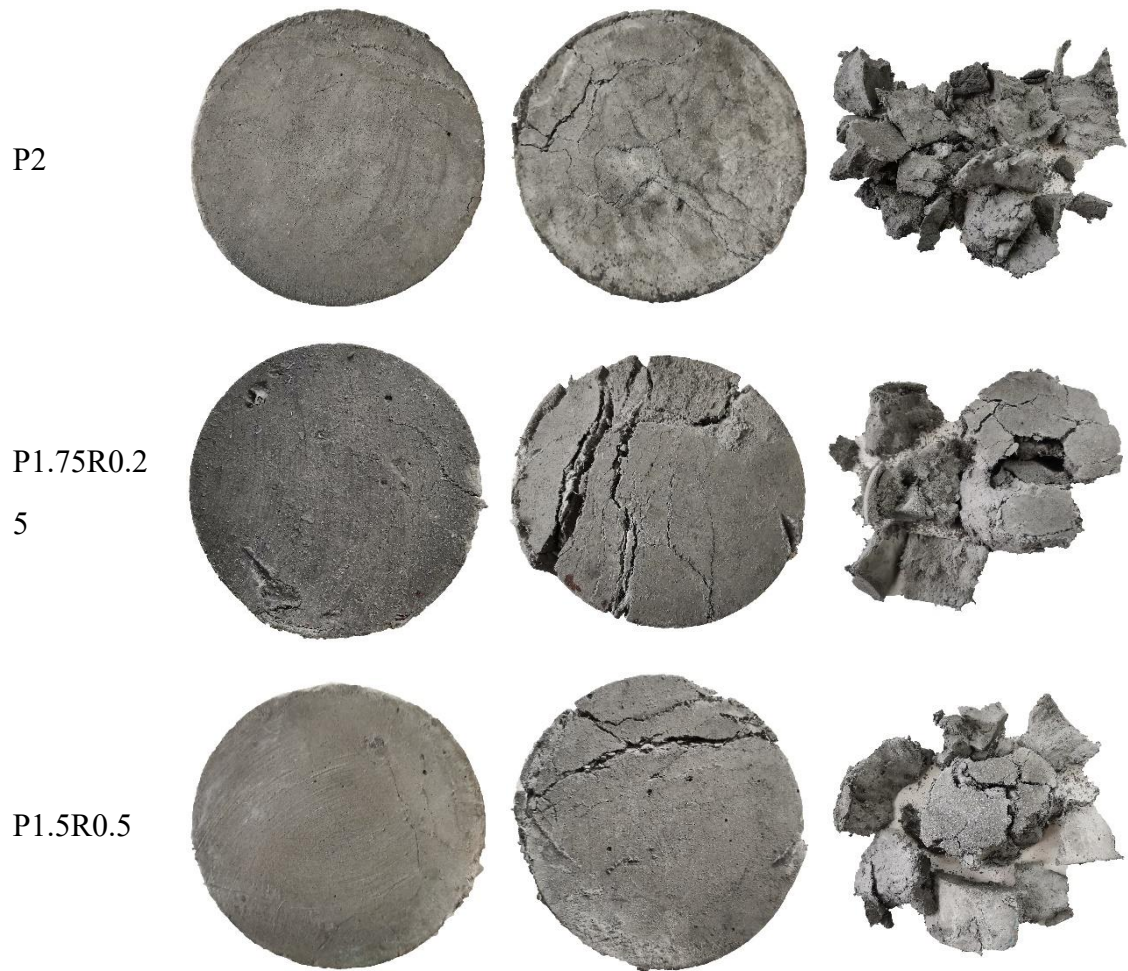
Figure 6-10 Typical failure patterns of all mixtures under dynamic compression at various strain rates.

6.3.6.2 Stress-strain response

Figure 6-11 shows the dynamic compressive stress-strain curves of SHGC specimens reinforced with various hybrid fibre content at different strain rates. Overall, with increasing strain rate, all SHGC mixtures exhibited an increase in dynamic compressive strength, strain at peak stress, and ultimate strain. This is known as the strain rate effect that the strength of concrete can be significantly enhanced by the loading rate (Zhang et al., 2018, Chen et al., 2019, Sun et al., 2018). The enhancement of dynamic compressive strength was resulted from lateral inertia associated with friction to the contact surface under rapid impact loading, which leads to stress transfer and stress redistribution between fibre and matrix through adhesive interface (Lee and Jacobsen, 2011, Cotsovos and Pavlović, 2008, Li and Meng, 2003). Based on these dynamic compressive stress-strain curves, the effects of PVA and RTS fibres on different dynamic parameters can be investigated in detail in a quantitative manner, as illustrated below.
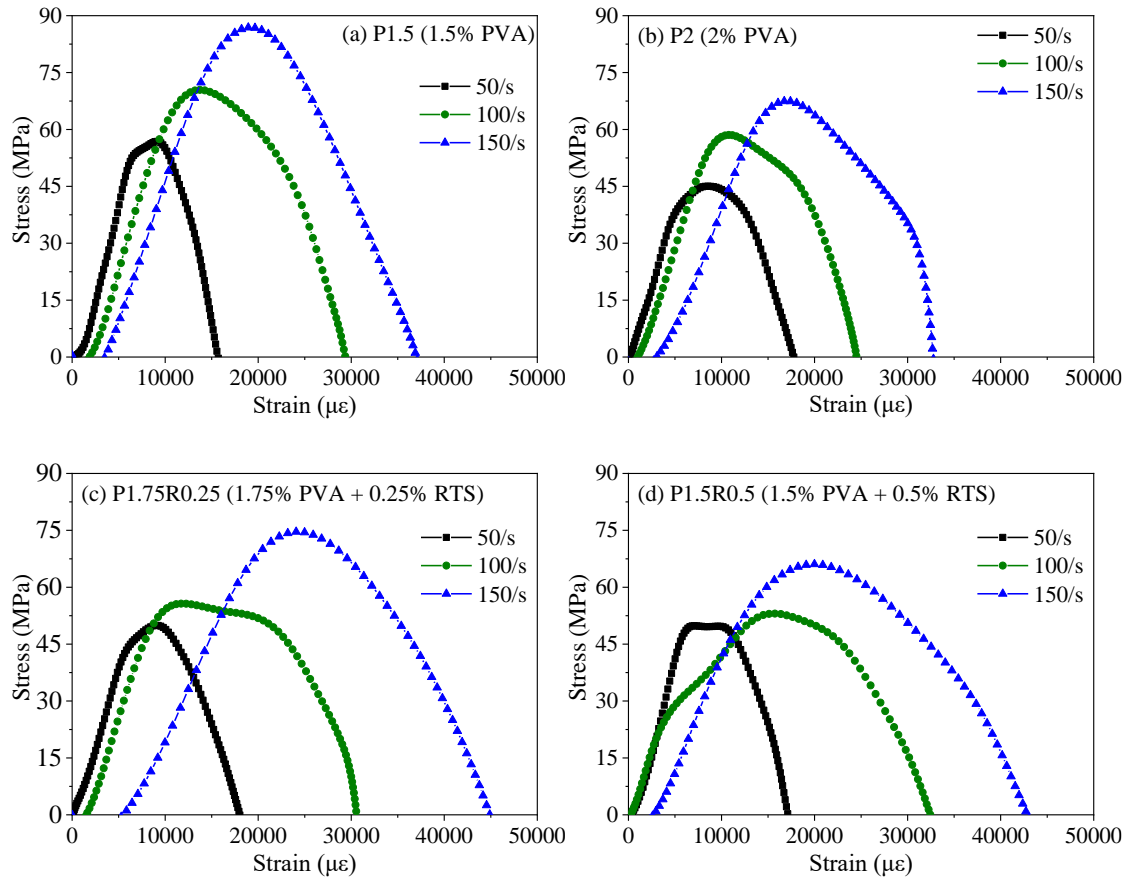
Figure 6-11 Dynamic compressive stress-strain curves of all mixtures at different strain rates.

6.3.6.3 Dynamic compressive strength

Figure 6-12 shows the dynamic compressive strength of SHGC specimens containing various hybrid fibre content at different strain rates. Overall, the increase of strain rate resulted in a significant improvement of dynamic compressive strength for all mixtures. As the strain rate increased from 50/s to 100/s, and 150/s, the dynamic compressive strength of all mixtures went up by 6.43%-29.97%, and 32.54%-52.83%, respectively.

In SHGC reinforced with 1.5% PVA fibre (P1.5), the increase of PVA fibre content and the addition of RTS fibre both led to a decreased dynamic compressive strength. When the PVA fibre content was increased to 2%, the dynamic compressive strength of specimens dropped by 20.74%, 16.86%, and 22.36% at strain rates of 50/s, 100/s, and 150/s, respectively. When 0.5% RTS fibre was incorporated into P1.5, the dynamic compressive strength of specimens was declined by 12.30%, 24.67%, and 23.94% at strain rates of 50/s, 100/s, and 150/s, respectively. The improvement of dynamic compressive strength with RTS fibre replacement level varied at different strain rates. At

a low strain rate, the increase of RTS fibre replacement level by 0.25% and 0.5% resulted in an increase in dynamic compressive strength by 10.85% and 10.65%, respectively. At a medium strain rate, replacing 0.25% and 0.5% PVA fibre with RTS fibre resulted in a reduction in dynamic compressive strength by 4.91% and 9.39%, respectively. When the specimens subjected to a high strain rate, the replacement of 0.25% PVA fibre with RTS fibre led to a 10.63% rise in dynamic compressive strength, but further replacing 0.5% PVA fibre with RTS fibre resulted in a 2.05% decline in dynamic compressive strength.

Regarding failure patterns, the hybrid PVA-RTS fibre reinforced SHGC specimens kept intact under dynamic compression at the strain rate of 50/s, suggesting that the partial replacement of PVA fibre with RTS fibre can effectively improve the crack resistance of SHGC at a low strain rate, hereby 50/s, which became less effective when the strain rates were increased to 100/s and 150/s, and the specimens exhibited splitting failure and pulverise failure, respectively, without an obvious increase in dynamic compressive strength. This can be ascribed to the short time for microcracks to propagate and more cracks generated under a high impact velocity (Zhang et al., 2018, Chen et al., 2019).
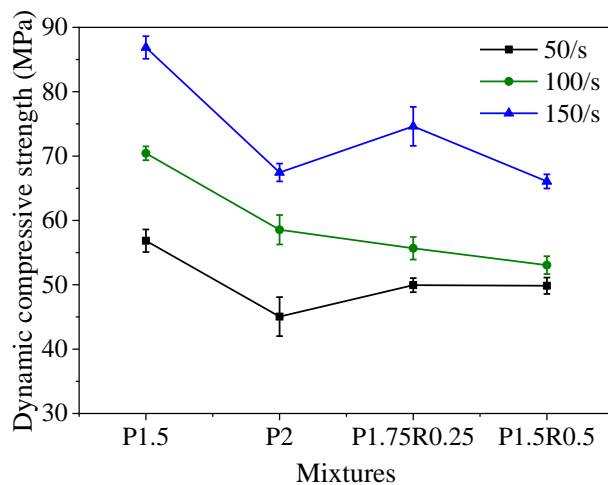
Figure 6-12 Dynamic compressive strength of all mixtures under dynamic compression.

6.3.6.4 Dynamic increase factor (DIF)

Dynamic increase factor (DIF) is defined as the ratio of dynamic compressive strength to the static compressive strength of the mixture, which has been widely used to evaluate the effect of strain rate on the material properties (Xiao et al., 2015). Figure 6-13 illustrates the DIF of all SHGC specimens under dynamic compression. To estimate the size effect, static compressive strength of SHGC was obtained from both cubes and cylinders.

Overall, SHGC cubes had a higher DIF than that of cylinders due to the lower static compressive strength of cubes compared to cylinders (Wang et al., 2011a).

As seen in Figure 6-13a, the increase of PVA fibre content and the addition of RTS fibre both resulted in a decrease in DIF. With the increase of PVA fibre content from 1.5% to 2%, the DIF of SHGC cubes dropped by 8.33%, 3.84%, and 10.19% at strain rates of 50/s, 100/s, and 150/s, respectively. The addition of 0.5% RTS fibre to P1.5 led to a 22.40%, 33.35%, and 32.70% reduction in DIF of SHGC at strain rates of 50/s, 100/s, and 150/s, respectively. When 0.25% PVA fibre was replaced with RTS fibre, the DIF of SHGC was slightly increased by 2.61% and 2.40% at low and high strain rates, respectively, whereas a reduction of 11.98% in DIF can be observed at a medium strain rate. Compared with P2, the replacement of PVA fibre with RTS fibre by 0.5% resulted in a decline of 15.35%, 30.69%, and 25.07%, respectively in DIF. Similar changing trends can be observed for DIF of SHGC cylinders, as illustrated in Figure 6-13b. The addition of 0.5% PVA fibre and 0.5% RTS fibre both led to a significant decrease in DIF, whereas the partial replacement of PVA fibre with RTS fibre indicated an insignificant influence on DIF of SHGC cylinders. This can be attributed to the complex stress state in cylinders under static and dynamic compression that the inner core of cylinders failed due to crushing (Wang et al., 2011b, Kim and Yi, 2002).
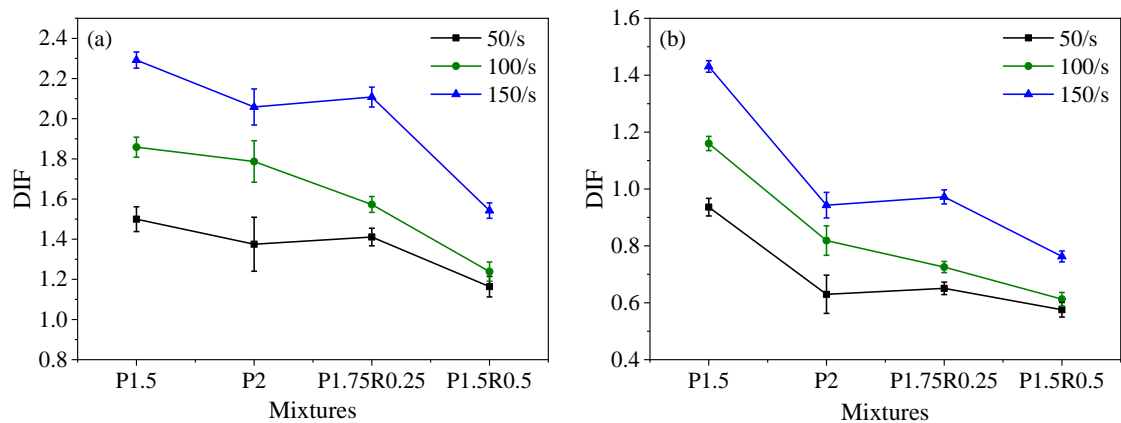
Figure 6-13 DIF of all specimens under dynamic compression: (a) cubes and (b) cylinders.

6.3.6.5 Energy absorption capacity.

Figure 6-14 shows the energy absorption capacity of SHGC specimens reinforced with various hybrid fibre content at different strain rates. During the SHPB test, the energy

absorbed by the specimen up to the peak stress was defined as fracture energy (Figure 6-14a), while the energy absorbed in both pre-peak and post-peak regions was defined as total energy (Figure 6-14b). It can be observed that the energy absorbed by specimens in the post-peak region was higher than that in the pre-peak region, which can be ascribed to higher energy demand in fibre pull-out or rupture than that in the initiation of microcracks (Chen et al., 2019).

Both fracture energy and total energy were increased with increasing strain rate, which is consistent with the other dynamic parameters discussed above and a previous study (Chen et al., 2019). The enhancement of fracture energy and total energy with the increase of strain rate can be attributed to the cracks generated in the limited loading time at high strain rates. The increased energy absorption capacity of SHGC can be observed with the partial replacement of PVA fibre with RTS fibre by up to 0.25%, which can be attributed to the higher elastic modulus and hydrophilicity of RTS fibre compared to PVA fibre, which led to a stronger bond between fibre and geopolymer matrix (Ranjbar et al., 2016b). However, after this replacement level the influence of RTS fibre on the energy absorption capacity of SHGC was negligible mainly due to fibre-balling effect.
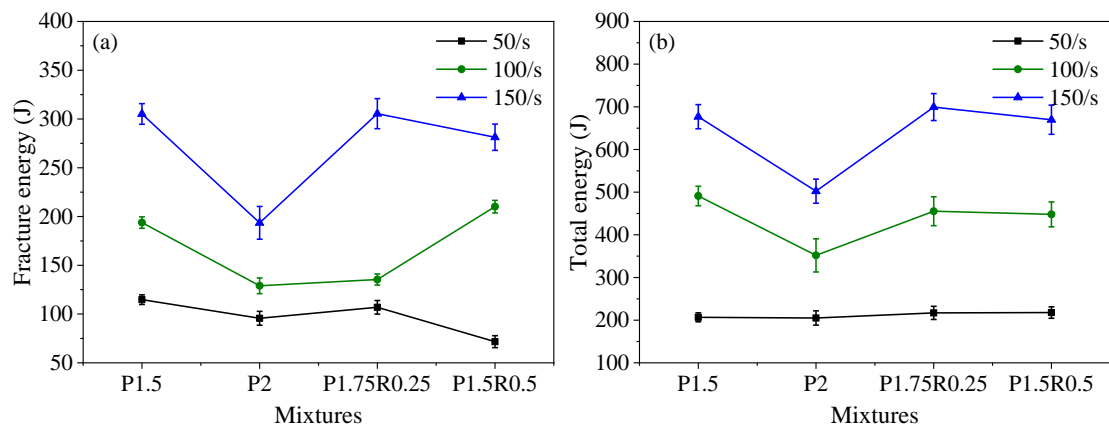
Figure 6-14 Energy absorption capacity of all mixtures under dynamic compression at various strain rates: (a) fracture energy and (b) total energy.

6.3.7 Dynamic splitting tensile behaviour

6.3.7.1 Failure patterns

Figure 6-15 shows the typical failure patterns of all mixtures. At low impact velocity, all specimens remained the shape integrity with a straight crack along the surface of the specimen. At medium and high impact velocity, all SHGC specimens were broken into

two or three parts, and the formed crack along the surface was not straight. Triangular crush at both ends of the specimen, where impact load was applied, was observed, which could be attributed to the cracks appearing before the stress equilibrium state was reached (Chen et al., 2016), and the increased friction at the interface between the specimen and loading points (Feng et al., 2018).
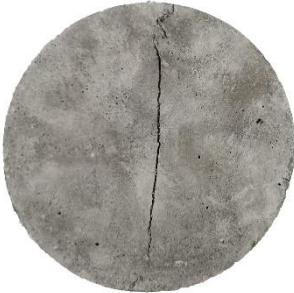
Mix No.	Impact velocity (m/s)		
	6	8	10
P1.5			
P2			
P1.75R0.25			
P1.5R0.5			

Figure 6-15 Typical failure patterns of all mixtures

6.3.7.2 Dynamic splitting tensile strength

Figure 6-16 shows the effect of hybrid PVA-RTS fibre content on the dynamic splitting tensile strength of all mixtures at different impact velocity. The trend of dynamic splitting tensile strength was similar to other dynamic properties and directly associated with strain rate. When strain rate increased (generated by increased impact velocity), the dynamic splitting tensile strength increased in all mixtures.
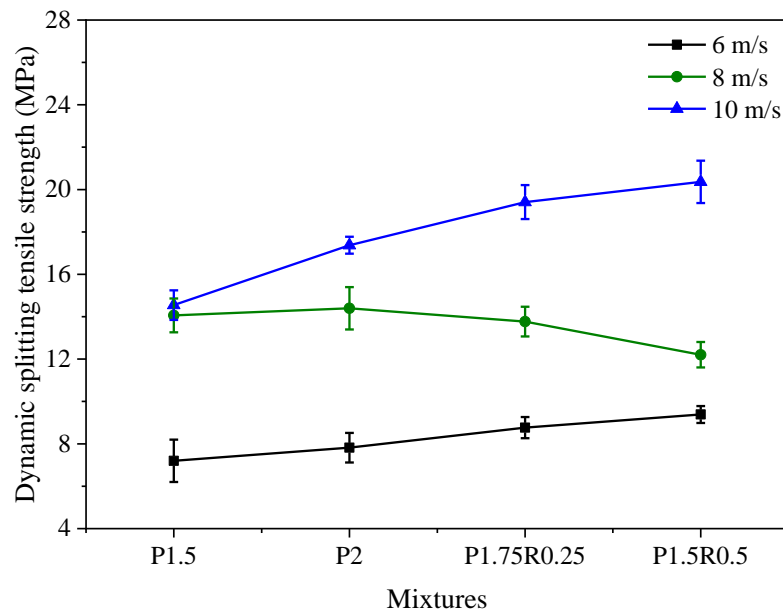
Figure 6-16 Effect of hybrid fibre content on dynamic splitting tensile strength of all mixtures at different impact velocity

At low and high impact velocity, the increase of PVA fibre from 1.5% to 2% resulted in the increase of dynamic splitting tensile strength by 8.60% and 19.43%, respectively. When adding 0.5% RTS fibre into P1.5, the dynamic splitting tensile strength showed an enhancement by 30.36% and 39.99% at low and high impact velocity, respectively. Regarding the partial replacement series, the increase of replacement level led to an increase in dynamic splitting tensile strength at low and high impact velocity. When PVA fibre was replaced with RTS fibre by 0.25%, the dynamic splitting tensile strength increased by 12.12% and 11.72% at low and high impact velocity, respectively. Further increasing the replacement level to 0.5% RTS in P2 could result in the enhancement of dynamic splitting tensile strength by 20.04% and 17.21% at low and high impact velocity,

respectively. The increase of dynamic splitting tensile strength with the increase RTS fibre content in the composite could be attributed to the higher elastic modulus of RTS fibre.

6.4 Concluding remarks

In this chapter, a series of tests were conducted to systematically investigate the effects of polyvinyl alcohol (PVA) and recycled tyre steel (RTS) fibres and strain rate on mechanical properties of FA-GGBS based SHGC cured at ambient temperature. Based on the obtained experimental results, the main conclusions can be drawn as follows:

- The increase of PVA fibre content, the addition of RTS fibre, and the partial replacement of PVA fibre with RTS fibre all resulted in a decline in flowability of SHGC due to random fibre balling and agglomeration in the mixing process. The incorporation of RTS fibre can effectively reduce the drying shrinkage of SHGC because of the high elastic modulus of RTS fibre and its strong interaction with geopolymer matrix due to the hydrophilic nature and large surface area.

- All SHGC specimens exhibited strain-hardening behaviour under uniaxial tension. For SHGC containing 1.5% mono PVA fibre, the increase of PVA fibre content to 2% resulted in a 2.31% rise in tensile strength, while the addition of 0.5% RTS fibre led to a 30.72% drop in tensile strength due to fibre balling effect. The tensile strength of SHGC was increased by 11.06% when 0.25%PVA fibre was replaced with RTS fibre, which can be ascribed to the enhanced fibre-bridging effect because of the higher stiffness and hydrophilic surface of RTS fibre.

- Under static compression, all SHGC specimens retained the shape integrity because of the fibre bridging effect. The compressive strength of SHGC cube declined by 13.54% with the increase of PVA fibre content by 0.5% but went up by 13.02% with the addition of 0.5% RTS fibre into P1.5. The partial replacement of PVA fibre with RTS fibre caused an enhanced compressive strength of SHGC as well. For SHGC cylinders, the compressive strength was also improved with increasing PVA content, the addition of RTS fibre and replacement of PVA fibre with RTS fibre.

- Under dynamic compression, all SHGC mixtures failed with microcracks at a low strain rate of 50 s^{-1} but exhibited pulverised failure at a high strain rate of 150 s^{-1}. With the increase of strain rate from 50 s^{-1} to 100 s^{-1}, and 150 s^{-1}, the dynamic compressive

strength of SHGC mixtures was increased by 6.43%-29.97%, and 32.54%-52.83%, respectively.

- Failure patterns of all mixtures changed with the increase of impact velocity under dynamic splitting tension. At low and high impact velocity, the dynamic splitting tensile strength increase with the increase of PVA fibre content, addition of RTS fibre, and the partial replacement of PVA fibre with RTS fibre. The incorporation of RTS fibre contributed to the increase of dynamic splitting tensile strength due to the higher elastic modulus and hydrophilic nature.

Chapter 7 Conclusions and Future Remarks

7.1 Conclusions

This thesis developed a hybrid PVA-RTS fibre reinforced SHGC with desired engineering properties based on micromechanics and fracture mechanics theory, and experimentally and systematically investigated the effects of sand and fibres on the engineering properties of SHGC. This thesis provides a comprehensive understanding of the strain-hardening behaviour and engineering properties of FA-GGBS based SHGC reinforced with hybrid PVA-RTS fibre and cured at ambient temperature for civil infrastructure applications. The main conclusions are drawn as follows:

- With the increase of sand content, the flowability, setting time, drying shrinkage, and compressive strength of SHGC reduced at early ages up to 28 d. However, at 28 d, the incorporation of sand up to 20 wt% increased the flexural strength and toughness of SHGC, but the further increase of sand content up to 40 wt% results in a decrease in flexural strength and toughness, which was associated with the brittleness of the geopolymer matrix. All SHGC specimens exhibited deflection hardening characteristics along with large deflection and multiple microcracks distributed over the tensile side of the specimens, and the widths of microcracks are within 300 μm and mostly smaller than 45 μm. The deflection-hardening behaviour of SHGC was governed by fibre toughening mechanisms, including fibre rupture, fibre pull-out, and fibre bridging.

- SHGC specimens reinforced with 2% PVA fibre exhibited strain-hardening behaviour with the average first-crack strength and ultimate tensile strength of 2.68 MPa and 4.45 MPa, respectively. The tensile strain capacity of specimens reached 4.91% with an average crack width of 85.39 μm. Both strength and energy-based criteria were met and the micromechanics of SHGC was valid.

- The increase of PVA fibre content resulted in reductions in flowability, drying shrinkage and compressive strength of SHGC, but significant improvement in tensile strength and ultimate strain of SHGC under uniaxial tension due to the fibre bridging

effect. Dynamic compressive behaviour of SHGC is strongly associated with the strain rate. The dynamic compressive strength of SHGC with various PVA fibre dosages is increased by 9.26%-29.97% and 41.59%-69.78% as the strain rate increases from 50/s to 100/s and 150/s, respectively. Overall, the mixture containing 1.5% PVA fibre can be regarded as the optimal mixture for SHGC considering static mechanical properties and dynamic compressive behaviour.

- The hybridisation of PVA fibre with RTS fibre resulted in a slight reduction in flowability but a significant improvement in resistance to drying shrinkage. Moreover, all specimens exhibited the desired strain-hardening behaviour with multiple microcracks formed under uniaxial tension. Compared to SHGC containing 2% PVA fibre, replacing PVA fibre with 0.25% RTS fibre led to an improvement in tensile strength by 11.06%. The dynamic compressive behaviour of SHGC was highly associated with the strain rate. With the increase of strain rate from 50/s to 100/s and 150/s, the dynamic compressive strength of SHGC was increased by 6.43%-29.97% and 32.54%-52.83%, respectively.

7.2 Prospects

Although the effects of fine silica sand and fibres on the engineering properties of SHGC and the development of a hybrid PVA-RTS fibre reinforced SHGC have been presented in this thesis, there are still worthwhile aspects that should be further explore in the future, including the effects of geopolymer precursors and matrix, long-term durability, sustainability assessment, engineering application. The future works associated with the study developed in this thesis are highlighted below.

- In this study, FA and GGBS were used as raw materials to produce geopolymers with desired engineering properties. However, as the thesis has mentioned, chemical compositions and particle size distributions of FA and GGBS vary from different sources, which can significantly affect the engineering properties of SHGC. Therefore, it is important to investigate the effects of FA and GGBS with different characteristics on the engineering properties of SHGC.

- According to micromechanics criteria, strain-hardening behaviour of SHGC is governed by strength and energy-based criteria. This study used SHGC containing 2%

PVA fibre to verify the micromechanics criteria and investigated the effect of fine silica sand and fibres on the engineering properties of SHGC. However, the effects of matrix, such as the mix proportions of geopolymer precursor, alkaline activator, have not been systematically investigated, and therefore should be experimentally investigated in the future work. This will provide a systematic guideline in tailoring SHGC with desired engineering properties.

- This study investigated the effects of fine silica sand, PVA fibre, and hybrid PVA-RTS fibres on the engineering properties of SHGC, respectively. However, previous studies demonstrated that the addition of fibre could affect the effect of sand on the engineering properties of SHGC. For pure geopolymers, the addition of sand could result in the increase of the compressive strength of geopolymers. However, when the fibre is added, the compressive strength of SHGC could drop with the increase of sand content. Hence, the synergies between sand and fibre should be further analysed to understand the effect of sand and fibres on the engineering properties of SHGC.

- This thesis characterised the flowability, drying shrinkage, and static and dynamic mechanical properties of SHGC considering the effects of fine silica sand and fibres. However, it is important to have a comprehensive understanding of long-term durability of SHGC, such as chloride penetration, thermal stability, to ensure that the material is applicable for civil infrastructure in the long term.

- The application of geopolymers to replace cement has been demonstrated to have significantly reduced carbon emissions, and the incorporation of RTS fibre instead of industry manufactured steel fibre also contributes to the sustainability. However, this is still a lack of systematic evaluation of the life cycle assessment (LCA) on the application of SHGC, which could provide a profound understanding of the carbon emissions and serve as a reference for carbon tax assessment. Hence, the LCA of SHGC should be conducted in the future work.

References

Afroughsabet, V., Teng, S. 2020. Experiments on drying shrinkage and creep of high performance hybrid-fiber-reinforced concrete. *Cement and Concrete Composites,* 106**,** 103481.

Aghaee, K., Yazdi, M.A., Tsavdaridis, K.D. 2015. Investigation into the mechanical properties of structural lightweight concrete reinforced with waste steel wires. *Magazine of Concrete Research*, 67**,** 197-205.

Ahmed, S.F.U., Ronnie, Z. 2017. Ductile behavior of polyethylene fibre reinforced geopolymer composite. *Engineering Technology International Conference 2016 (Etic 2016),* 97.

Akkaya, Y., Peled, A., Picka, J.D. Shah, S.P. 2000. Effect of sand addition on properties of fiber-reinforced cement composites. *ACI Structural Journal,* 97**,** 393-400.

Al-Majidi, M.H., Lampropoulos, A. Cundy, A.B. 2017. Tensile properties of a novel fibre reinforced geopolymer composite with enhanced strain hardening characteristics. *Composite Structures,* 168**,** 402-427.

Aldabsheh, I., Garcia-Valles, M., Martinez, S. 2018. Interaction of micro/nano-metric size of Jordanian aluminosilicate raw materials with high pH solution. *Materials Letters,* 229**,** 57-59.

Alrefaei, Y., Dai, J.G. 2018. Tensile behavior and microstructure of hybrid fiber ambient cured one-part engineered geopolymer composites. *Construction and Building Materials,* 184**,** 419-431.

Alshaaer, M., Mallouh, S.A., Al-Kafawein, J., Al-Faiyz, Y., Fahmy, T., Kallel, A., Rocha, F. 2017. Fabrication, microstructural and mechanical characterization of Luffa Cylindrical Fibre - Reinforced geopolymer composite. *Applied Clay Science,* 143**,** 125-133.

Altwair, N.M., Johari, M.A.M., Hashim, S.F.S. 2012. Flexural performance of green engineered cementitious composites containing high volume of palm oil fuel ash. *Construction and Building Materials,* 37**,** 518-525.

ASTM. 2005. Standard Test Method for Flexural Performance of Fiber-Reinforced

143

Concrete (Using Beam With Third-Point Loading).

ASTM. 2012. Standard Specification for Coal Fly Ash and Raw or Calcined Natural Pozzolan for Use in Concrete.

ASTM. 2015. Standard Test Method for Flow of Hydraulic Cement Mortar.

ASTM. 2017. Standard Practice for Use of Apparatus for the Determination of Length Change of Hardened Cement Paste, Mortar, and Concrete.

ASTM. 2019a. Standard Specification for Coal Fly Ash and Raw or Calcined Natural Pozzolan for Use in Concrete.

ASTM. 2019b. Standard Test Methods for Time of Setting of Hydraulic Cement by Vicat Needle.

ASTM. 2020a. Standard Test Method for Compressive Strength of Hydraulic Cement Mortars (Using 2-in. or [50-mm] Cube Specimens).

ASTM. 2020b. Standard Test Method for Linear-Elastic Plane-Strain Fracture Toughness of Metallic Materials.

ASTM. 2021. Standard Test Method for Compressive Strength of Cylindrical Concrete Specimens. West Conshohocken, PA, United States: ASTM International.

Batista, R.P., Trindade, A.C.C., Borges, P.H.R., Silva, F.D. 2019. Silica Fume as Precursor in the Development of Sustainable and High-Performance MK-Based Alkali-Activated Materials Reinforced With Short PVA Fibers. *Frontiers in Materials,* 6.

Bentur, A., Mindess, S. 1990. *Fibre Reinforced Cementitious Composites,* London, CRC Press.

Bernal, S., Gutierrez, R.D., Delvasto, S., Rodriguez, E. 2010. Performance of an alkali-activated slag concrete reinforced with steel fibers. *Construction and Building Materials,* 24**,** 208-214.

Berthole, L.D., Karnes, C.H. 1975. Two-dimensional analysis of the split hopkinson pressure bar system. *Journal of the Mechanics and Physics of Solids,* 23**,** 1-19.

Bhutta, A., Borges, P. H. R., Zanotti, C., Farooq, M., Banthia, N. 2017. Flexural behavior of geopolymer composites reinforced with steel and polypropylene macro fibers. *Cement and Concrete Composites,* 80**,** 31-40.

Bischoff, P.H., Perry, S.H. 1991. Compressive behaviour of concrete at high strain rates.

Materials and Structures, 24, 425-450.

Bosoaga, A., Masek, O., Oakey, J. E. 2009. CO_2 Capture Technologies for Cement Industry. *Energy Procedia, 1*, 133-140.

Chen, M., Chen, W., Zhong, H., Chi, D., Wang, Y.H., Zhang, M.Z. 2019. Experimental study on dynamic compressive behaviour of recycled tyre polymer fibre reinforced concrete. *Cement and Concrete Composites, 98*, 95-112.

Chen, M., Zhong, H., Wang, H., Zhang, M.Z. 2020. Behaviour of recycled tyre polymer fibre reinforced concrete under dynamic splitting tension. *Cement and Concrete Composites, 114*, 103764.

Chen, X.D., Ge, L.M., Zhou, J.K., Wu, S.X. 2016. Dynamic Brazilian test of concrete using split Hopkinson pressure bar. *Materials and Structures, 50*, 1.

Chen, X.D., Wu, S.X., Zhou, J.K. 2013. Experimental and modeling study of dynamic mechanical properties of cement paste, mortar and concrete. *Construction and Building Materials, 47*, 419-430.

Choi, J.I., Lee, B.Y., Ranade, R., Li, V.C., Lee, Y. 2016. Ultra-high-ductile behavior of a polyethylene fiber-reinforced alkali-activated slag-based composite. *Cement & Concrete Composites, 70*, 153-158.

Choi, S.J., Choi, J.I., Song, J.K., Lee, B.Y. 2015. Rheological and mechanical properties of fiber-reinforced alkali-activated composite. *Construction and Building Materials, 96*, 112-118.

Japan Society of Civil Engineers. 2008. Recommendations for design and construction of high performance fiber reinforced cement composites with multiple fine cracks (HPFRCC). Concrete engineering series no. 82, July 2008.

Trindade, A.C.C., Curosu, I., Liebscher, M., Mechtcherine, V., Silva, F.D.A. 2020. On the mechanical performance of K- and Na-based strain-hardening geopolymer composites (SHGC) reinforced with PVA fibers. *Construction and Building Materials, 248*, 118558.

Cotsovos, D.M., Pavlovic, M.N. 2008. Numerical investigation of concrete subjected to compressive impact loading. Part 1: A fundamental explanation for the apparent strength gain at high loading rates. *Computers & Structures, 86*, 145-163.

Vargas, A.S.D., Molin, D.C.C.D., Vilela, A.C.F., Silva, F.J.D., Pavao, B., Veit, H. 2011. The effects of Na_2O/SiO_2 molar ratio, curing temperature and age on compressive strength, morphology and microstructure of alkali-activated fly ash-based geopolymers. *Cement and Concrete Composites,* 33**,** 653-660.

Domski, J., Katzer, J., Zakrzewski, M., Ponikiewski, T. 2017. Comparison of the mechanical characteristics of engineered and waste steel fiber used as reinforcement for concrete. *Journal of Cleaner Production,* 158**,** 18-28.

Fang, G.H., Bahrami, H., Zhang, M.Z. 2018a. Mechanisms of autogenous shrinkage of alkali-activated fly ash-slag pastes cured at ambient temperature within 24 h. *Construction and Building Materials,* 171**,** 377-387.

Fang, G.H., HO, W.K., TU, W.L., Zhang, M.Z. 2018b. Workability and mechanical properties of alkali-activated fly ash-slag concrete cured at ambient temperature. *Construction and Building Materials,* 172**,** 476-487.

Fang, G.H., Zhang, M.Z. 2020. Multiscale micromechanical analysis of alkali-activated fly ash-slag paste. *Cement and Concrete Research,* 135**,** 106141.

Farhan, A.H., Dawson, A.R., Thom, N.H. 2018a. Recycled hybrid fiber-reinforced & cement-stabilized pavement mixtures: Tensile properties and cracking characterization. *Construction and Building Materials,* 179**,** 488-499.

Farhan, N.A., Sheikh, M.N., Hadi, M.N.S. 2018b. Engineering Properties of Ambient Cured Alkali-Activated Fly Ash-Slag Concrete Reinforced with Different Types of Steel Fiber. 30**,** 04018142.

Farooq, M., Bhutta, A., Banthia, N. 2019. Tensile performance of eco-friendly ductile geopolymer composites (EDGC) incorporating different micro-fibers. *Cement and Concrete Composites,* 103**,** 183-192.

Feng, W.H., Liu, F., Yang, F., Li, L.J., Jing, L. 2018. Experimental study on dynamic split tensile properties of rubber concrete. *Construction and Building Materials,* 165**,** 675-687.

Fernandez-Jimenez, A., Garcia-Lodeiro, I., Palomo, A. 2007. Durability of alkali-activated fly ash cementitious materials. *Journal of Materials Science*, 42**,** 3055-3065.

Fischer, G., Li, V.C. 2002. Influence of Matrix Ductility on Tension-Stiffening Behavior of Steel Reinforced Engineered Cementitious Composites (ECC). *Aci Structural Journal*.

Fischer, G., Li, V.C. 2003. Deformation behavior of fiber-reinforced polymer reinforced engineered cementitious composite (ECC) flexural, members under reversed cyclic loading conditions. *Aci Structural Journal,* 100**,** 25-35.

Fu, Q., Zhang, Z., Zhao, X., Hong, M., Guo, B., Yuan, Q., Niu, D. 2021. Water saturation effect on the dynamic mechanical behaviour and scaling law effect on the dynamic strength of coral aggregate concrete. *Cement and Concrete Composites,* 120.

Gigli, S., Landi, D., Germani, M. 2019. Cost-benefit analysis of a circular economy project: a study on a recycling system for end-of-life tyres. *Journal of Cleaner Production,* 229**,** 680-694.

Gregor, F., Li, V.C. 2002. Effect of Matrix Ductility on Deformation Behavior of Steel-Reinforced ECC Flexural Members under Reversed Cyclic Loading Conditions. *Structural Journal,* 99.

Guo, X.L., Xiong, G.Y., Zhang, H.M. 2020. In-situ evaluation of self-healing performance of Engineered Geopolymer Composites (EGC) by ultrasonic method. *Materials Letters,* 280**,** 128546.

Hao, Y., Hao, H., Jiang, G.P., Zhou, Y. 2013. Experimental confirmation of some factors influencing dynamic concrete compressive strengths in high-speed impact tests. *Cement and Concrete Research,* 52**,** 63-70.

Hardjito, D., Wallah, S.E., Sumajouw, D.M.J., Rangan, B.V. 2004. On The Development of Fly Ash-based Geopolymer Concrete. *Aci Materials Journal*, 101, 467-472.

Hossain, M.A., Hossain, K.M.A., Manzur, T., Hasan, M., Sood, D. Fresh and Hardened Properties of Engineered Geo-Polymer Composite with MgO. Proceedings of the 5th International Conference on Civil Structural and Transportation Engineering (ICCSTE'20), Virtual, Niagara, ON, Canada, 2020. 12-14.

Hou, X., Cao, S., Zheng, W., Rong, Q., Li, G. 2018. Experimental study on dynamic compressive properties of fiber-reinforced reactive powder concrete at high strain rates. *Engineering Structures,* 169**,** 119-130.

Huseien, G.F., Ismail, M., Khalid, N.H.A., Hussin, M.W., Mirza, J. 2018. Compressive strength and microstructure of assorted wastes incorporated geopolymer mortars: Effect of solution molarity. *Alexandria Engineering Journal,* 57**,** 3375-3386.

Jenq, Y.S., Shah, S.P. 1986. Crack Propagation in Fiber-Reinforced Concrete. *Journal of Structural Engineering*, 112**,** 19-34.

Kan, L.L., Lv, J.W., Duan, B.B., Wu, M. 2019. Self-healing of Engineered Geopolymer Composites prepared by fly ash and metakaolin. *Cement and Concrete Research,* 125**,** 105895.

Kan, L.L., Wang, W.S., Liu, W.D., Wu, M. 2020a. Development and characterization of fly ash based PVA fiber reinforced Engineered Geopolymer Composites incorporating metakaolin. *Cement and Concrete Composites,* 108**,** 103521.

Kan, L.L., Zhang, L., Zhao, Y.J., Wu, M. 2020b. Properties of polyvinyl alcohol fiber reinforced fly ash based Engineered Geopolymer Composites with zeolite replacement. *Construction and Building Materials,* 231**,** 117161.

Kanda, T., Li, V. 1998. Multiple cracking sequence and saturation in fiber reinforced cementitious composites.

Kanda, T., Li, V. 2006. Practical Design Criteria for Saturated Pseudo Strain Hardening Behavior in ECC. *Journal of Advanced Concrete Technology,* 4**,** 59-72.

Khan, M.I., Fares, G., Mourad, S., Abbass, W. 2016. Optimized Fresh and Hardened Properties of Strain-Hardening Cementitious Composites: Effect of Sand Size and Workability. *Journal of Materials in Civil Engineering*, 28**,** 04016152.

Khan, M.Z.N., Hao, Y., Hao, H., Shaikh, F.U.A. 2018. Experimental evaluation of quasi-static and dynamic compressive properties of ambient-cured high-strength plain and fiber reinforced geopolymer composites. *Construction and Building Materials,* 166**,** 482-499.

Khan, M.Z.N., Hao, Y.F., Hao, H., Shaikh, F.U.A. 2019. Mechanical properties and behaviour of high-strength plain and hybrid-fiber reinforced geopolymer composites under dynamic splitting tension. *Cement and Concrete Composites,* 104**,** 103343.

Kim, J.K., Yi, S.T. 2002. Application of size effect to compressive strength of concrete

members. *Sadhana,* 27**,** 467.

Kuenzel, C., Vandeperre, L.J., Donatello, S., Boccaccini, A.R., Cheeseman, C. 2012. Ambient Temperature Drying Shrinkage and Cracking in Metakaolin-Based Geopolymers. *Journal of the American Ceramic Society,* 95**,** 3270-3277.

Kumar, S., Kumar, R., Mehrotra, S.P. 2010. Influence of granulated blast furnace slag on the reaction, structure and properties of fly ash based geopolymer. *Journal of Materials Science,* 45**,** 607-615.

Lai, J., Sun, W. 2009. Dynamic behaviour and visco-elastic damage model of ultra-high performance cementitious composite. *Cement and Concrete Research,* 39**,** 1044-1051.

Lee, B.Y., Cho, C.G., Lim, H.J., Song, J.K., Yang, K.H., Li, V. 2012. Strain hardening fiber reinforced alkali-activated mortar - A feasibility study. *Construction and Building Materials,* 37**,** 15-20.

Lee, S.F., Jacobsen, S. 2011. Study of interfacial microstructure, fracture energy, compressive energy and debonding load of steel fiber-reinforced mortar. *Materials and Structures,* 44**,** 1451-1465.

Lehne, J., Preston, F. 2018. Making Concrete Change: Innovation in Low-carbon Cement and Concrete*,* London, The Royal Institute of International Affairs.

Leone, M., Centonze, G., Colonna, D., Micelli, F., Aiello, M. A. 2018. Fiber-reinforced concrete with low content of recycled steel fiber: Shear behaviour. *Construction and Building Materials,* 161**,** 141-155.

Lepech, M.D., Li, V.C. 2006. Long term durability performance of engineered cementitious composites/Langzeitbeständigkeit systematisch entwickelter zusammengesetzter Zement gebundener Werkstoffe. Restoration of Buildings and Monuments, 12(2), 119-132.

Li, F., Yang, Z.M., Zheng, A.H., Li, S. 2021. Properties of modified engineered geopolymer composites incorporating multi-walled carbon Nanotubes(MWCNTs) and granulated blast furnace Slag(GBFS). *Ceramics International,* 47**,** 14244-14259.

Li, M., Li, V.C. 2011. High-Early-Strength Engineered Cementitious Composites for Fast,

Durable Concrete Repair-Material Properties. *Aci Materials Journal,* 108**,** 3-12.

Li, N., Jin, Z., Long, G., Chen, L., Fu, Q., Yu, Y., Zhang, X., Xiong, C. 2021. Impact resistance of steel fiber-reinforced self-compacting concrete (SCC) at high strain rates. *Journal of Building Engineering,* 38**,** 102212.

Li, Q.H., Zhao, X., Xu, S.L., Leung, C.K.Y., Wang, B. 2019. Multiple Impact Resistance of Hybrid Fiber Ultrahigh Toughness Cementitious Composites with Different Degrees of Initial Damage. *Journal of Materials in Civil Engineering*, 31**,** 04018368.

Li, Q. M., Meng, H. 2003. About the dynamic strength enhancement of concrete-like materials in a split Hopkinson pressure bar test. *International Journal of Solids and Structures,* 40**,** 343-360.

Li, V., Wu, C., Wang, S.X., Ogawa, A., Saito, T. 2002. Interface tailoring for strain-hardening polyvinyl alcohol-engineered cementitious composite (PVA-ECC). *ACI Materials Journal,* 99**,** 463-472.

Li, V. C. 1993. From micromechanics to structural engineering-the design of cementitous composites for civil engineering applications.

Li, V. 2003. On Engineered Cementitious Composites (ECC), A Review of the Material and Its Applications. *Journal of Advanced Concrete Technology*, 1, 215-230.

Li, V. 2019. Engineered Cementitious Composites (ECC): Bendable Concrete for Sustainable and Resilient Infrastructure, Springer.

Li, V., Kanda, T. 1998. Engineered Cementitious Composites for Structural Applications. *Journal of Materials in Civil Engineering*, 10**,** 66-69.

Li, V., Leung, C.K.Y. 1992. Steady-State and Multiple Cracking of Short Random Fiber Composites. *Journal of Engineering Mechanics*, 118**,** 2246-2264.

Li, V., Wu, H.C., Maalej, M., Mishra, D.K., Hashida, T. 1996. Tensile Behavior of Cement-Based Composites with Random Discontinuous Steel Fibers. *Journal of the American Ceramic Society*, 79**,** 74-78.

Li, W., Xu, J. 2009. Impact characterization of basalt fiber reinforced geopolymeric concrete using a 100-mm-diameter split Hopkinson pressure bar. *Materials Science and Engineering: A,* 513-514**,** 145-153.

Liew, K.M., Akbar, A. 2020. The recent progress of recycled steel fiber reinforced concrete. *Construction and Building Materials,* 232**,** 117232.

Lin, J.X., Song, Y., Xie, Z.H., Guo, Y.C., Yuan, B., Zeng, J.J., Wei, X. 2020. Static and dynamic mechanical behavior of engineered cementitious composites with PP and PVA fibers. *Journal of Building Engineering,* 29**,** 101097.

Ling, Y.F., Wang, K.J., Li, W.G., Shi, G.Y., Lu, P. 2019. Effect of slag on the mechanical properties and bond strength of fly ash-based engineered geopolymer composites. *Composites Part B: Engineering,* 164**,** 747-757.

Ma, Y., Ye, G. 2015. The shrinkage of alkali activated fly ash. *Cement and Concrete Research,* 68**,** 75-82.

Maalej, M., Quek, S.T., Ahmed, S.F.U., Zhang, J., Lin, V.W.J., Leong, K.S. 2012. Review of potential structural applications of hybrid fiber Engineered Cementitious Composites. *Construction and Building Materials,* 36**,** 216-227.

Martinelli, E., Caggiano, A., Xargay, H. 2015. An experimental study on the post-cracking behaviour of Hybrid Industrial/Recycled Steel Fibre-Reinforced Concrete. *Construction and Building Materials,* 94**,** 290-298.

Martinie, L., Rossi, P., Roussel, N. 2010. Rheology of fiber reinforced cementitious materials: classification and prediction. *Cement and Concrete Research,* 40**,** 226-234.

Mastali, M., Kinnunen, P., Dalvand, A., Firouz, R.M., Illikainen, M. 2018. Drying shrinkage in alkali-activated binders - A critical review. *Construction and Building Materials,* 190**,** 533-550.

Matsumoto, T., Mihashi, H. 2002. JCI-DFRCC summary report on DFRCC terminologies and application concepts. *Proceedings of JCI international workshop on ductile fibre reinforced cementitious composites*. Citeseer, 59-66.

Mohammed, B.S., Khed, V.C., Liew, M.S. 2018. Optimization of hybrid fibres in engineered cementitious composites. *Construction and Building Materials,* 190**,** 24-37.

Sahmaran, M., Li, M., & Li, V. C. (2007). Transport properties of engineered cementitious composites under chloride exposure. *ACI Materials Journal*, 104(6), 604-611.

Mwangi, J.P.M. 2001. Flexural Behavior of Sisal Fiber Reinforced Concrete Beams, University of California, Davis.

Nath, P., Sarker, P.K. 2016. Fracture properties of GGBFS-blended fly ash geopolymer concrete cured in ambient temperature. *Materials and Structures*, 50**,** 32.

Nedeljkovic, M., Lukovic, M., Breugel, K.V., Hordijk, D., Ye, G. 2018. Development and application of an environmentally friendly ductile alkali-activated composite. *Journal of Cleaner Production,* 180**,** 524-538.

Nematollahi, B., Qiu, J.S., Yang, E.H., Sanjayan, J. 2017a. Micromechanics constitutive modelling and optimization of strain hardening geopolymer composite. *Ceramics International,* 43**,** 5999-6007.

Nematollahi, B., Qiu, J.S., Yang, E.H., Sanjayan, J. 2017b. Microscale investigation of fiber-matrix interface properties of strain-hardening geopolymer composite. *Ceramics International,* 43**,** 15616-15625.

Nematollahi, B., Ranade, R., Sanjayan, J., Ramakrishnan, S. 2017c. Thermal and mechanical properties of sustainable lightweight strain hardening geopolymer composites. *Archives of Civil and Mechanical Engineering,* 17**,** 55-64.

Nematollahi, B., Sanjayan, J. 2014. Effect of different superplasticizers and activator combinations on workability and strength of fly ash based geopolymer. *Materials & Design,* 57**,** 667-672.

Nematollahi, B., Sanjayan, J., Qiu, J.S., Yang, E.H. 2017d. Micromechanics-based investigation of a sustainable ambient temperature cured one-part strain hardening geopolymer composite. *Construction and Building Materials,* 131**,** 552-563.

Nematollahi, B., Sanjayan, J., Qiu, J.S., Yang, E.H. 2017e. High ductile behavior of a polyethylene fiber-reinforced one-part geopolymer composite: A micromechanics-based investigation. *Archives of Civil and Mechanical Engineering,* 17**,** 555-563.

Nematollahi, B., Sanjayan, J., Shaikh, F.U.A. 2014. Comparative deflection hardening behavior of short fiber reinforced geopolymer composites. *Construction and Building Materials,* 70**,** 54-64.

Nematollahi, B., Sanjayan, J., Shaikh, F.U.A. 2015. Tensile Strain Hardening Behavior

of PVA Fiber-Reinforced Engineered Geopolymer Composite. *Journal of Materials in Civil Engineering,* 27, 04015001.

Nematollahi, B., Sanjayan, J., Shaikh, F.U.A. 2016a. Matrix design of strain hardening fiber reinforced engineered geopolymer composite. *Composites Part B-Engineering,* 89**,** 253-265.

Nguyen, H., Carvelli, V., Adesanya, E., Kinnunen, P., Illikainen, M. 2018. High performance cementitious composite from alkali-activated ladle slag reinforced with polypropylene fibers. *Cement & Concrete Composites,* 90**,** 150-160.

Nguyen, H., Staudacher, M., Kinnunen, P., Carvelli, V., Illikainen, M. 2019. Multi-fiber reinforced ettringite-based composites from industrial side streams. *Journal of Cleaner Production,* 211**,** 1065-1077.

Noushini, A., Hastings, M., Castel, A., Aslani, F. 2018. Mechanical and flexural performance of synthetic fibre reinforced geopolymer concrete. *Construction and Building Materials,* 186**,** 454-475.

Ohno, M., Li, V. 2014. A feasibility study of strain hardening fiber reinforced fly ash-based geopolymer composites. *Construction and Building Materials,* 57**,** 163-168.

Ohno, M., Li, V. 2018. An integrated design method of Engineered Geopolymer Composite. *Cement and Concrete Composites,* 88**,** 73-85.

Pakravan, H.R., Jamshidi, M., Latifi, M. 2016. Study on fiber hybridization effect of engineered cementitious composites with low- and high-modulus polymeric fibers. *Construction and Building Materials,* 112**,** 739-746.

Parra-Montesinos, G., Wight, J. K. 2000. Seismic response of exterior RC column-to-steel beam connections. Journal of structural engineering, 126(10), 1113-1121.

Paulay, T., Binney, J. R. 1974. Diagonally Reinforced Coupling Beams of Shear Walls. *ACI Symposium Publication,* 42, 579-598.

Provis, J.L., Deventer, J.S.J.D. 2009. Geopolymers: structures, processing, properties and industrial applications, Elsevier.

Puertas, F., Amat, T., Fernandez-Jimenez, A., Vazquez, T. 2003a. Mechanical and durable behaviour of alkaline cement mortars reinforced with polypropylene fibres. *Cement and Concrete Research,* 33**,** 2031-2036.

Puertas, F., Palomo, A., Fernandez-Jimenez, A., Izquierdo, J.D., Granizo, M.L. 2003b. Effect of superplasticisers on the behaviour and properties of alkaline cements. *Advances in Cement Research*, 15**,** 23-28.

Ramarad, S., Khalid, M., Ratnam, C.T., Chuah, A.L., Rashmi, W. 2015. Waste tire rubber in polymer blends: A review on the evolution, properties and future. *Progress in Materials Science,* 72**,** 100-140.

Ranjbar, N., Mehrali, M., Mehrali, M., Alengaram, U.J., Jumaat, M.Z. 2016a. High tensile strength fly ash based geopolymer composite using copper coated micro steel fiber. *Construction and Building Materials,* 112**,** 629-638.

Ranjbar, N., Talebian, S., Mehrali, M., Kuenzel, C., Metselaar, H.S.C., Jumaat, M.Z. 2016c. Mechanisms of interfacial bond in steel and polypropylene fiber reinforced geopolymer composites. *Composites Science and Technology,* 122**,** 73-81.

Ranjbar, N., Zhang, M.Z. 2020. Fiber-reinforced geopolymer composites: A review. *Cement and Concrete Composites,* 107**,** 103498.

Ren, G.M., Wu, H., Fang, Q., Liu, J. Z. 2018. Effects of steel fiber content and type on dynamic compressive mechanical properties of UHPCC. *Construction and Building Materials,* 164**,** 29-43.

Rokugo, K., Kanda, T. 2013. Strain Hardening Cement Composites: Structural Design and Performance, State-of-the-Art Report of the RILEM Technical Committee 208-HFC, SC3, Springer.

Rokugo, K., Kanda, T., Yokota, H., Sakata, N. 2009. Applications and recommendations of high performance fiber reinforced cement composites with multiple fine cracking (HPFRCC) in Japan. *Materials and Structures,* 42**,** 1197.

Ross, C.A., Tedesco, J. W., Kuennen, S.T. 1995. Effects of Strain Rate on Concrete Strength. *ACI Materials Journal,* 92.

Rossi, P., Van Mier, J.G.M., Boulay, C., Le Maou, F. 1992. The dynamic behaviour of concrete: influence of free water. *Materials and Structures,* 25**,** 509-514.

Salami, B.A., Johari, M.A.M., Ahmad, Z.A., Maslehuddin, M. 2016. Impact of added water and superplasticizer on early compressive strength of selected mixtures of palm oil fuel ash-based engineered geopolymer composites. *Construction and*

Building Materials, 109**,** 198-206.

Salami, B.A., Johari, M.A.M., Ahmad, Z.A., Maslehuddin, M. 2017. Durability performance of Palm Oil Fuel Ash-based Engineered Alkaline-activated Cementitious Composite (POFA-EACC) mortar in sulfate environment. *Construction and Building Materials,* 131**,** 229-244.

Scherer, G.W. 1990. Theory of Drying. *Journal of the American Ceramic Society*, 73**,** 3-14.

Shaikh, F.U.A. 2013. Deflection hardening behaviour of short fibre reinforced fly ash based geopolymer composites. *Materials & Design,* 50**,** 674-682.

Shaikh, F.U.A. 2020. Tensile and flexural behaviour of recycled polyethylene terephthalate (PET) fibre reinforced geopolymer composites. *Construction and Building Materials,* 245**,** 118438.

Shaikh, F.U.A., Fairchild, A., Zammar, R. 2018. Comparative strain and deflection hardening behaviour of polyethylene fibre reinforced ambient air and heat cured geopolymer composites. *Construction and Building Materials,* 163**,** 890-900.

Singh, B., Ishwarya, G., Gupta, M., Bhattacharyya, S.K. 2015. Geopolymer concrete: A review of some recent developments. *Construction and Building Materials,* 85**,** 78-90.

Singh, M., Saini, B., Chalak, H.D. 2019. Performance and composition analysis of engineered cementitious composite (ECC) – A review. *Journal of Building Engineering,* 26**,** 100851.

Siyal, A.A., Azizli, K.A., Man, Z., Ullah, H. 2016. Effects of Parameters on the Setting Time of Fly Ash Based Geopolymers Using Taguchi Method. *Procedia Engineering,* 148**,** 302-307.

Soe, K.T., Zhang, Y.X., Zhang, L.C. 2013. Material properties of a new hybrid fibre-reinforced engineered cementitious composite. *Construction and Building Materials,* 43**,** 399-407.

Somna, K., Jaturapitakkul, C., Kajitvichyanukul, P., Chindaprasirt, P. 2011. NaOH-activated ground fly ash geopolymer cured at ambient temperature. *Fuel,* 90**,** 2118-2124.

Stang, H. 1999. 18 EXTRUSION OF ECC-MATERIAL. In PRO 6: 3rd International RILEM Workshop on High Performance Fiber Reinforced Cement Composites (HPFRCC 3) (Vol. 3, p. 203). Rilem publications.

Sun, X.W., Zhao, K., Li, Y.C., Huang, R.Y., Ye, Z.B., Zhang, Y.L., Ma, J. 2018. A study of strain-rate effect and fiber reinforcement effect on dynamic behavior of steel fiber-reinforced concrete. *Construction and Building Materials,* 158**,** 657-669.

Suthiwarapirak, P., Matsumoto, T., Kanda, T. 2002. Flexural fatigue failure characteristics of an engineered cementitious composite and polymer cement mortars. Doboku Gakkai Ronbunshu, 2002(718), 121-134.

Takashima, H., Miyagai, K., Hashida, T., Li, V. C. 2003. A design approach for the mechanical properties of polypropylene discontinuous fiber reinforced cementitious composites by extrusion molding. *Engineering Fracture Mechanics,* 70**,** 853-870.

Tedesco, J.W., Powell, J.C., Ross, C.A., Hughes, M.L. 1997. A strain-rate-dependent concrete material model for ADINA. *Computers & Structures,* 64**,** 1053-1067.

Temuujin, J., Riessen, A.V., Mackenzie, K.J.D. 2010. Preparation and characterisation of fly ash based geopolymer mortars. *Construction and Building Materials,* 24**,** 1906-1910.

Toutanji, H., Xu, B., Gilbert, J., Lavin, T. 2010. Properties of poly(vinyl alcohol) fiber reinforced high-performance organic aggregate cementitious material: Converting brittle to plastic. *Construction and Building Materials,* 24**,** 1-10.

Trindade, A.C.C., Borges, P.H.R., Silva, F.D. 2019. Mechanical behavior of strain-hardening geopolymer composites reinforced with natural and PVA fibers. *Materials Today-Proceedings,* 8**,** 753-759.

Trindade, A.C.C., Heravi, A.A., Curosu, I., Liebscher, M., Silva, F.D.A., Mechtcherine, V. 2020. Tensile behavior of strain-hardening geopolymer composites (SHGC) under impact loading. *Cement and Concrete Composites,* 113**,** 103703.

Tu, W.L., Zhu, Y., Fang, G.H., Wang, X.G., Zhang, M.Z. 2019. Internal curing of alkali-activated fly ash-slag pastes using superabsorbent polymer. *Cement and Concrete Research,* 116**,** 179-190.

Vargas, A.S.D., Molin, D.C.C.D., Vilela, A.C.F., Silva, F.J.D., Pavao, B., Veit, H. 2011. The effects of Na_2O/SiO_2 molar ratio, curing temperature and age on compressive strength, morphology and microstructure of alkali-activated fly ash-based geopolymers. *Cement and Concrete Composites,* 33**,** 653-660.

Wan, X.M., Shen, C., Wang, P.G., Zhao, T.J., Lu, Y. 2020. A study on fracture toughness of ultra-high toughness geopolymer composites based on Double-K Criterion. *Construction and Building Materials,* 251**,** 118851.

Wang, A.Q., Zhang, C.Z., Sun, W. 2003. Fly ash effects: I. The morphological effect of fly ash. *Cement and Concrete Research,* 33**,** 2023-2029.

Wang, Q.S., Yong, Y., Ma, G., Luo, H.W. 2019. Hybrid effects of steel fibers, basalt fibers and calcium sulfate on mechanical performance of PVA-ECC containing high-volume fly ash. *Cement and Concrete Composites,* 97**,** 357-368.

Wang, S., Li, V. 2006. Polyvinyl Alcohol Fiber Reinforced Engineered Cementitious Composites: Material Design and Performances. *Proceedings of International RILEM workshop on HPFRCC in structural applications*, 65-73.

Wang, S., & Li, V. C. 2007. Engineered cementitious composites with high-volume fly ash. ACI materials journal, 104(3), 233.

Wang, S.S., Zhang, M.H., Quek, S. T. 2012. Mechanical behavior of fiber-reinforced high-strength concrete subjected to high strain-rate compressive loading. *Construction and Building Materials,* 31**,** 1-11.

Wang, S.S., Zhang, M.H., Quek, S.T. 2011a. Effect of specimen size on static strength and dynamic increase factor of high-strength concrete from SHPB test. *Journal of Testing and Evaluation,* 39**,** 898-907.

Wang, Y., CHAN, C.L., Leong, S.H., Zhang, M.Z. 2020. Engineering properties of strain hardening geopolymer composites with hybrid polyvinyl alcohol and recycled steel fibres. *Construction and Building Materials,* 261**,** 120585.

Wang, Y., Wang, Y.S., Zhang, M.Z. 2021. Effect of sand content on engineering properties of fly ash-slag based strain hardening geopolymer composites. *Journal of Building Engineering,* 34**,** 101951.

Wu, Z.M., Shi, C.J., He, W., Wang, D.H. 2017. Static and dynamic compressive properties

of ultra-high performance concrete (UHPC) with hybrid steel fiber reinforcements. *Cement and Concrete Composites, 79***,** 148-157.

Xiao, J.Z., Li, L., Shen, L.M., Poon, C.S. 2015. Compressive behaviour of recycled aggregate concrete under impact loading. *Cement and Concrete Research, 71***,** 46-55.

Xiao, S.H., Liao, S.J., Zhong, G.Q., Guo, Y.C., Lin, J.X., Xie, Z.H., Song, Y. 2021. Dynamic properties of PVA short fiber reinforced low-calcium fly ash - slag geopolymer under an SHPB impact load. *Journal of Building Engineering, 44.*

Xu, B., Toutanji, H.A., Gilbert, J. 2010. Impact resistance of poly(vinyl alcohol) fiber reinforced high-performance organic aggregate cementitious material. *Cement and Concrete Research, 40***,** 347-351.

Xu, F., Deng, X., Peng, C., Zhu, J., Chen, J.P. 2017. Mix design and flexural toughness of PVA fiber reinforced fly ash-geopolymer composites. *Construction and Building Materials, 150***,** 179-189.

Yan, D., Lin, G. 2006. Dynamic properties of concrete in direct tension. *Cement and Concrete Research, 36***,** 1371-1378.

Yang, E.H., Sahmaran, M., Yang, Y., Li, V. C. 2009. Rheological control in production of engineered cementitious composites. *ACI Materials Journal, 106***,** 357-366.

Yang, E. H., Yang, Y., Li, V. C. 2007. Use of high volumes of fly ash to improve ECC mechanical properties and material greenness. ACI materials journal, 104(6), 620.

Yang, K.H., Song, J.K., Song, K.I. 2013. Assessment of CO_2 reduction of alkali-activated concrete. *Journal of Cleaner Production, 39***,** 265-272.

Yang, T., Zhu, H.J., Zhang, Z.H. 2017. Influence of fly ash on the pore structure and shrinkage characteristics of metakaolin-based geopolymer pastes and mortars. *Construction and Building Materials, 153***,** 284-293.

Yang, W.J., Fang, Y.H., Gu, Y.M. 2014. Effect of Basalt and Polypropylene Fiber on the Mechanical Properties of Alkali-Activated Slag Cement Paste. *International Conference on Material Science and Material Engineering (Msme 2014)***,** 350-353.

Yazici, S., Inan, G., Tabak, V. 2007. Effect of aspect ratio and volume fraction of steel

fiber on the mechanical properties of SFRC. *Construction and Building Materials,* 21**,** 1250-1253.

Ye, J., Cui, C., Yu, J., Yu, K., Dong, F. 2021. Effect of polyethylene fiber content on workability and mechanical-anisotropic properties of 3D printed ultra-high ductile concrete. *Construction and Building Materials,* 281**,** 122586.

Yu, J., Chen, Y.X., Leung, C.K.Y. 2018. Micromechanical modeling of crack-bridging relations of hybrid-fiber Strain-Hardening Cementitious Composites considering interaction between different fibers. *Construction and Building Materials,* 182**,** 629-636.

Yu, K., Ding, Y., Zhang, Y.X. 2020. Size effects on tensile properties and compressive strength of engineered cementitious composites. *Cement and Concrete Composites,* 113**,** 103691.

Yu, K., Wang, Y., Yu, J., Xu, S. 2017. A strain-hardening cementitious composites with the tensile capacity up to 8%. *Construction and Building Materials,* 137**,** 410-419.

Yu, Q., Zhuang, W., Shi, C. 2021. Research progress on the dynamic compressive properties of ultra-high performance concrete under high strain rates. *Cement and Concrete Composites,* 124.

Zhang Y.S., Sun, W., Li, Z.J., Zhou X.M., Eddie, Chau, C.K. 2008. Impact properties of geopolymer based extrudates incorporated with fly ash and PVA short fiber. *Construction and Building Materials,* 22**,** 370-383.

Zahid, M., Shafiq, N., Isa, M.H., Gil, L. 2018. Statistical modeling and mix design optimization of fly ash based engineered geopolymer composite using response surface methodology. *Journal of Cleaner Production,* 194**,** 483-498.

Zamanzadeh, Z., Lourenco, L., Barros, J. 2015. Recycled Steel Fibre Reinforced Concrete failing in bending and in shear. *Construction and Building Materials,* 85**,** 195-207.

Zhang, H., Wang, L., Zheng, K., Bakura, T. J., Totakhil, P.G. 2018. Research on compressive impact dynamic behavior and constitutive model of polypropylene fiber reinforced concrete. *Construction and Building Materials,* 187**,** 584-595.

Zhang, Q., Li, V.C. 2016. Ductile cement-based spray-applied fire-resistive materials. *Journal of Structural Fire Engineering,* 7**,** 114-125.

Zhang, S.Z., Li, V., Ye, G. 2020. Micromechanics-guided development of a slag/fly ash-based strain-hardening geopolymer composite. *Cement and Concrete Composites,* 109**,** 103510.

Zhang, W., Zhang, Y., Zhang, G. 2012. Static, dynamic mechanical properties and microstructure characteristics of ultra-high performance cementitious composites. Science and Engineering of Composite Materials, 19(3), 237-245.

Zhang, Z., Kong, D., Gong, G., Chong, X., Wu, Y.G., Li, Q., Meng, B. 2007. Dynamic mechanical behavior of concrete under high strain rate using SHPB. *Journal of PLA University of Science Technology,* 8**,** 611-618.

Zhong, H., Poon, E.W., Chen, K., Zhang, M.Z. 2019. Engineering properties of crumb rubber alkali-activated mortar reinforced with recycled steel fibres. *Journal of Cleaner Production*, 238**,** 117950.

Zhong, H., Zhang, M.Z. 2020. Experimental study on engineering properties of concrete reinforced with hybrid recycled tyre steel and polypropylene fibres. *Journal of Cleaner Production,* 259**,** 120914.

Zhong, H., Zhang, M.Z. 2021. Effect of recycled tyre polymer fibre on engineering properties of sustainable strain hardening geopolymer composites. *Cement and Concrete Composites,* 122**,** 104167.

Zhu, B., Pan, J., Nematollahi, B., Zhou, Z., Zhang, Y., Sanjayan, J. 2019. Development of 3D printable engineered cementitious composites with ultra-high tensile ductility for digital construction. *Materials & Design,* 181**,** 108088.

Appendix. Mix Proportion Calculation

Method 1 – Experimental data

The mix proportion of control specimens for the first batch of materials is presented in Table A-1. Based on the mix proportion, the first batch is casted with the assumption of 24.22 L and the batch weight is shown in Table A-2.

Table A-1. Mix proportions of control specimens.

Mix No.	Binder	FA/GGBS	AL/B	Molarity of SH (M)	SS/SH ratio	SPs (wt.% of B)	Fine silica sand/B
M0	400	80/20	0.4	10	2	1	0.3

Table A-2. Batch weight of control specimens (kg).

Mix No.	FA	GGBS	NaOH	Na_2SiO_3	SPs	Fine silica sand	Total weight
M0	7.75	1.94	1.29	2.58	0.10	2.91	16.57

After casting, the geopolymer mortar were filled in moulds shown in Table A-3.

Table A-3. Geopolymer mortar filled in the casting.

Moulds filled	Number of moulds filled	Dimensions of each mould (mm)	Volume of each mould (L)	Total volume (L)
Compressive strength	6	50 x 50 x 50	0.125	0.75
Rebound hammer test	1	100 x 100 x 100	1	1.00
Elastic modulus	1	D100 x 200	1.57	1.57
Four-point bending test	3	400 x 100 x 20	0.8	2.40
Drying shrinkage	3	50 x 50 x 250	0.625	1.88

Hence, the first batch has a total weight of 16.57 kg and total volume of 7.60 L, leading to a fresh density of 2.18 kg/L.

According to the calculation, in order to cast specimens of 25.27L, which is 3.27 times the total volume of casted specimens, the weight of each raw material in one batch is multiplied by 3.27 and shown in Table A-4.

Table A-4. Revised batch weight of control specimens (kg).

Mix No.	FA	GGBS	NaOH	Na2SiO3	SPs	Fine silica sand	Total weight
M0	25.34	6.34	4.22	8.44	0.33	9.52	54.18

Method 2 – Unit Weight

According to the mix proportions shown in Table A-1, assume the unit weight for calculation (superplasticiser is neglected), leading to the following equation:

$$x + 0.4x + 0.3x = 1 \ (unit \ weight)$$

$$x = 0.588$$

In this batch, each 1kg geopolymer mortar contains 0.588kg binder, 0.235kg activator, and 0.176kg sand.

The required geopolymer mortar is 25.27L, and the fresh density is assumed to be 2.2kg/L, hence the total weight required is 55.594 kg.

Further to this ratio, in order to prepare geopolymer mortar with total weight of 55.594kg, the total weight of each type should be 32.69 kg for binder, 13.06kg for activator, and 9.78kg for sand. Hence, the batch weight of each material is shown in Table A-5.

Table A-5. Batch weight of each material.

Mix No.	FA	GGBS	NaOH	Na$_2$SiO$_3$	SPs	Fine silica sand	Total weight (with SPs)
M0	26.15	6.54	4.35	8.71	0.26	9.78	55.8

Method 3 – Unit Volume

According to the mix design shown in Table A-1, assume the unit volume for calculation (superplasticiser is neglected), leading to the following equation:

$$\frac{x}{density \ of \ binder} + \frac{0.4x}{density \ of \ activator} + \frac{0.3x}{density \ of \ sand} = 1 \ (unit \ volume)$$

In this batch, densities of binder, activator, and sand should be available:

- Density of binder:

The specific gravity of fly ash is 2.65 and GGBS is 2.9. Therefore the density of binder could be derived by

2.65 x 0.8 + 2.9 x 0.2 = 2.7 kg/L

- Density of activator:

The density of NaOH solution is 1.31kg/L, and Na_2SiO_3 solution is 1.45kg/L. Therefore the density of activator solution could be derived by

1.31 x 0.33 + 1.45 x 0.67 = 1.40kg/L

- Density of fine silica sand is 2.65 kg/L

Therefore, the equation could be expressed as

$$\frac{x}{2.7} + \frac{0.4x}{1.4} + \frac{0.3x}{2.65} = 1 \ (unit \ volume)$$

$$x = 1.30 \ (kg)$$

The total volume for each batch is 25.27L, the total weight of each type should be 32.85kg for binder, 13.14kg for activator, and 9.86kg for sand. Hence, the batch weight of each material is shown in Table A-6.

Table A-6. Batch weight of each material.

Mix No.	FA	GGBS	NaOH	Na₂SiO₃	SPs	Fine silica sand	Total weight (with SPs)
M0	26.28	6.57	4.38	8.76	0.33	9.86	56.18

Table A-7. Comparisons of batch weight derived by three methods.

Methods	FA	GGBS	NaOH	Na2SiO3	SPs	Fine silica sand	Total weight (with SPs)
Experiment	25.34	6.34	4.22	8.44	0.33	9.52	54.18
Unit weight	26.15	6.54	4.35	8.71	0.26	9.78	55.8
Unit volume	26.28	6.57	4.38	8.76	0.33	9.86	56.18